

FINAL REPORT

Graphene/graphene oxide based polymer
nanocomposites and their applications as biosensor
and supercapacitor

Sponsored by

COUNCIL OF SCIENTIFIC AND INDUSTRIAL RESEARCH

(CSIR Scheme No.: 02(0066)/12/EMR-II)



Submitted by

Prof. S.K. Dolui, C. Bora, C. Sarkar

Department of Chemical Sciences

Tezpur University

Napaam-784028

Assam



FORM-F

COUNCIL OF SCIENTIFIC AND INDUSTRIAL RESEARCH
Human Resource Development Group
(Extra Mural Research Division)
CSIR Complex, Library Avenue, Pusa, New Delhi – 110012

PROFORMA FOR PREPARING FINAL TECHNICAL REPORT
(Five copies of the report must be submitted immediately after completion of the research scheme)

1. Title of the scheme

Graphene/graphene oxide based polymer nanocomposites and their applications as biosensor and supercapacitor.	Scheme No.:	02(0066)/12/EMR-II
	Date of Commencement :	16/05/2012
	Date of termination :	31/08/2015

2. Name and address of Principal Investigator

Prof. Swapan Kr. Dolui Professor, Department of Chemical Sciences, Tezpur University, Napaam, Tezpur-784028, Assam, India
--

3. Name of Sponsoring laboratory of CSIR (If applicable)

NA

4. Total grant sanctioned and expenditure during the entire tenure

	Amount Sanctioned	Expenditure
Staff		

Contingency		
Equipment		
Total		

5. Equipment(s) purchased out of CSIR grant

Name	Cost
Centrifuge	19,800/-+VAT
Membrane filter	19,250/-+1600/-+13.5%VAT
Hot Oven	23,400/-+VAT
Rotor evaporator	3,03,774/-

6. Research fellows associated with scheme

Name& Designation	Date of Joining	Date of leaving
Chandramika Bora (SRF)	14/08/2012	30/04/2013
Chandrama Sarkar (JRF)	24/08/2013	31/08/2015

7. Name(s) of the fellow(s) who received Ph.D. by working in the scheme, along with the Title(s) of thesis:

Name : Chandramika Bora

Title of thesis: "Graphene/graphene oxide based polymer nanocomposites and their applications"

8. List of research papers published/communicated, based on the research work done under the scheme (Name(s) of author(s), Title, Journal, Volume number, Year and Pages should be given for each paper published and a copy of each of them should be enclosed; reprints/copies of papers appearing after submission of FTR should also be sent to CSIR):

- i. C. Bora, P. Bharali, S. Baglari, S.K. Dolui. Strong and conductive reduced graphene oxide/polyester resin composite films with improved mechanical strength and thermal stability. *Composites Science and Technology* **87** (2013) 1-7.

- ii. C. Bora, S.K. Dolui. Interfacial synthesis of polypyrrole/graphene nanocomposites by liquid/liquid interfacial polymerization and their optical, electrical and electrochemical properties. *Polymer International* **63** (2013) 1439-1446.
- iii. C. Bora, S.K. Dolui. Synthesis of polythiophene/graphene oxide composite by interfacial polymerization and evaluation of their electrical and electrochemical properties. *Polymer International* 2014, DOI 10.1002/pi.4739.
- iv. C. Sarkar, S.K. Dolui. Synthesis of copper oxide/reduced graphene oxide nanocomposite and its enhanced catalytic activity towards reduction of 4-nitrophenol. *RSC Advances* **5** (2015) 60763-60769.

9. Details of new apparatus or equipment designed or constructed during the investigation: No

10. The likely impact of the completed work on the scientific/technological potential in the country (this may be attached as Enclosure-I): Enclosure-I is attached separately.

11. Is the research work done of some industrial or agricultural importance and whether patent(s) should be taken? Yes/No; if yes, what action has been/should be taken: Yes, Patent has been filed as "Sulfonated graphene/ polypyrrole composite as supercapacitor electrode." (Patent application no. E-2/749/2014 KOL)

12. How has the research work complemented the work of CSIR Laboratory that sponsored your scheme?

This work is useful for CSIR-Central Electronics Engineering Research Institute.

13. Detailed account of the work carried out in terms of the objective(s) of the project and how for they have been achieved; results and discussion should be presented in the manner of a scientific paper/project report in about 5000 words; and this should be submitted as Enclosure-II to this report.
Enclosure-II is attached separately.

14. An abstract of research achievements in about 200-500 words, suitable for publication.

Abstract of research achievement is summarized below:

Graphene (GR)/graphene oxide (GO) based polymer nanocomposites are an exciting field of research today. These wonderful materials have shown diverse range of applications in many areas. The research work under this project demonstrates the successful synthesis of a series of GR/GO based nanocomposites with polymers such as polypyrrole (PPy), polythiophene (PTh) and polyester (PE) resin. The composites were characterized by various spectroscopic and analytical techniques. The electrical and electrochemical properties of the composites were also studied. All the composites showed superior properties compared to the pure polymer at low

filler loading. We have also studied some of the applications of the composites in sensor and supercapacitor. The major findings of the work are summarized below:

GR and GO based PPy and PTh composites was successfully prepared by liquid/liquid interfacial polymerization. Both Raman spectroscopy and XRD results indicated the incorporation of the nanofillers in the polymer matrix. TEM and SEM study showed uniform distribution of the GR/GO throughout the polymer matrix. The composites exhibited an improved thermal stability compared to pure polymer. The PPy/GR composites exhibited a higher value of conductivity ($2.51-8.45 \text{ S cm}^{-1}$) compared to PPy (0.210 S cm^{-1}) and PPy/GO composites ($0.360-0.507 \text{ S cm}^{-1}$). Electrical conductivity of the PTh/GR composites was found to be higher ($7.4 \times 10^{-3} \text{ Scm}^{-1}$ for PTGR3 composite) than that of pure PTh ($5.8 \times 10^{-5} \text{ S cm}^{-1}$). Both the composites showed reversible electrochemical response and a good cycling stability even up to 100th cycles. A charging-discharging study also revealed a high capacitance value (260 F g^{-1}) for the PPy/GR composite and 210 F/g for PTh/GR composites at 3 wt.% of GR loading. GR and GO based polyester (PE) resin composites with high thermal stability and mechanical strength was also prepared. Around 123% increase of tensile strength and 87% increase in Young's modulus are obtained with 3 wt.% of GR loading. The PE/GR composite film was found to possess a higher value of conductivity ($3.7 \times 10^{-4} \text{ S cm}^{-1}$) compared to pure resin due to the incorporation of highly conducting GR sheets. The PE/GR composites imply proficient antibacterial activity towards the five different kinds of bacterial strains.

Also we have studied some of their applications. We have fabricated of a glucose biosensor based on PPy/GR nanocomposites. This biosensor showed a high value of sensitivity ($29.6 \mu\text{M/cm}^2.\text{mM}$) and lower limit of detection ($0.1 \mu\text{M}$) compared to other GR and CNT based biosensor. Sulfonated graphene (SG) based PPy composite was used as electrode material for supercapacitor. Charging-discharging study revealed a high specific capacitance value (360 F g^{-1}) of PPy/SG composite at a current density of 1 A g^{-1} . Furthermore, the composite exhibited a good electrochemical stability. Thus the results obtained from this work may be useful for development of new high performance GR based polymer nanocomposites in future.

15. Mention here whether or not the unspent grant has been refunded to CSIR: Last grant yet to be released.

Date: 5/11/15

Signature of PI

Enclosure-I

The likely impact of the completed work on the scientific/technological potential is given below:

Graphene (GR) based polymer composites have been explored for a wide range of applications in many areas such energy storage device, sensors, solar cells, liquid crystal devices, organic light emitting diodes, field emission devices and biomedical applications etc. Graphene based polymer composites exhibit a moderate conductivity, high chemical stability and excellent electrochemical properties. They are also found to be attractive for electrochemical applications due to its high surface area and good interaction with water and organic solvents. Graphene oxide (GO) based electrodes are widely used in various electrochemical applications such as electrochemical sensors, electrochemiluminescence and electrocatalysis.

The research work under this project demonstrates the successful synthesis of a series of GR/GO based nanocomposites with polymers such as polypyrrole (PPy), polythiophene (PTh) and polyester (PE) resin. The electrical and electrochemical properties of the composites were studied. All the composites showed superior properties compared to the pure polymer at low filler loading. We have also studied some of the applications of the composites in sensor and supercapacitor. GR and GO based PPy and PTh composites exhibited an improved thermal stability compared to pure polymer.

GR and GO based PPy and PTh composites was successfully prepared by liquid/liquid interfacial polymerization which have vast application potential in supercapacitors, biosensors and many other fields. The PPy/GR composites exhibited a higher value of conductivity ($2.51-8.45 \text{ S cm}^{-1}$) compared to PPy (0.210 S cm^{-1}) and PPy/GO composites ($0.360-0.507 \text{ S cm}^{-1}$). Electrical conductivity of the PTh/GR composites was found to be higher ($7.4 \times 10^{-3} \text{ S cm}^{-1}$ for PTGR3 composite) than that of pure PTh ($5.8 \times 10^{-5} \text{ S cm}^{-1}$). Both the composites showed reversible electrochemical response and a good cycling stability even up to 100th cycles. A charging-discharging study also revealed a high capacitance value (260 F g^{-1}) for the PPy/GR composite and 210 F/g for PTh/GR composites at 3 wt.% of GR loading. This work show that the GO/GR based PPy and PTh composites prepared using the interfacial polymerization method possess great promise for a range of potential applications in batteries and optoelectronic devices. Also this work suggests that GR based PPy composites have superior thermal stability, electrical and electrochemical properties than that of GO based composites.

GR and GO based PE resin composites with high thermal stability and mechanical strength was also prepared. Around 123% increase of tensile strength and 87% increase in Young's modulus are obtained with 3 wt.% of GR loading. The PE/GR composite film was found to possess a higher value of conductivity ($3.7 \times 10^{-4} \text{ S cm}^{-1}$) compared to pure resin. The PE/GR composites imply proficient antibacterial activity towards the five different kinds of

bacterial strains. These mechanically strong and ductile PE/GO and PE/GR composite films exhibit good potential in industrial applications. GR based PE resin composites with improved antibacterial activity could offer new opportunities for the development of a new range of environmental friendly and high strength structural material.

Also we have demonstrated the fabrication of a glucose biosensor based on PPy/GR nanocomposites. This biosensor showed a high value of sensitivity ($29.6 \mu\text{M}/\text{cm}^2.\text{mM}$) and lower limit of detection ($0.1 \mu\text{M}$) compared to other GR and CNT based biosensor. The biosensor is able to detect glucose with high sensitivity and fast response. It also showed reasonable stability which is crucial for practical application of biosensors. This method may be used for the fabrication of other biosensors. In another work sulfonated graphene (SG) based PPy composite was used as electrode material for supercapacitor. The composite showed higher electrical conductivity and superior electrochemical reversibility compared to PPy. Charging-discharging study revealed a high specific capacitance value (360 F g^{-1}) of PPy/SG composite at a current density of 1 A g^{-1} . Furthermore, the composite exhibited a good electrochemical stability. Thus this method opens a new way to fabricate other SG based nanocomposites for energy storage applications.

Enclosure II

Final report on

Graphene/graphene oxide based polymer nanocomposites and
their applications as biosensor and supercapacitor.

Sponsored by

COUNCIL OF SCIENTIFIC AND INDUSTRIAL RESEARCH

CSIR Scheme No.: 02(0066)/12/EMR-II

1. Introduction:

Polymer nanocomposites show substantial property enhancements at much lower loadings than polymer composites with conventional micron-scale fillers which ultimately results in lower component weight and can simplify processing. Moreover, the multifunctional property enhancements made possible with nanocomposites may create new applications of polymers. Majority of research has focused on polymer nanocomposites based on layered materials of a natural origin like montmorillonite type of layered silicate compounds or synthetic clay (layered double hydroxide). But the electrical and thermal conductivity of clay minerals are quite poor. In order to overcome these shortcomings, carbon-based nanofillers, such as carbon black, EG, CNT, have been introduced to the preparation of polymer nanocomposites. Among these, CNTs have proven to be very effective as conductive fillers. But one drawback of CNTs is that their production cost is very high. To overcome these difficulties nanofillers like graphene and graphene oxide have been introduced which show superior properties than the conventional fillers. [1-2]

Polymer/graphene nanocomposites show superior mechanical, thermal, gas barrier, electrical and flame retardant properties compared to the neat polymer. It was also reported that the improvement in mechanical and electrical properties of graphene based polymer nanocomposites are much better in comparison to that of clay or other carbon filler-based polymer nanocomposites. However, the improvement in the physicochemical properties of the nanocomposites depends on the distribution of graphene layers in the polymer matrix as well as interfacial bonding between the graphene layers and polymer matrix. Interfacial bonding between graphene and the host polymer influences the final properties of the graphene reinforced polymer nanocomposite. [3]

What is graphene?

Graphene has become one of the most exciting topics of research due to its extraordinarily high electrical and thermal conductivities, great mechanical strength and low cost. Particularly composites of graphene and polymers have attracted increasing attention because of their enhanced properties such as their high conductivity. The discovery of graphene

with its combination of extraordinary physical properties and ability to be dispersed in various polymer matrices has created a new class of polymer nanocomposites. Graphene is a one atom thick planar sheet of sp^2 -bonded carbon atoms that are densely packed in a honeycomb crystal lattice. It is the basic building block of some carbon allotropes.^[4]

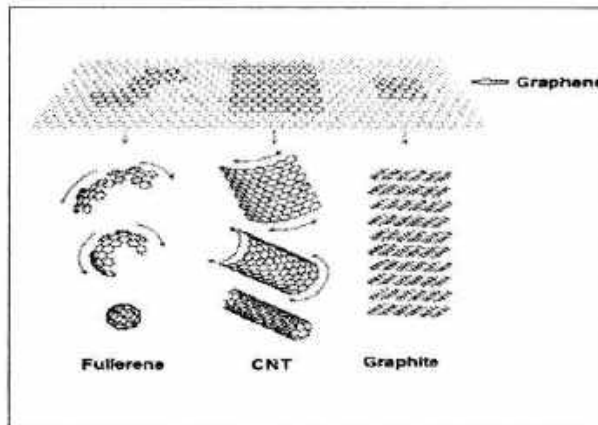


Fig.1. Different carbon allotropes

The Nobel Prize in Physics for 2010 was awarded to Andre Geim and Konstantin Novoselov "for groundbreaking experiments regarding the two-dimensional material graphene. The modification of graphene/graphene oxide and the utilization of these materials in the fabrication of nanocomposites with different polymer matrixes have been explored. Graphene, as a nanofiller, may be preferred over other conventional nanofillers (Na-MMT, LDH, CNT, CNF, EG, etc.) due to high aspect ratio, tensile strength (TS), thermal conductivity and electrical conductivity, flexibility etc.

What is Graphene oxide?

Graphene oxide consists of a two dimensional (2D) sheet of covalently bonded carbon atoms bearing various oxygen functional groups (e.g. hydroxyl, epoxide and carbonyl groups) on their basal planes and edges. Although single GO sheet has been predicted to have strong mechanical strength (fracture stress = about 63Gpa) by Monte Carlo simulations, up to date, few work concerned the use of GO as effective mechanical reinforcement nanofillers for polymer

composite. Unlike graphene, graphene oxide is electrically insulating, which makes it unsuitable for the synthesis of conducting nanocomposites. [5,6]

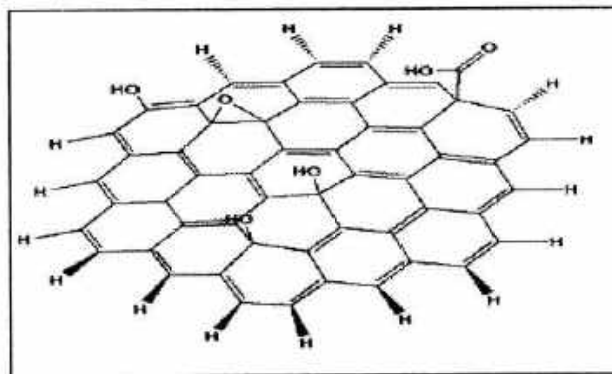


Fig. 2 Structure of graphene oxide.

Tung *et al* [7] prepared polymer nanocomposites based on polyaniline (PANI) and graphene nanosheets (GNS) modified with poly(sodium-4-styrenesulfonate) (PSS-GNS). The composite was found to have more electrical conductivity than that of pure PANI. The TGA results showed that thermal stability of the PANI was also improved significantly to approximately 100°C in the nanocomposite. Hao *et al* [8] synthesised sulfonated graphene/polyaniline (SGEP) nanocomposite by liquid/liquid interfacial polymerization method. Sulfonated graphene (SGE) sheets were used as both a macromolecular acid dopant and substrate for the polymerization of polyaniline (PANI). Nanocomposite SGEP-1 with PANI nanorods randomly attached to the surface of SGE was shown to have an excellent electrochemical performance with a highest specific capacity of 763 F/g, and capacitance retention of 96% after 100 cycles and 85% after 1000 cycles. The electrochemical measurements show the high potential of SGEP composites for use in energy storage and conversion devices, as well as other fields. Zhao *et al* [9] reported that the graphene based poly(vinyl alcohol) was successfully prepared by incorporating graphene oxide into PVA matrix and reducing graphene oxide into graphene. The composite films showed good uniformity and dispersion and exhibited a significant improvement in mechanical properties. Around 150% improvement of tensile strength and a nearly 10 times increase of Young's modulus are achieved at a graphene loading of 1.8 vol %. Xu *et al*. [10] prepared mechanically strong poly(vinyl alcohol)/graphene oxide composite film by

vacuum filtration. The Young's modulus and tensile strength of the composite film with 3 wt% GO was found to be 4.8 GPa and $110 \pm$ MPa, respectively which was higher than that of pure polymer. Vadukumpully *et al* ^[11] synthesized ultrathin composite films of graphene nanoflakes and poly(vinyl chloride) by a simple solution blending, drop casting. The composite films showed 58% increase in Young's modulus and an almost 130% improvement of tensile strength. The films were found to possess high electrical conductivity (0.058 S/cm at 6.47 vol.% of the graphene loading) with a low percolation threshold of 0.6 vol.%. Eda *et al.*^[12] prepared PS/FGS composite thin films using a solution blending method. The composite thin films were semi-conducting in nature and exhibited an ambipolar field effect. The composite thin films were electrically conducting with a conductivity ranging from 1 to 24 Sm⁻¹, which is good in agreement with the values reported for bulk composites by Stankovich S *et al.* ^[13].The conductivity of the thin films decreased with decreasing temperature to approximately 50K and increased slightly with further decreases in temperature.

DETAILS OF THE WORK DONE

2. Preparation of polypyrrole/graphene composites and evaluation of their optical electrical and electrochemical properties

2.1. Experimental section

2.1.1 Materials. Pyrrole (Merck), Sodium nitrate (Merck), sulfuric acid (Merck), potassium permanganate (Merck), hydrogen peroxide (Qualigens Fine Chemicals), ferric chloride (Aldrich), chloroform (Merck), acetonitrile (Merck) are commercial products and were used as received. For all purposes double-distilled water was used.

2.1.2. Preparation of GR.

Graphite oxide dispersion was prepared using a modified Hummers method²⁴ using KMnO_4 and H_2SO_4 as oxidizing agent. For purification, the mixture was washed with 5% of HCl and then DI H_2O for several times. The powdered graphite oxide filtered and dried under vacuum at $65\text{ }^\circ\text{C}$. To prepare GR, 0.1 g of graphite oxide was dispersed in 50 mL of DI water. Then 1 mL of hydrazine monohydrate was added to it and heated at $95\text{ }^\circ\text{C}$ for 12 h. After that the mixture was filtered was washed with DI water several times.

2.1.3. Preparation of PPy/GR composites.

PPy/GR composites were prepared by liquid/liquid interfacial polymerization involving pyrrole and GR. Required amount of GR and $\text{FeCl}_3 \cdot 6\text{H}_2\text{O}$ were dispersed in 15 ml of H_2O . Pyrrole (0.08 mL) was dissolved in 15 ml chloroform in beaker and was kept for 24 h. Both are mixed and a black film appeared on the interface between the two phases. Finally, the product was filtered and washed several times with water and air dried. Composites containing 1, 2 and 3 wt % of GR were prepared and named as GRPPy1, GRPPy2 and GRPPy3.

2.2.Characterization:

Fourier transform infrared (FTIR) spectra were recorded at room temperature, over a frequency range of 4000-500 cm^{-1} , using a Nicolet spectrometer. Raman spectra were recorded using a Nanofinder 30 confocal Raman with He-Ne laser. The X-ray diffraction (XRD) study was carried out at room temperature using a Rigaku X-ray diffractometer with Cu-K α radiation using a scanning rate of 0.05 θ /s in the range of $2\theta = (10^\circ\text{-}70^\circ)$. Scanning electron micrographs (SEM) were taken out on a JSM-6390LV. Transmission electron microscope (TEM) measurements were taken out on a PHILIPS CM 200 microscope. Thermogravimetric analysis (TGA) was performed using, Simadzu thermogravimetric analyser, Japan from temperature range 298 to 973K under the nitrogen flow. The DC electrical conductivity of PPy and PPY/GR composites was measured using four probe techniques. The electrochemical behavior of the prepared samples was studied using Sycopl AEW2-10 cyclic voltammeter. The electrochemical behavior of the prepared samples was studied using Sycopal AE2-10 cyclic voltammeter.

2.4. Results and discussion

2.4.1 FTIR analysis.

FTIR analyses of pure PPy, GO, GR and PPY/GR composites are shown in Figure 1. In the FTIR spectrum of GO the broad peak at 3409 cm^{-1} and a peak at 1719 cm^{-1} can be assigned to O-H stretching vibration and the carbonyl (C=O) stretching respectively. The peaks at 1370 and 1250 cm^{-1} represent the C-O-C and C-OH stretching vibration. Upon reduction of GO, the peaks at 1370, 1250 and 1060 cm^{-1} disappears which indicates the removal of epoxide and the hydroxyl groups. In the FTIR spectrum of PPY/GR composite we have observed peaks for both PPy and GR. This indicates that GR have been successfully incorporated in the polymer matrix in the composite.

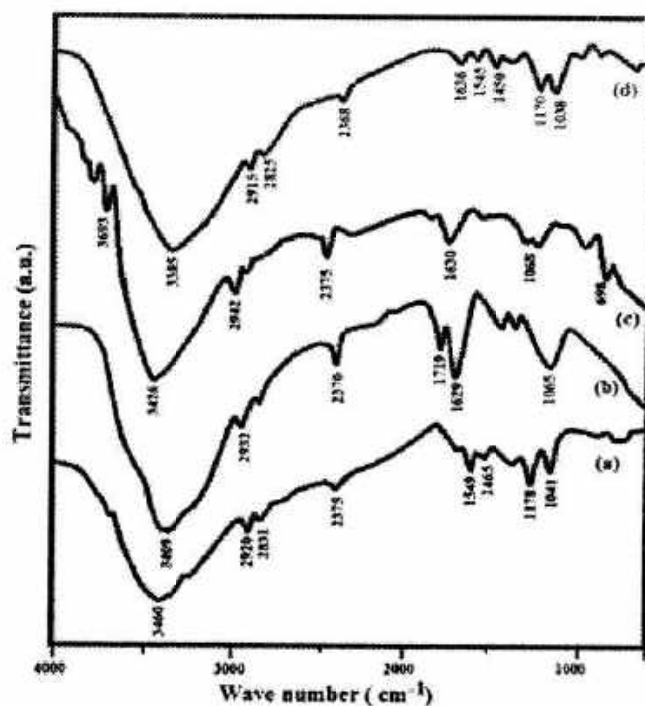


Fig. 1. FTIR spectroscopic analysis of (a) pure PPy, (b) GO, (c) GR and (d) PPy/GR composites.

2.4.2. Raman analysis.

The Raman spectra of PPy/GR pure GR are shown in Figure 2. In the Raman spectra of pure GR, D and G bands which appear at about 1340 cm^{-1} and 1585 cm^{-1} respectively. The D band is attributed to the K-point phonons of A_{1g} symmetry, and the G band corresponding to ordered sp^2 -bonded carbon atoms. The intensity ratio (I_D/I_G) is found to be 1.17 for pure GR due to the presence of unrepaired defects that remained after the removal of functional groups. The peak intensity ratio, I_D/I_G of the composites was 1.14. This indicates the presence of defects within the sp^2 carbon network.

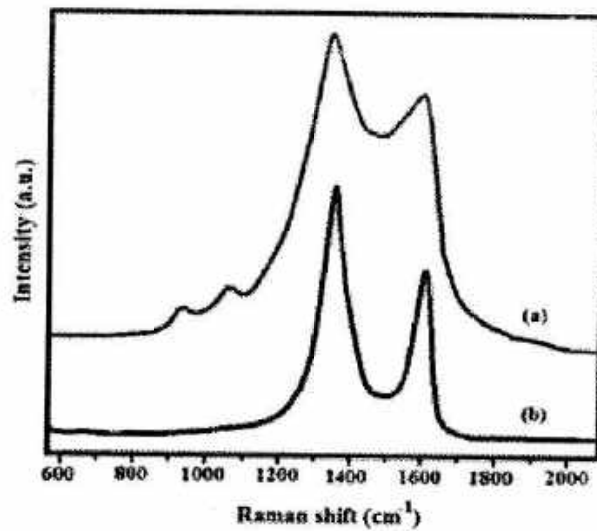


Fig. 2. Raman spectra of (a) PPy/GR composite and (b) GR.

2.4.3. XRD analysis.

The XRD patterns of PPy/GR composite and pure PPy are shown in Figure 3. Pure GR shows a broad reflection peak centered at $2\theta = 24.5^\circ$ and 43° . Pure PPy exhibit a characteristic peak at $2\theta = 26^\circ$. The XRD data of PPy/GR composite is almost similar to that of pure PPy, however, the shifting of peak reveals the full interaction between PPy and GR.

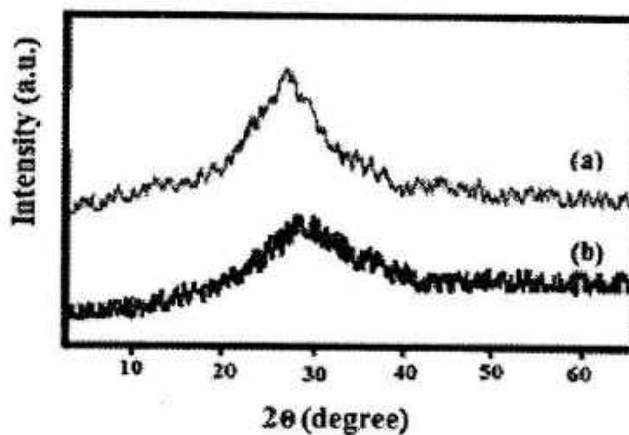


Fig. 3. XRD patterns of (a) PPy/GR composite and (b) Pure PPy.

2.4.4. Morphology and Structure.

The structure of the PPy, GR and PPy/GR composites were investigated using scanning electron microscope (SEM) and transmission electron microscope (TEM). In the SEM and TEM images of GR a layered structure is observed. PPy showed a sphere-like structure (Figure 4c). In case of PPy/GR composite, this sphere like structure of PPy disappears and a rough structure is observed due to the polymerization of PPy on the surface of GR sheets.

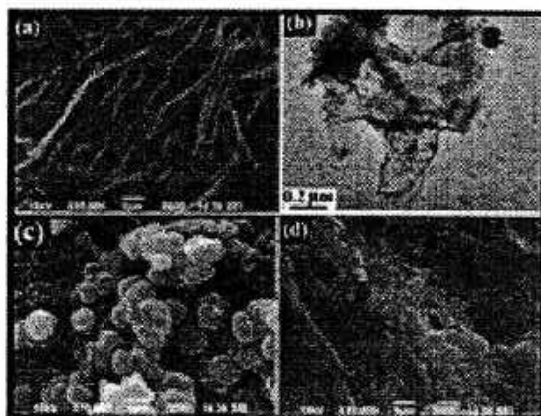


Fig. 4. (a) SEM images of GR, (b) TEM images of GR, (c) SEM image of PPy and (d) PPy/GR composite.

2.4.5. Thermal Gravimetric Analysis.

The TGA curves of pure PPy, GR and PPy/GR composites are shown in Figure 5. GR exhibited around 20% weight loss at the temperature range of 250 to 500 °C, due to the removal of most of the oxygen-containing functional groups during reduction. Pure PPy displays a major weight loss in the temperature scale of 250 to 500 °C corresponds to the complete degradation of the polymer. In case of the composites, the major decomposition starts at higher temperatures compared to pure PPy indicating better thermal stability of the composites. The major weight loss in the temperature range of 250 to 500 °C is due to the decomposition of the PPy and functional groups of GR from the composite.

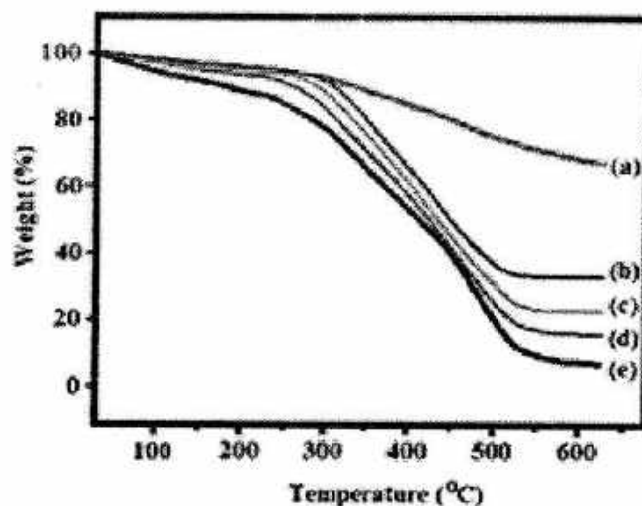


Fig. 5. TGA curves of (a) GR, (b) PPyGR1, (c) PPyGR2, (d) PPyGR3 composite and (e) PPy.

2.4.6. Measurements of electrical conductivity.

The electrical conductivities of pure PPy and PPy/GR composites are determined using a fourpoint probe resistivity measurement system. Pure PPy shows a conductivity of 0.210 S/cm. For GRPPy1, GRPPy2 and GRPPy3, the conductivities are 2.51, 4.52 and 8.45 S/cm respectively. Increase in magnitude of conductivity as compared to pure PPy is due to the incorporation of highly conducting GR sheets.

2.4.7 Electrochemical Properties.

Cyclic voltammogram (CV) of PPy and PPy/GR composites in 0.1M LiClO₄ - acetonitrile solution solution at 50 mV/s are shown in Figure 6. CVs of PPy/GR composites have large rectangular areas, indicating higher capacitances and better charge propagation within the electrode compared to PPy. However, CV of GR exhibits a much smaller rectangular area, perhaps due to its compact. For PPy/GR composites the redox waves became wider. This is possibly due to the increased conductivity of the composite on introduction of GR.

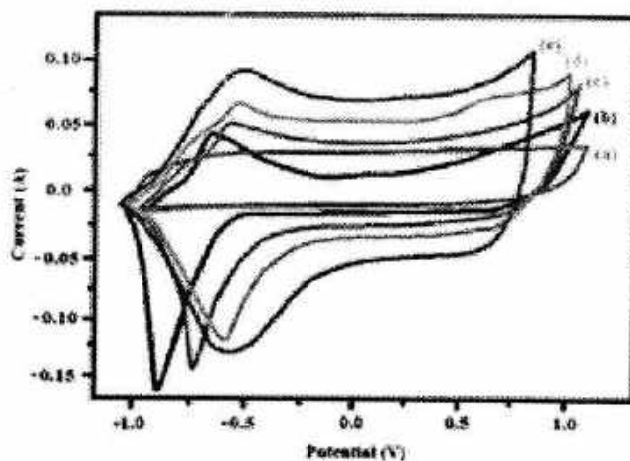


Fig. 6. Cyclic voltammogram of (a) GR, (b) PPy, (c) PPyGR1, (d) PPyGR2, and (e) PPyGR3 composites at a scan rate of 50 mV/s.

The composite was exposed to cyclic oxidation and reduction upto 100th cycles (Figure 7). There was no significant change in redox potentials and the composite was quite stable even upto 100th repeated cycles indicating a good cycling stability.

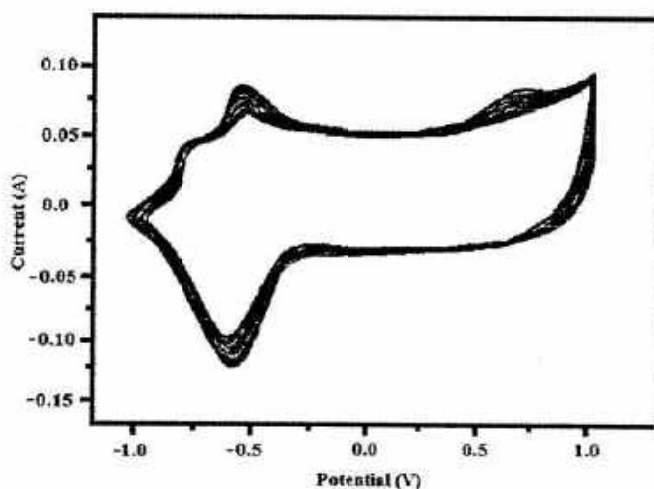


Fig. 7. Successive electrochemical cycles of the PPy/GR (3%) composite up to 100th cycles.

2.5. Conclusion

PPy/GR composite with improved properties was successfully prepared by liquid/liquid interfacial polymerization. Both XRD study and FTIR spectroscopic analysis indicate successful formation of the composite. TEM and SEM study showed uniform distribution of GR in the PPy matrix. The PPy/GR composites exhibited a high value of conductivity on incorporation of

highly conducting GR nanosheets within the polymer matrix. The composite shows good cycling stability even upto 100th cycles. Thus, the liquid/liquid interfacial polymerization has been found to be an effective method to prepare PPy/GR composites with great application potential.

3. Fabrication of glucose biosensor based on polypyrrole/graphene composite

3.1 Experimental

3.1.1 Chemicals

Glucose oxidase (Type X-S, *Aspergillus niger* (EC 1.1.3.4)), d-glucose, phosphate buffer saline, Nafion (5 wt% in lower aliphatic alcohol and water mixture), 2-propanol, H₂O₂ were obtained from Sigma-Aldrich and used as received. All solutions used in the experiments were prepared with ultra-pure water. Pyrrole monomer was purchased from Sigma Aldrich and was used as received. Sodium nitrate (Merck), sulfuric acid (Merck), potassium permanganate (Merck), ferric chloride (Aldrich), hydrazine monohydrate (Aldrich) and Lithium perchlorate (Fluka) are commercial products and were used as received.

3.1.2. Preparation of PPy/GR/Nafion Composite Film

PPy/GR composites were prepared by liquid/liquid interfacial polymerization involving pyrrole and GR as described in the previous section. Then PPy/GR nanocomposites were mixed with of 0.5 wt% Nafion–isopropyl-alcohol solution (1mg/ml) by ultrasonication for 30 mins. Then the PPy/GR/Nafion paste was drop cast on the GCE. The solvent was allowed to evaporate at room temperature.

3.2. Instrumentation

Cyclic voltammetric and amperometric measurements were performed on an electrochemical analyzer (CHI Instruments, Inc., Austin, TX). Measurements were performed with a standard one compartment three electrode configuration cell with a modified GCE as the working electrode, platinum as the counter electrode and an Ag/AgCl as the reference electrode. The cyclic voltammograms (CVs) of the PPy/GR/Nafion composite film were obtained in 5 mM K₄Fe(CN)₆ and 0.1 M KCl solution. An amperometric response of the

GOD/PPy/GR/Nafion/GCE to the sequential addition of a desired amount of glucose with continuous gentle stirring in a 50 mM phosphate buffer solution (pH 7.4). All TEM measurements were carried out on a JEOL JEM-2100 transmission electron microscope at an accelerating voltage of 200 kV.

3.3. Results and discussion

PPy/GR composites were prepared by interfacial polymerization. The prepared composite was then dispersed in a 0.5 wt% Nafion–isopropyl-alcohol solution and cast on a glassy-carbon electrode (GCE). Then glucose oxidase (GOD) was immobilized on PPy/GR/Nafion/GCE, forming a bionanocomposite film.

Electrochemical study of the biosensor electrode. Cyclic voltammetry is a useful technique to evaluate electrochemical performance of PPy/GR/Nafion/GCE. Fig. 1 shows the cyclic voltammograms of PPy/GR composite at the different GR loading recorded in an electrolyte solution containing 0.1 M KCl. The electrochemical responses obtained at the PPy/GR/Nafion/GCE are much larger than that obtained at the Nafion/GCE. The Nafion/GCE shows no redox peaks. CVs of PPy/GR/Nafion/GCE have large rectangular areas, indicating higher double-layer capacitances within the electrode.

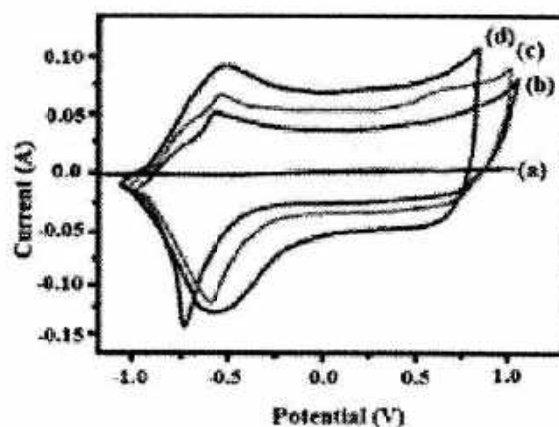


Fig. 1. Cyclic voltammetric response for (a) Nafion and PPy/GR/Nafion composite with (b) 1 wt%, (c) 2 wt%, (d) 3 wt% of GR loading at scan rate, 100 mV/s

Fig. 2 shows the cyclic voltammograms of PPY/GR/Nafion/GCE in a 50 mM phosphate buffer solution containing 2mM H₂O₂ in comparison to nafion modified GCE. The electrochemical response obtained at the PPY/GR/Nafion/GCE is much larger than Nafion modified electrode. PPY/GR/Nafion modified electrode showed significant oxidation and reduction currents. The higher electrochemical response in case of PPY/GR/Nafion modified electrode indicates that PPY/GR composites catalyze the oxidation- reduction of H₂O₂. The decrease of the overpotential of H₂O₂ can be attributed to the increase in electrical conductivity of the composite system.

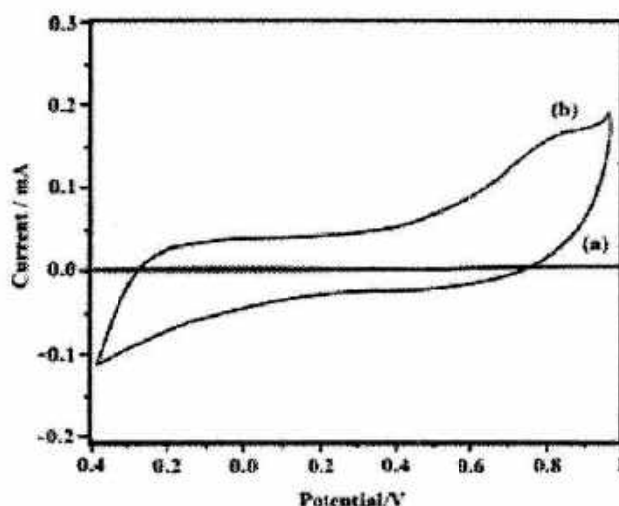


Fig. 2. Cyclic voltammograms obtained at (a) bare GCE; (b) PPY/GR/Nafion/GCE; in 50 mM PBS buffer.

Amperometric Measurement. The amperometric responses of PPY/GR/GOD/Nafion biosensor are compared to GOD/Nafion at successive additions of various amounts of glucose at an applied potential of +0.9 V which are shown in Fig. 4. The GOD/Nafion biosensor gives much weaker current response than PPY/GR/GOD/Nafion biosensor. The electrochemical response increased in proportion with the increase in the glucose concentration. It can be seen that the sensor is responsive to a low concentration of glucose, such as 6 μ M glucose. The sensitivity of PPY/GR based glucose biosensor is calculated and it was found to be 19 μ A/(mM.cm²) at a glucose oxidase concentration of 3 mg/mL.

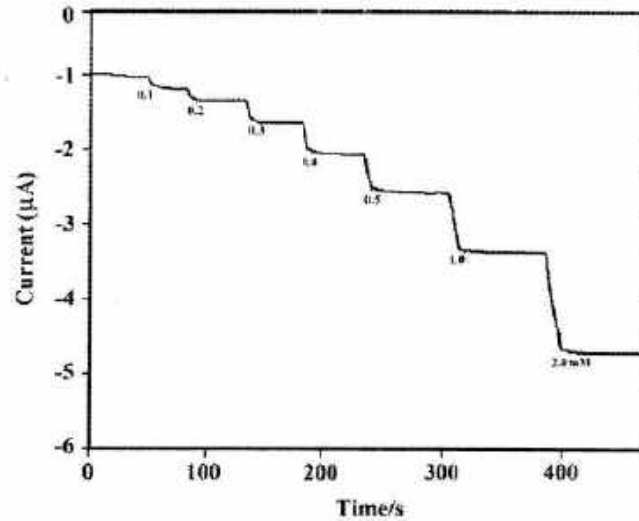


Fig. 3. Amperometric response of PPy/GR/GOD/Nafion glucose biosensor (glucose oxidase, 3 mg/mL) at an applied potential of +0.9 V to successive addition of varied amount of glucose in a stirred 50mM, PH 7.4, phosphate buffer solution.

3.4. Conclusion

In this work, we have demonstrated the fabrication of a glucose biosensor based on PPy/GR nanocomposites prepared by interfacial polymerization. The PPy/GR/Nafion/GOD film modified glassy carbon electrode is found to be active for the electro-oxidation of hydrogen peroxide. This PPy/GR based biosensor showed a superior value of sensitivity ($19\mu\text{M}/\text{cm}^2.\text{mM}$) compared to other carbon nanotube based biosensor. The biosensor is able to detect glucose as substrate with high sensitivity and fast response.

4. Polypyrrole/Sulfonated Graphene Composite as Electrode Material for Supercapacitor

4.1. Experimental

4.1.1. Chemicals. All the chemicals such as graphite, pyrrole, sulfuric acid, potassium permanganate sodium nitrate, ferric chloride, hydrogen peroxide, hydrazine monohydrate and chlorosulfonic acid were purchased from Sigma Aldrich and was used as received.

4.2.2. Preparation of sulfonated graphene (SG). 6 mg of GR was suspended in 30 ml of dichloromethane. To this 10 ml of chlorosulfonic acid was added dropwise and the reaction mixture was stirred at room temperature (25 °C) for 1 h. The reaction was stopped by neutralisation with 20 wt.% NaOH. The obtained precipitate was filtered and purified by washing with DI water and then dried at 80 °C.

4.2.3. Preparation of PPy/SG composite. The PPy/SG composites were synthesized using interfacial polymerization as follows as described in the previous sections. final product was filtered and washed with DI water and then dried at room temperature (25 °C). Different compositions of the composites were prepared with 1, 2 and 3 wt.% of SG loading and termed as PPySG1, PPySG2 and PPySG3, respectively.

4.2.4. Preparation of Supercapacitor Electrodes. About 5 mg of the PPy/SG composite was mixed with 5 wt.% Nafion solution and coated over a stainless steel net. Then it was dried at 100 °C for 10 h and was used as a working electrode. The supercapacitor setup was designed by placing a separator immersed in 1 M H₂SO₄ electrolyte solution in between two electrodes and then pressed tightly.

4.3. Characterization Techniques. Fourier transform infrared (FTIR) spectra were analysed with a Nicolet spectrometer, in a frequency range of 4000-500 cm⁻¹. Scanning electron microscope (SEM) analysis was taken out using a JEOL JSM-6390LV.

Electrochemical Analysis. Cyclic voltammetry (CV) of the electrode was studied with a Sycopel AEW2-10 cyclic voltammeter. The analysis was performed in a three electrode cell where the composite, platinum and Ag/AgCl electrodes were used as a working, counter and

reference electrode, respectively. The galvanostatic charge–discharge test was performed on an Autolab PGSTAT302N with the current density range between 0.5 to 5 A g⁻¹. For both the tests, 1 M H₂SO₄ solution was used as an electrolyte. Specific capacitance (C_s) was measured from the charge-discharge method by the following equation¹⁶

$$C_s = (I \times \Delta t) / (m \times \Delta V) \quad (3)$$

where I is the discharge current, Δt is the discharge time, ΔV is the voltage drop and m is the weight of active material (5 mg) per electrode.

4.4. Results and Discussion:

4.4.1. FTIR Analysis. Figure 1 represents the FTIR spectra of SG, PPy and PPy/SG composite. The FTIR spectrum of SG shows peaks at 1112 cm⁻¹ and 1196 cm⁻¹ (two νS-O) indicates that sulfonic acid group is present in SG. PPy shows peaks at 3460 and 1549 cm⁻¹ due to the N-H and C-N stretching vibration of pyrrole. FTIR spectrum of the composite, shows peaks associated with both PPy and SG. The shifting of the and also lowering in the peak intensity for the composite compared to pure PPy indicates successful incorporation of SG in PPy matrix.

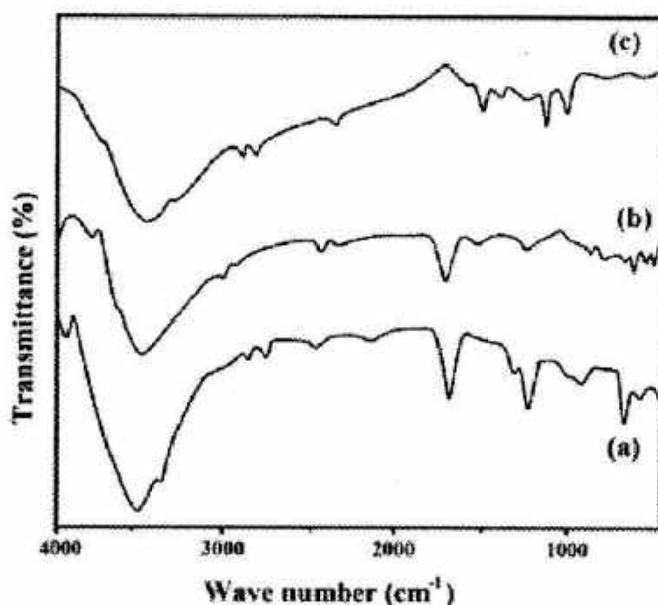


Figure 1. FTIR spectra for (a) SG, (b) PPySG3 composite and (c) PPy.

4.4.2. Morphological Studies. Pure PPy displays a regular, sphere-like structure (Figure 2a) whereas, a rough structure appears in the PPySG3 composites (Figure 2b). This morphological change in the composites results from the polymerization of PPy on the SG surface.

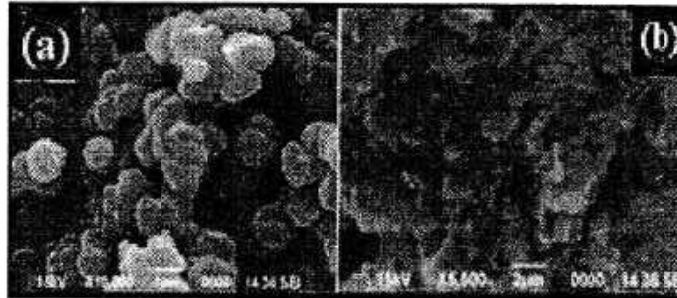


Figure 2. SEM images of (a) PPy and (b) PPySG3 composite.

4.4.3. Electrochemical Properties.

Cyclic Voltammetry (CV) Studies. Figure 3 illustrates the CV of SG, PPy and PPy/SG composite electrode with a voltage range from -0.4 to 0.8 V. CV curve of PPy exhibits peaks for reduction and oxidation at around -0.35 V and +4.6 V respectively. The CV curve of PPySG3 composite shows nearly rectangular shape with a larger area, indicating ideal capacitive nature and better charge transport than that of PPy due to the presence of highly conducting SG.

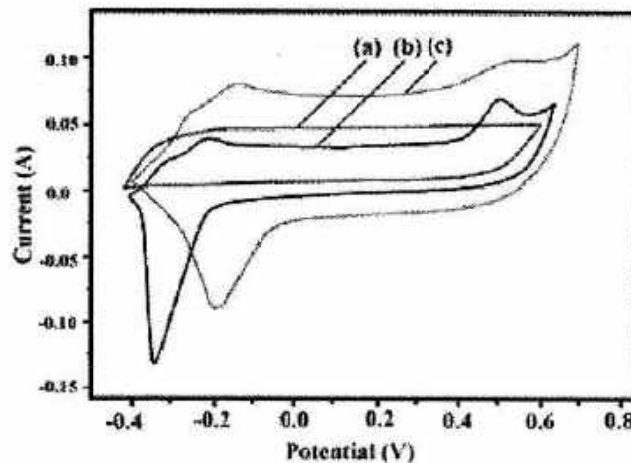


Figure 3. CV curves of (a) SG, (b) PPy, (c) PPySG3 composite.

Galvanostatic Charge-Discharge Study. Galvanostatic charge/discharge curves of PPy, SG and PPy/SG composite are demonstrated in Figure 4 with a potential range between -0.4 to 0.8 V. Composite showed a longer discharge time compared to pure PPy at the same current density. Table 1 summarizes the specific capacitances (C_s) of the samples that are calculated from the charge-discharge curves.

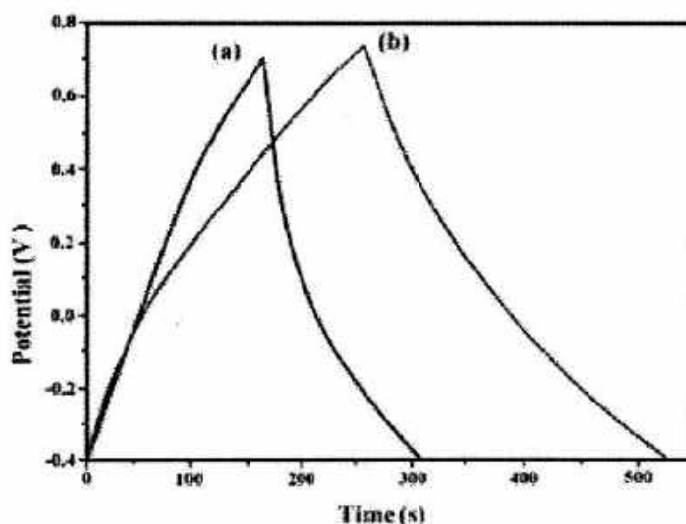


Figure 4. Charge/discharge curves of (a) PPy and (b) PPySG3 .

Table 1. Specific Capacitance of PPy, SG and PPy/SG Composite

Sample	specific capacitance ($F g^{-1}$) (galvanostatic)
PPy	155
PPySG3	360

A higher value of specific capacitance of $360 F g^{-1}$ is observed for PPy/SG (3 wt.%) composite compared to PPy and SG under the same current density (Table 1). This is due to the fact that highly conductive SG sheets favors redox process and thus increases its capacitance.

4.5. Conclusions.

PPy/SG composite was synthesized via interfacial polymerization and was found to be promising for supercapacitor electrode. The composite showed higher electrical conductivity and superior electrochemical reversibility compared to PPy. Charging-discharging study revealed a

high specific capacitance value (360 F g^{-1}) of PPySG3 composite at a current density of 1 A g^{-1} . This simple method opens a new way to fabricate other GR based nanocomposites for supercapacitor applications.

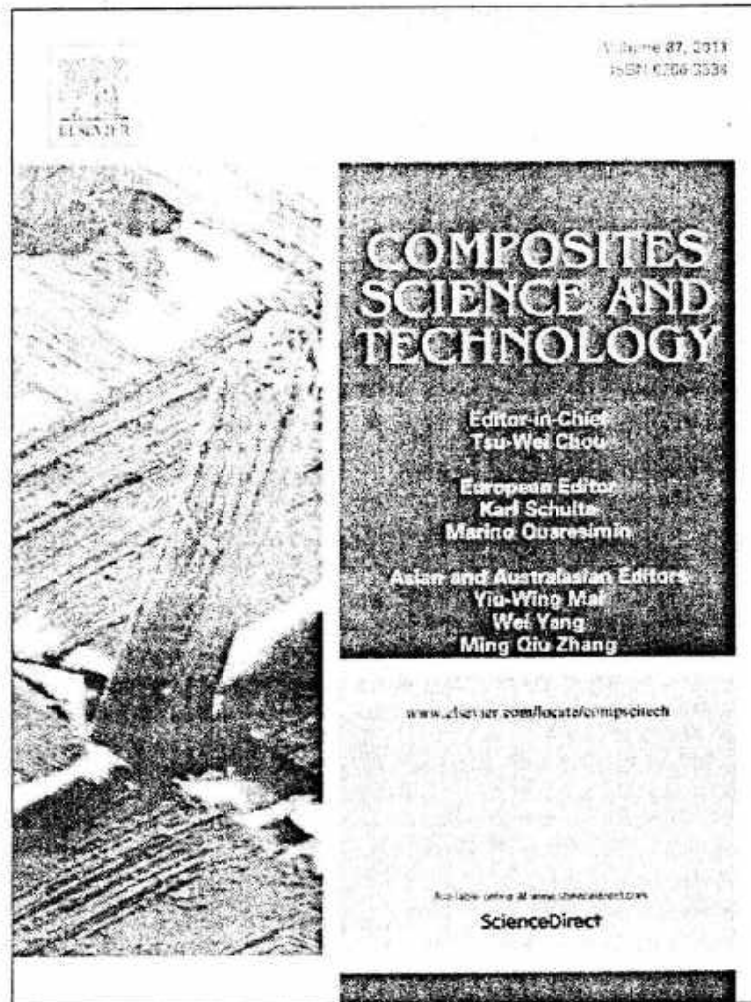
5. SUMMARY OF THE WORK

- GR based PPy composites have been successfully prepared by liquid/liquid interfacial polymerization.
- The PPy/GR composites exhibited a higher value of conductivity compared to pure polypyrrole.
- The composites showed good cycling stability even up to 100th cycles.
- With this PPy/GR composite we have demonstrated the fabrication of a glucose biosensor. The PPy/GR/Nafion/GOD film modified GCE is found to be active for the electro-oxidation of hydrogen peroxide.
- This PPy/GR based biosensor showed a high value of sensitivity ($29.6 \mu\text{M}/\text{cm}^2 \cdot \text{mM}$) and lower limit of detection ($0.1 \mu\text{M}$) compared to other GR and CNT based biosensor.
- PPy/SG composite was synthesized via interfacial polymerization and was found to be a promising candidate for supercapacitor electrode.
- The composite showed higher electrical conductivity and electrochemical reversibility compared to pure polypyrrole.
- Charging-discharging study revealed a high specific capacitance value (360 F g^{-1}) of PPySG3 composite at a current density of 1 A g^{-1} .

References:

1. Rao, C.N.R., Sood, A. K., Subrahmanyam, K. S., Govindaraj, A. *Angew. Chem. Eng.* **4**, 7752–7777, 2009.
2. Kuilla, T., et al. *Prog. Polym. Sci.* **35**, 1356–1375, 2010.
3. Kim, H., Abdala, A.A., Macosko, C.W. *Prog. Polym. Sci.* **43**, 6515–6530 2010.
4. Allen, M.J, Tung, C.V., Kaner, R.B. *Chem. Rev.* **10**, 132–145, 2010.
5. Potts, J.R., Dreyer, D.R., Bielawski, C.W. Ruoff, R.S. *Chem. Rev.* **52**, 5-25, 2011.

6. Kotov, N.A. Carbon sheet solutions, *Nature* **442**, 254–255, 2006.
7. Tung, N.T., et al. *Macromol. Res.* **19**, 203-208, 2011.
8. Hao, Q., Wang, H., Yang, X., Lu, L. *Nano Res.* **4**, 323-333, 2011.
9. Zhao, X., Zhang, Q., Chen, D. *Macromolecules* **43**, 2357–2363, 2010.
10. Xu, Y., et al. *Carbon* **47**, 3538-3543, 2009.
11. Vadukumpully, S., et al. *Carbon* **49**, 198-205, 2011.
12. Eda, G., & Chhowalla, M. *Nano Lett.* **9**, 814–818, 2009.
13. Stankovich, S., et al. *Nature* **442**, 282–286, 2006.



This article appeared in a journal published by Elsevier. The attached copy is furnished to the author for internal non-commercial research and education use, including for instruction at the authors institution and sharing with colleagues.

Other uses, including reproduction and distribution, or selling or licensing copies, or posting to personal, institutional or third party websites are prohibited.

In most cases authors are permitted to post their version of the article (e.g. in Word or Tex form) to their personal website or institutional repository. Authors requiring further information regarding Elsevier's archiving and manuscript policies are encouraged to visit:

<http://www.elsevier.com/authorsrights>



Strong and conductive reduced graphene oxide/polyester resin composite films with improved mechanical strength, thermal stability and its antibacterial activity

Chandramika Bora^a, Pranjal Bharali^b, Silpi Baglari^a, Swapan K. Dolui^{a,*}, Bolin K. Konwar^b

^a Department of Chemical Sciences, Tezpur University, Napaam, Tezpur, Assam 784028, India

^b Department of Molecular Biology and Biotechnology, Tezpur University, Napaam, Assam, India

ARTICLE INFO

Article history:

Received 8 April 2013

Received in revised form 20 July 2013

Accepted 22 July 2013

Available online 6 August 2013

Keywords:

A. Nanocomposites

A. Polymers

A. Nanomaterial

B. Mechanical properties

B. Thermal properties

ABSTRACT

In this work, we report a simple method of preparation of reduced graphene oxide (rGO) based unsaturated polyester (PE) resin nanocomposite. The synthesized samples were characterized by Fourier transform infrared spectroscopy (FTIR), X-ray diffraction (XRD), scanning electron microscopy (SEM), atomic force microscopy (AFM), thermogravimetric analysis (TGA), differential scanning calorimetry (DSC) and tensile strength measurements. The SEM analyses revealed good dispersion as well as the interaction of rGO with the matrix. The composite exhibited significant improvement in mechanical properties at a low rGO loading. The tensile strength and Young's modulus of the composites increased by 123% and 87% respectively at 3 wt.% loading of the rGO. The thermal property of the PE resin was also improved with the incorporation of rGO in the composite. Moreover, the composite film showed a higher value of electrical conductivity (3.7×10^{-4} S/cm) compared to that of neat resin. The PE/rGO nanocomposites displayed good antimicrobial activity against a number of bacteria.

© 2013 Elsevier Ltd. All rights reserved.

1. Introduction

Polymer nanocomposites have attracted considerable interest in the last decades owing to their enhanced properties arising from the reinforcement of nanofillers [1,2]. The dispersion of the nanofillers within the polymer matrix has significant influence on the properties of the composites compared to conventional micron scale fillers [3]. Recently, graphene, a one-atom-thick planar sheet of sp^2 -bonded carbon atoms is considered as promising versatile nanofiller due to its extraordinarily high electrical and thermal conductivities, great mechanical strength and low manufacturing cost. Graphene based nanocomposites have attracted enormous interest due to its wide variety of applications in the areas of materials science and engineering [4–6].

PE resin is one of the most widely used polymers due to its excellent processability, good dimensional stability, low moisture absorption, good chemical resistance and low-cost. It has found applications in many industrial areas such as coating, automotive, transportation, storage tanks and piping [7,8]. Glass fiber reinforced polyester resin has been utilized for decades in many applications including automotive and construction due to their good cost/property relation. However, mechanical strength and thermal stability of polyester resin is low compared to other resin. Also it is

electrically insulating in nature which hinders some of its applications. Several fillers like silicates, clay, carbon fibers and carbon nanotubes have been incorporated to improve properties of polyester resin. Bharadwaj et al. prepared crosslinked polyester-clay nanocomposite by dispersing organically modified montmorillonite and crosslinked by methyl ethyl ketone peroxide catalyst [9]. The composite showed good thermal, mechanical and rheological behavior. The oxygen permeability of the composites was found to be reduced progressively. Vilcakova et al. investigated the electrical conductivity of composites of a polyester resin filled with short carbon fibers with a special attention to the properties in the percolation threshold region. A very low percolation threshold (0.7–0.8 vol% of the filler) was confirmed [10]. Seyhan et al. reported preparation of carbon nanotube/unsaturated thermoset polyester nanocomposites using 3-roll mill and sonication techniques [11]. The CNT/polyester blend exhibited a shear thinning behavior, while polyester resin blends act as a Newtonian fluid. It was also observed that nanotubes with aminefunctional groups have better tensile strength, as compared to those with untreated CNTs. Battisti et al. developed electrically conductive nanocomposites containing multiwalled carbon nanotubes in an unsaturated polyester matrix [12]. The conductivity of the cured nanocomposite follows a statistical percolation model, with percolation threshold at 0.026 wt.% loading of nanotubes. Salavagione et al. prepared reduced graphene oxide (rGO) based polyvinyl alcohol composite with improved thermal and electrical properties [13].

* Corresponding author. Tel.: +91 9957198489; fax: +91 03712 267006.

E-mail address: swapankdolui@gmail.com (S.K. Dolui).

The composite exhibited around 100 °C increase in thermal stability and an electrical percolation threshold. However, to our knowledge, works based on PE/rGO composite is rare in the literature. Therefore in our present investigation we have used rGO as filler in the polyester resin matrix to improve mechanical strength, thermal stability as well as to introduce new characteristic like electrical conductivity of the resin at very low filler content. Moreover, rGO has been found to have good antibacterial activity towards microorganisms. Hu et al. reported the antibacterial activity of water dispersible GO and rGO nanosheets. They found that such rGO-based nanomaterials can effectively inhibit the growth of *Escherichia coli* bacteria while showing minimal cytotoxicity.

Here we are reporting a simple method of preparation of PE/rGO composite by dispersing rGO in polyester resin and subsequently crosslinked using methyl ethyl ketone peroxide (MEKP) catalyst at different rGO concentration. The effect of rGO on various properties like thermal, mechanical and electrical property of polyester resin has been investigated. The antibacterial activity of the nanocomposite was evaluated against a number of bacterial strains.

2. Experimental

2.1. Materials

Water-clear PE resin (acid value 10 mg KOH/gm, hydroxyl value 45 and viscosity 2500–3000 Cps) and hardener methyl ethyl ketone peroxide (MEKP) were obtained from Kumud Enterprise, West Bengal. Graphite powder, concentrated sulfuric acid (98%), sodium nitrate, potassium permanganate, 30% H₂O₂ solution, hydrochloric acid, acetone, N, N dimethylformamide (DMF) and hydrazine monohydrate were of reagent grade and purchased from Merck. All the reagents were used without further purification.

2.2. Preparation of rGO by reduction of graphite oxide

Graphite oxide dispersion was prepared from natural graphite using a modified Hummers method [14] using KMnO₄ and H₂SO₄ as oxidizing agents. For purification, the mixture was washed with 5% of HCl and then DI H₂O for several times. The powdered graphite oxide was obtained by filtration and then drying the reaction mixture under vacuum at 65 °C. To prepare rGO, 0.1 g of graphite oxide was dispersed in 50 mL of DI water. Then 1 mL of hydrazine monohydrate was added to the mixture and heated at 95 °C for 12 h. After that the mixture was filtered and the reduced GO was obtained as a black powder. The product thus obtained was washed with DI water several times.

2.3. Preparation of PE resin/rGO nanocomposites

PE/rGO composites of different weight percentage of rGO to PE resin (1–3 wt.%) were prepared as follows: The required amount of rGO was dispersed in a minimum amount of THF (solvent) by ultrasonication for 1 h. Then required amount of polyester resin was introduced into the above dispersion and mixed under vigorous mechanical stirring followed by ultrasonication for 30 min. The mixture was then degassed for about 20 min under vacuum until it was completely bubble free. Afterwards, 4% of the hardener (MEKP) with respect to PE resin was added into the mixture and the mixture was cast on teflon plates and dried under vacuum in desiccators for overnight at room temperature. Then they were allowed to cure at 120 °C for further study.

2.4. Characterization

Fourier transform infrared (FTIR) spectra were recorded using a Nicolet Impact 410 spectrophotometer at room temperature, over a frequency range of 500–4000 cm⁻¹. The samples were crushed well and then examined in KBr pellets. The X-ray diffraction (XRD) study was carried out at room temperature (25 °C) using a Rigaku X-ray diffractometer (Miniflex, UK) with Cu K α radiation ($\lambda = 0.15418$ nm) at 30 kV and 15 mA with a scanning rate of 0.050/s in the range of $2\theta = (10\text{--}70^\circ)$. The surface morphology of the composites was observed by scanning electron microscope (SEM) of model JSM-6390LV, JEOL, Japan at an accelerating voltage of 5–15 kV. The surface of the sample was coated with platinum before SEM analysis. Transmission electron microscope (TEM) measurement was carried out by a PHILIPS CM 200 microscope at 200 kV. The TEM sample was prepared by dispensing a small amount of dry powder in ethanol. Then, one drop of the suspension was dropped on 300 mesh copper TEM grids covered with thin amorphous carbon films. Atomic force microscopy (AFM) observation was performed on the DI Multimode V in tapping-mode. To study the thermal degradation of the samples, thermogravimetric analysis (TGA) was performed using Shimadzu TGA 50 thermal analyzer, Japan from temperature range 25–700 °C with a heating rate of 10 °C min⁻¹ under the nitrogen flow rate of 30 mL min⁻¹. Differential scanning calorimetric (DSC) analysis of the samples was done using Shimadzu DSC-60. The analysis was run in the presence of nitrogen gas at a scanning speed 10 °C/min in the temperature range of 0–300 °C. For measurement of the mechanical properties, the composite films were cut to a width of 10 mm and a thickness of 3 mm. The tensile strength measurements were conducted with a Zwick Z010 (Germany) UTM with a 10-kN load cell and at jaw separation speed of 50 mm/min at room temperature (25 °C). Measurements of electrical conductivities of the samples were performed using Keithley 2000 (Keithley Instruments Inc., USA) instrument. The resistivity of the samples was measured in a four-point probe unit using the following equation:

$$\text{Resistivity } (\rho, \Omega \text{ cm}) = (V/I)2\pi S \quad (1)$$

$$\text{Conductivity } (\sigma, S/\text{cm}) = 1/\rho \quad (2)$$

where V is the applied voltage, I is the measured current through the sample and S is the distance between the probes.

2.4.1. Antimicrobial activity test

The well diffusion technique was used in the present investigation. 200 μ L of the log phase culture of the test microbes (10^7 – 10^8 cell as per McFarland standard) which includes *Staphylococcus aureus* (ATCC 11632), *Bacillus subtilis* (ATCC 11774), *Escherichia coli* (MTCC 40), *Pseudomonas aeruginosa* (MTCC 7812) and *Klebsilla pneumoniae* (ATCC10031) were seeded on the surface of the Muller Hinton agar medium, using a micropipette and spread over the medium uniformly using a sterile glass spreader. Further, with the help of a sterile cork borer three wells, each with a diameter of 6 mm were made on Muller Hinton agar (MHA) plate. Samples were dissolved in sterilized dimethyl sulfoxide (DMSO) (10%, v/v) and introduced into each of the wells. Streptomycin sulfate (1 mg/mL) was taken as a positive control. The culture plates were incubated at 37 ± 2 °C for 24 h. The observed zones of inhibition were measured using transparent metric ruler. The experiment was done thrice and the mean values were determined.

3. Results and discussion

PE/rGO composite film at different rGO concentration was prepared by dispersing rGO in polyester resin and subsequently

crosslinked using methyl ethyl ketone peroxide (MEKP) catalyst at different rGO concentration. The synthetic process of PE/rGO composite is illustrated in Fig. 1.

3.1. FTIR study

FTIR spectra of pure PE resin, GO, rGO and PE/rGO resin composite are represented in Fig. 2(a). In the FTIR spectrum of GO, the broad peak at 3409 cm^{-1} and a peak at 1719 cm^{-1} can be assigned to O–H stretching vibration and the carbonyl (C=O) stretching respectively. The peaks at 1370 and 1250 cm^{-1} represent the C–O–C and C–OH stretching vibration [15]. The peak near 1065 cm^{-1} represents C–O stretching vibrations which confirm the presence of the epoxide groups in the GO layers. In the FTIR spectrum of rGO, a broad peak appears at 3426 cm^{-1} corresponding to O–H stretching vibration which is due to the absorption of moisture by the rGO sheets. The peaks at 2850 and 2915 cm^{-1} corresponds to aromatic C–H stretching vibration [16]. Upon reduction of GO, the absorption bands at 1719 , 1370 , 1250 and 1060 cm^{-1} decreased indicating successful reduction of GO into rGO.

The PE resin film shows important characteristic absorption bands at 1732 cm^{-1} for carbonyl group (C=O), 3428 cm^{-1} for O–H stretching and 1629 cm^{-1} for aromatic C=C stretching. The peaks at 1166 cm^{-1} and 1263 cm^{-1} band appears for C–O–C stretching vibrations attached with aliphatic and aromatic moiety. From the FTIR spectrum of PE/rGO resin composite, it is seen that the absorption peaks are almost similar to pure PE resin. However some peaks have shifted to lower frequencies than the pristine polyester. The shifting of the peaks indicates the interactions of the polyester segments (–COOH and –OH) with the remaining oxygen functional groups of rGO through H-bonding or other polar–polar interactions. Thus from the FTIR results we can say that rGO has been successfully incorporated in the polymer matrix.

3.2. XRD analysis

The X-ray analysis was used to determine the structure and crystallinity of polymer matrices. The XRD patterns of GO, rGO,

pristine PE resin and PE/rGO (3 wt.%) composite are shown in Fig. 2(b). The X-ray pattern of GO displays the presence of a strong peak at $2\theta = 11.2^\circ$, corresponding to d-spacing of 0.78 nm [17]. rGO exhibits a broader diffraction peak at $2\theta = 24^\circ$ which can be correlated to an interlayer spacing of 0.36 nm in the graphene sample. A weak and broad diffraction peak of PE resin is observed at $2\theta = 25.5^\circ$ which indicates that the resin is amorphous in nature. The PE/rGO composite (3 wt.%) exhibits a weaker diffraction peak compared to the neat resin indicating strong interaction between the polymer chains and the filler. However the reflection peak of rGO disappears in the nanocomposite which can be attributed to the exfoliation and homogeneous dispersion of GO in the polyester matrix. Similar results were observed for other rGO based polymer composites [13].

3.3. Morphological studies

In the SEM of rGO a layered, wrinkle-like structure is observed (Fig. 3(a)). The TEM image of rGO (Fig. 3(e)) shows a crumpled and agglomerated sheet like structure with hundreds of nanometers. The wrinkled structure observed in the TEM image of rGO sheets is due to the rapid removal of intercalated functional groups in graphitic oxide during exfoliation. SEM image of the composite (Fig. 3(c)) displays a rough, layered structure compared to the smooth surface of the neat PE resin (Fig. 3(b)). Appearance of this layered structure in the composites results from the uniform dispersion of rGO sheets in the polymer matrix and the strong interaction between remaining oxygen functional groups. Fig. 3(d) shows a fractured surface of the PE/rGO (3 wt.%) composite film. The image reveals the random dispersion of rGO sheets in the polymer matrix with a few restacking which may affect the mechanical and other properties of the composite.

AFM is used to measure the thickness of the rGO sheets. Fig. 3(f) shows a typical tapping-mode AFM image of rGO sheets deposited onto a mica substrate. It revealed that the average thickness of the rGO sheets was around 4 nm , indicating well exfoliated nanosheets.

Fig. 3(g) shows the EDX spectra of GO and rGO. GO exhibits oxygen content of 45 atom\% , as shown in Fig. 3(g) and the atomic ratio

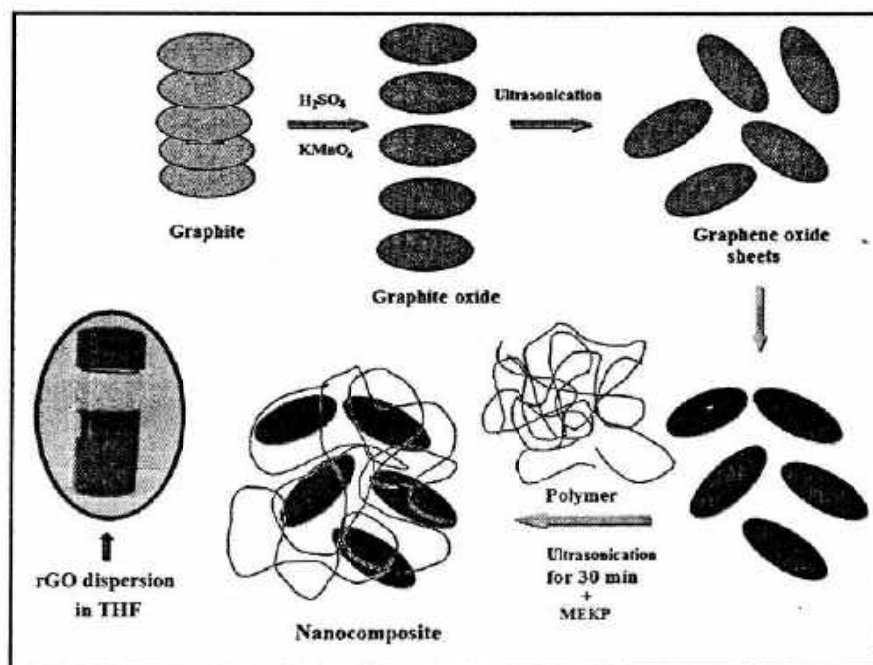


Fig. 1. Fabrication process of PE/rGO composite.

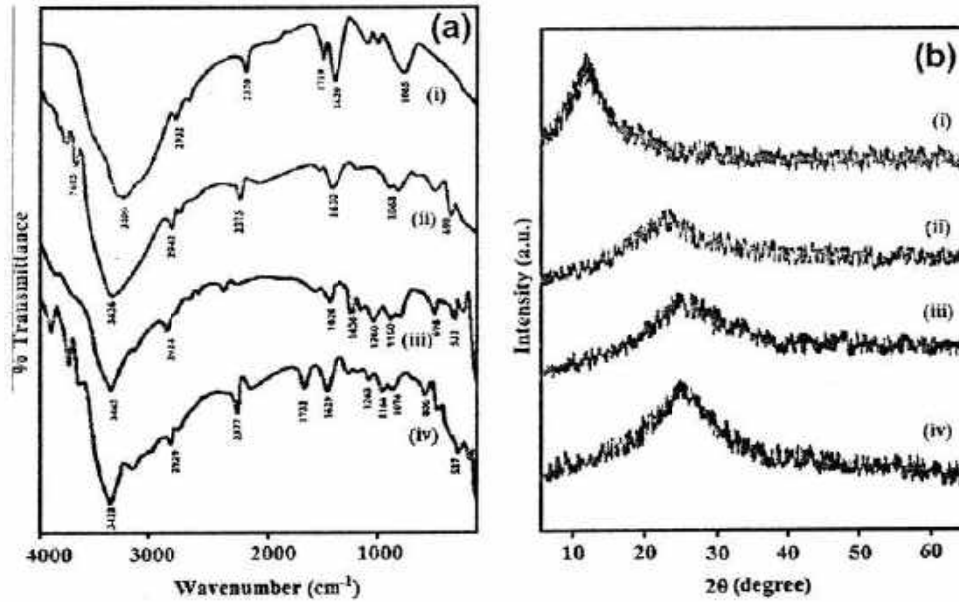


Fig. 2. (a) FTIR spectra of (i) GO, (ii) rGO, (iii) PE/rGO composite, (iv) PE resin; (b) XRD patterns of (i) GO, (ii) rGO, (iii) PE/rGO composite and (iv) PE resin.

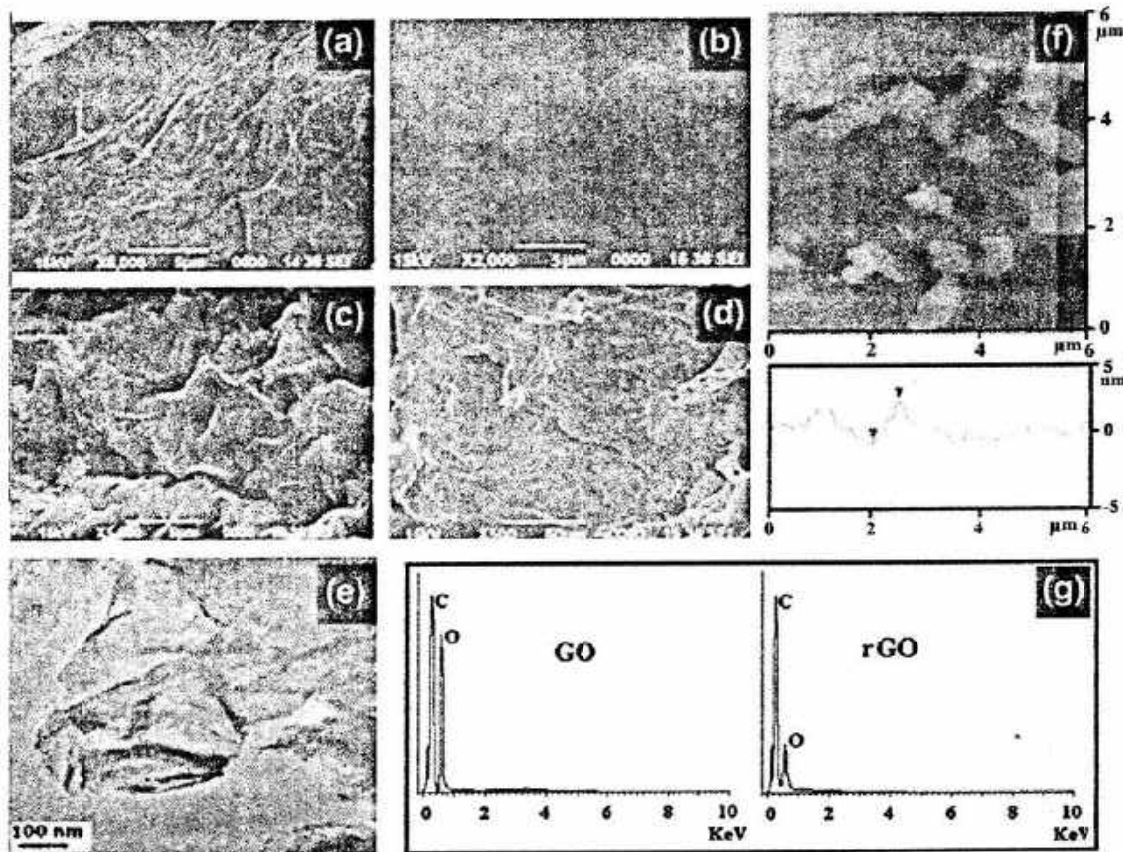


Fig. 3. (a–c) SEM images of rGO, PE resin and PE/rGO composite (3 wt.%) respectively, (d) SEM image of cross section of the composite, (e) TEM image of rGO, (f) tapping mode AFM image of rGO and (g) EDX spectra of GO and rGO.

of carbon to oxygen was found to be 1.25. After reduction, the atomic ratio of carbon to oxygen was 9, as shown in the EDX spectra of rGO (Fig. 3(g)). Only 15% oxygen content remained in the rGO which indicates successful reduction of the GO.

3.4. Thermal properties

Thermal properties of the PE/rGO composite films were evaluated with thermo gravimetric analysis (TGA) and differential

scanning calorimetry (DSC). TGA curve for PE resin, PE/rGO composite and rGO are shown in Fig. 4(a). GO shows a major weight loss at the temperature range of 200–320 °C which is attributed to the removal of most of the oxygen-containing functional groups. The 60% residual weight of GO indicates that some functional groups existed on GO surface before the thermal treatment. rGO showed around 20% weight loss at the temperature range of 250–500 °C, which is due to the removal of most of the oxygen-containing functional groups during the chemical reduction

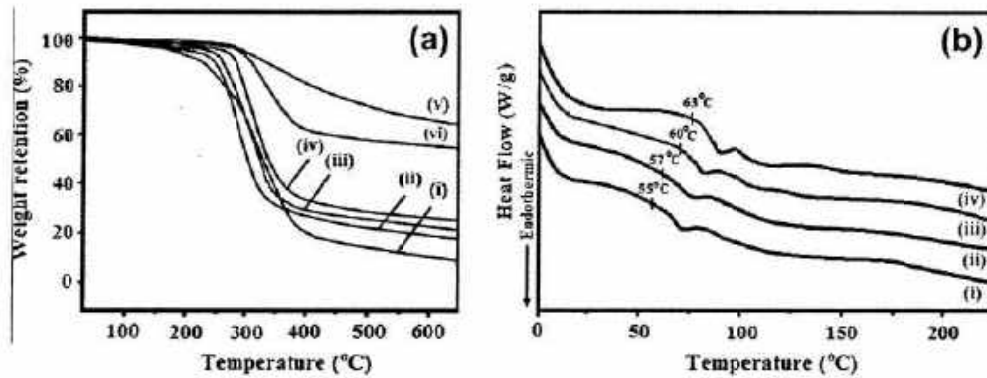


Fig. 4. (a) TGA curves of (i) PE resin, (ii) PE/rGO (1 wt.%), (iii) PE/rGO (2 wt.%), (iv) PE/rGO (3 wt.%) composite, (v) rGO and (vi) GO, (b) DSC curves of (i) PE resin, (ii) PE/rGO (1 wt.%), (iii) PE/rGO (2 wt.%) and (iv) PE/rGO (3 wt.%) composite.

process. rGO exhibited about 70% residual weight at 600 °C indicating its excellent thermal stability. In the TGA curve of PE resin, initial weight loss occurs at a temperature of 240 °C. The weight loss after 300 °C is due to the complete degradation of the polymer. The major degradation temperature of polyester was found to be improved from 245 to 289 °C on incorporation of the rGO. This improvement in thermal stability is ascribed to the strong interaction between rGO and PE resin which restricts the mobility of the polymer chains. The interaction may be due to the formation of hydrogen bonding between residual oxygen functionality on rGO and polymer or some dipolar interactions between the two components. Also the weight retention value increases with the incorporation of rGO with PE resin matrix. Almost 25–30% weight retention values were observed in the TGA curves of the composites at 600 °C which is probably due to the existence of a carbon net structure in the composite [18]. The PE/rGO composites have shown better thermal stability compared to other PE resin composites [10,11].

The glass transition behavior of PE/rGO composites was obtained from DSC. PE resin exhibits glass-transition temperature (T_g) at around 55 °C (Fig. 4(b)). The T_g of PE resin increases from 55 °C to 63 °C with an increase in the rGO content. This increase in T_g can be attributed to the reinforcing effect of rGO which reduces segmental motion of the polymer chain.

3.5. Mechanical properties

The incorporation of rGO into the polymer matrix has a significant influence on the mechanical behavior of the composite due to its large aspect ratio and excellent mechanical strength. The representative stress–strain curves of neat PE resin and its composites at various rGO loadings are shown in Fig. 5. The mechanical properties of the composite films were found to be increased significantly compared to pure PE resin. The slope of the curves increases with the increasing rGO content. Based on the slope of the elastic region, the Young's modulus values are calculated and are shown in Table 1. On introduction of rGO sheets the Young's modulus values are found to be increased. For the composite film with 3 wt.% of rGO loading, Young's modulus increased to 3 GPa, corresponding to an increase of 87% compared to pure polyester resin.

The tensile strength and the percentage elongation at break of the PE/rGO films are represented in Table 1. The average tensile strength for pure PE resin is 26 MPa. The tensile strength values are found to be increased with increasing rGO loading. PE/rGO composite with 3 wt.% of rGO loading showed the tensile strength value of 58 MPa, corresponding to an improvement of 123% compared to neat resin. The value is higher than carbon nanofiber and carbon nanotube based PE resin composites [11,19]. This enhanced tensile property can be attributed to the well dispersion

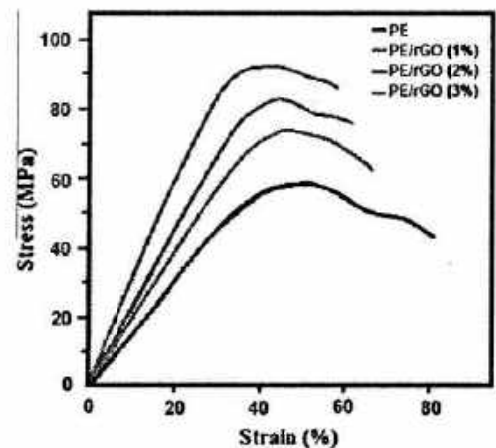


Fig. 5. Representative stress–strain curves of the composites with various rGO loadings.

Table 1
Properties of PE/rGO composites.

Sample	Tensile strength/MPa	Elongation (%)	Young's modulus (GPa)	Conductivity (σ , S/cm)	Glass transition temperature (T_g , °C)
PE resin	26	81	1.4	3.09×10^{-12}	55
PE/rGO (1%)	35	58	1.9	1.10×10^{-5}	57
PE/rGO (2%)	47	50	2.3	7.5×10^{-5}	60
PE/rGO (3%)	58	45	3.07	3.7×10^{-4}	63

of rGO in the polymer matrix and strong interfacial interactions between both the components.

On the other hand, a gradual decrease in the elongation at break of the composites was observed with increasing rGO content. For the 3 wt.% rGO loading, the elongation at break decreased to 45% from 81% for the pure polymer. It could be due to the large aspect ratio and the interaction between rGO and the polymer matrix, which restricts the movement of the polymer chains. The results were similar to that of other graphene based polymer composites [20–22].

3.6. Electrical properties

The electrical conductivities of pure PE resin and PE/rGO composites at different rGO content are determined using a fourpoint probe resistivity measurement system (Table 1). The conductivity of pristine PE resin is around 3.09×10^{-12} S/cm. On incorporation of rGO the conductivity of the composites increases rapidly and

Table 2
Antibacterial activities of synthesized compounds against different bacterial strains.

Test sample	Zone of Inhibition (mm) against				
	<i>Staphylococcus aureus</i> (ATCC11632)	<i>Bacillus subtilis</i> (ATCC11774)	<i>Escherichia coli</i> (MTCC40)	<i>Pseudomonas aeruginosa</i> (MTCC7812)	<i>Klebsilla pneumoniae</i> (ATCC10031)
10% DMSO (v/v)	0	0	0	0	0
PE resin	10	10	10	11	10
PE/rGO (1%)	11	11	10	12	12
PE/rGO (2%)	12	11	11	13	13
PE/rGO (3%)	13	12	12	15	14

the highest conductivity of 3.7×10^{-4} S/cm is achieved for composite containing 3 wt.% rGO. Such an improvement in conductivity can be explained by the large specific surface area and excellent homogeneous dispersion of rGO sheets which form a conducting network in the insulating resin matrix. The conductivity obtained here is higher than that of carbon fiber and CNT based PE resin composite [10,12].

3.7. Antibacterial activity

An organized glimpse of data for the antibacterial property of the synthesized composites is illustrated in Table 2, which shows a highly significant and pronounced antibacterial behavior of the tested samples against five different bacterial growths of *Staphylococcus aureus*, *Bacillus subtilis*, *Escherichia coli*, *Pseudomonas aeruginosa* and *Klebsilla pneumoniae*. Samples were dissolved and tested for corresponding antimicrobial activities in 10% DMSO (v/v) aqueous solution. It was found from literature that 10% DMSO (v/v) has been used for antimicrobial and other biological activities as it is highly miscible with water, highly polar and stable [23,24]. In the presence of 10% DMSO (v/v) both the gram positive and gram negative bacteria showed no detectable effect on bacterial growth. Both gram positive and gram negative bacteria were found sensitive to the composites; predominantly the composites were appeared to be more effective towards the gram negative. It is clear from the above set of tests that *Pseudomonas aeruginosa* bacteria is very sensitive toward the PE/rGO composites and *Escherichia coli* shows the lowest degree of inhibition. The antibacterial effect of composites increases with the rGO content. The composite containing 3 wt.% of rGO has showed the highest degree of inhibition against all the five kinds of bacterial strains for which the diameter of the zone of inhibition is more (Fig. 6). The reason for the growth inhibitory property of the nanocomposites might be due to the cellular damages of the bacterial cells. Such cellular damages are

caused due to the effect of either oxidative stress or physical disorder caused by rGO. Similar observation was also reported in other carbon nanomaterials like CNTs and fullerene [25,26].

4. Conclusion

The rGO based PE resin composite films with high mechanical strength; thermal stability and improved electrical property have been successfully prepared by incorporating rGO sheets into the resin matrix. Both FTIR and XRD results exhibit successful incorporation of rGO in the polymer matrix. The morphological analysis revealed uniform distribution of rGO within the polymer matrix. TGA analysis showed significant improvement in major degradation temperature (260–289 °C) and weight retention value (15–25%) of the composite compared to neat resin. The composite demonstrated a significant improvement in mechanical properties with very low rGO loading. A 123% increase of tensile strength and 87% increase in Young's modulus are obtained with 3 wt.% of rGO loading, which reveals the efficient load transfer between rGO and the polymer matrix. The composite film with 3 wt.% rGO loading was found to possess a higher value of conductivity (3.7×10^{-4} S/cm) compared to pure resin. The composites imply proficient antibacterial activity towards the five different kinds of bacterial strains and the antibacterial activity was found to be increased with increasing rGO content. Among all the bacterial strains, *Pseudomonas aeruginosa* was much more sensitive toward the PE/rGO composites. These rGO based PE resin composites with improved mechanical strength and antibacterial activity could offer new opportunities for the development of a new range of environmental friendly and high strength structural material.

Acknowledgements

The authors would like to thank the Council of Scientific and Industrial Research (CSIR) India, for their financial support in the research under Contract No. 02(0066)/12/EMR-II). The financial support received from UGC under SAP program and DST under FIST program is kindly acknowledged by the authors.

References

- [1] Kim H, Abdala AA, Macosko CW. Graphene/Polymer nanocomposites. *Macromolecules* 2010;43:6515–30.
- [2] Potts JR, Dreyer DR, Bielawski CW, Ruoff RS. Graphene-based polymer nanocomposites. *Polymer* 2011;52:5–25.
- [3] Kujala T, Bhadrab S, Yao D, Kim NH, Bose S, Lee JH. Recent advances in Graphene based polymer composites. *Prog Polym Sci* 2010;35:1350–75.
- [4] Rao CNR, Soed AK, Subrahmanyam KS, Govindaraj A. Graphene: the new two-dimensional nanomaterials. *Angew Chem Int Ed* 2009;48:7752–7.
- [5] Wang S, Tambraparni M, Qiu J, Tipton J, Dean D. Thermal expansion of graphene composites. *Macromolecules* 2009;42:5251–5.
- [6] Fang M, Wang KG, Yang YL, Nutt S. Covalent polymer functionalization of graphene nanosheets and mechanical properties of composites. *J Mater Chem* 2009;19:7098–105.
- [7] Aziz SH, Ansell MP, Clarke SJ, Panteny SR. Modified polyester resins for natural fibre composites. *Compos Sci Technol* 2005;65:525–35.

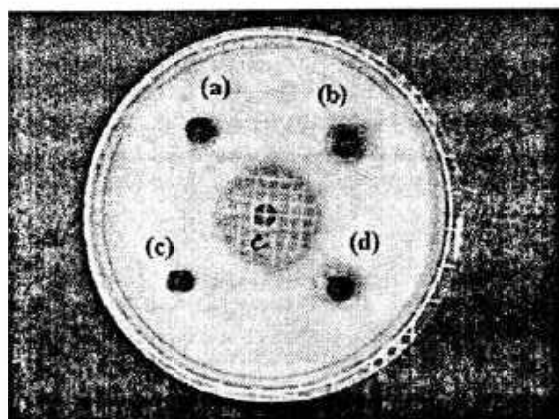


Fig. 6. Antibacterial test against *Escherichia coli*. (a) Pure PE resin. (b) PE/rGO (1 wt.%), PE/rGO (2 wt.%), PE/rGO (3 wt.%) composite.

- [8] Tibiletti L, Longuet C, Ferry L, Coustou P, Mas A, Robin JJ, et al. Thermal degradation and fire behaviour of unsaturated polyesters filled with metallic oxides. *Polym Degrad Stab* 2011;96:67–75.
- [9] Bharadwaj RK, Mehrabi AR, Hamilton C. Structure–property relationships in cross-linked polyester–clay nanocomposites. *Polymer* 2002;43:3699–705.
- [10] Vileakova J, Saha P, Quadrat O. Electrical conductivity of carbon fibres/polyester resin composites in the percolation threshold region. *Eur Polym J* 2002;38:2343–7.
- [11] Seyhan T, Gajny FH, Tanoglu M, Schulte K. Critical aspects related to processing of carbon nanotube/unsaturated thermoset polyester nanocomposites. *Eur Polym J* 2007;43:374–9.
- [12] Battisti A, Skordos AA, Partridge IK. Percolation threshold of carbon nanotubes filled unsaturated polyesters. *Compos Sci Technol* 2010;70:633–7.
- [13] Salavagione HJ, Martinez G, Gomez MA. Synthesis of poly(vinyl alcohol)/reduced graphite oxide nanocomposites with improved thermal and electrical properties. *J Mater Chem* 2009;19:5027–32.
- [14] Hummers WS, Offeman RE. Preparation of graphitic oxide. *J Am Chem Soc* 1958;80:1339.
- [15] Patole AS, Patole SP, Kang H, Yoo JB, Kim TH, Ahn JH. A facile approach to the fabrication of graphene/polystyrene nanocomposites by in situ microemulsion polymerization. *J Colloid Interface Sci* 2010;350:530–7.
- [16] Pandey RK, Lakshminarayanan V, Pandey RK, Lakshminarayanan V. Electro-oxidation of formic acid, methanol, and ethanol on electrodeposited Pd-polyaniline nanofiber films in acidic and alkaline medium. *J Phys Chem C* 2009;113:21596–603.
- [17] Yang X, Shang S, Liang L. Layer-structured poly(vinyl alcohol)/graphene oxide nanocomposites with improved thermal and mechanical properties. *J Appl Polym Sci* 2011;120:1355–60.
- [18] Bora C, Dofui SK. Fabrication of polypyrrole/graphene oxide nanocomposites by liquid/liquid interfacial polymerization and evaluation of their optical, electrical and electrochemical properties. *Polymer* 2012;53:923–32.
- [19] Aguiló JV, Pereira AC, Rizo HV, González JL, Gullón JM. Comparative study of the dispersion and functional properties of multiwall carbon nanotubes and helical-ribbon carbon nanofibers in polyester nanocomposites. *Compos Sci Technol* 2009;69:1521–32.
- [20] Zhao X, Zhang Q, Chen D. Enhanced mechanical properties of graphene-based Poly(vinyl alcohol) composites. *Macromolecules* 2010;43:2357–63.
- [21] Kong J, Choi MC, Kim CY, Park JJ, Selvaraj M, Han M. Preparation and properties of polyimide/graphene oxide nanocomposite films with Mg ion crosslinker. *Eur Polym J* 2012;48:1394–405.
- [22] Xu Y, Hong W, Bai H, Li C, Shi G. Strong and ductile poly(vinyl alcohol)/graphene oxide composite films with a layered structure. *Carbon* 2009;47:3538–43.
- [23] Hussain AI, Anwar F, Chatha SAS, Jabbar A, Mahboob S, Nigam PS. Rosmarinus officinalis essential oil: antiproliferative, antioxidant and antibacterial activities. *Braz J Microbiol* 2010;41:1070–8.
- [24] Das S, Thakur AJ, Medhi T, Das B. An efficient stereo-controlled synthesis of bis-pyrimido-[4,5-d]-pyrimidine derivatives via aza-Diels-Alder methodology and their preliminary bioactivity. *RSC Adv* 2013;3:3407–13.
- [25] Tang YJ, Ashcroft JM, Chen D, Min G, Kim CH, Murkbejee B, et al. Charge-associated effects of fullerene derivatives on microbial structural integrity and central metabolism. *Nano Lett* 2007;7:754–60.
- [26] Szabo T, Berkesi O, ForGO P, Josepovits K, Sanakis Y, Petridis D, et al. Evolution of surface functional groups in a series of progressively oxidized graphite oxides. *Chem Mater* 2006;18:2740–9.

Interfacial synthesis of polypyrrole/graphene composites and investigation of their optical, electrical and electrochemical properties

Chandramika Bora and Swapan Kr Dolui*

Abstract

We report the development of a novel route for the synthesis of polypyrrole/graphene (PPy/GR) composites by liquid–liquid interfacial polymerization, where GR and the initiator were dispersed in the aqueous phase and the monomer was dissolved in the organic phase. The synthesized samples were characterized by Fourier transform infrared spectroscopy, scanning electron microscopy, ultraviolet–visible spectroscopy, Raman spectroscopy, X-ray diffraction, thermogravimetric analysis, electrochemical and electrical conductivity measurements. Structural analysis reveals a uniform dispersion of GR sheets in the PPy matrix. The composites showed noticeable improvement in thermal stability and electrical conductivity (8.45 S cm^{-1}) and excellent electrochemical reversibility in comparison with pure PPy. A specific capacitance of 260 F g^{-1} at a current density of 100 mA g^{-1} was achieved for the composite during the charge–discharge process.

© 2013 Society of Chemical Industry

Keywords: graphene; polypyrrole; interfacial polymerization

INTRODUCTION

Graphene (GR), a one-atom-thick sp^2 -bonded carbon sheet, with unique properties has become like a rising star on the horizon of materials science since its discovery in 2004.^{1,2} The special physical and chemical properties of GR make it promising for many applications such as supercapacitors, sensors, solar cells, batteries, fuel cells and many others.^{3–6} Owing to its high surface area, excellent conductivity, good mechanical strength, easy availability and cost efficiency, GR can be used as an effective nanofiller in polymers compared with other carbon materials like carbon nanotubes, carbon fibers and fullerenes.⁷ Hence GR-based composites have attracted tremendous scientific interest recently. The incorporation of a small quantity of GR nanofiller into polymer matrices remarkably improves the properties of the composite material.^{8–10} Such improvement in the properties of GR-based composites results from the homogeneous dispersion of nanofillers in the polymer matrix due to the high aspect and surface-to-volume ratios of GR.

Several GR-based polymer composites show good enhancement in thermal, mechanical and electrical properties.^{11,12} On the other hand, conducting polymers such as polyaniline, polypyrrole and polythiophene have been studied extensively in the last few decades because of their good electrical properties, high specific capacity, easy processability and light weight. Amongst these, polypyrrole (PPy) is particularly attractive because of its low cost, easy synthesis and relatively high conductivity.¹³ However, PPy is usually mechanically weak and insulating in its neutral state which hinders some of its applications. It also exhibits poor stability during the charge–discharge process. Incorporation of GR in a conducting polymer matrix leads to the formation of composites with synergistic properties which have advantages of both the components. Hence, GR can be considered as an effective

nanofiller for PPy because of its high surface area, good mechanical strength and excellent conductivity.

Until recently, some efforts have been made to achieve improved properties of composites based on PPy and GR. Zhang *et al.*¹⁴ synthesized GR-based PPy composite by *in situ* polymerization of pyrrole monomer in the presence of GR under acidic conditions. The composite showed higher specific capacitance and better rate capability and cycling stability than pure PPy which allows its applications in supercapacitors. Bose *et al.*¹⁵ successfully prepared PPy/GR composites by *in situ* polymerization of graphite oxide (GO) and pyrrole monomer followed by chemical reduction using hydrazine monohydrate. The composite exhibited good improvement in thermal stability as well as electrical conductivity. Liu *et al.*¹⁶ synthesized composite films of sulfonated GR and PPy by electrochemical deposition from aqueous solutions containing pyrrole monomer, sulfonated GR sheets and dodecylbenzene sulfonic acid. The composite exhibited improved conductivity, electrochemical stability and rate performance. However, in most cases the preparation of polymer composites is done by *in situ* polymerization.

Here we have developed a novel route to fabricate PPy/GR composite by interfacial polymerization. Interfacial polymerization is a simple, controllable, easy and slow reaction compared with other conventional polymerization methods. It is recognized as an easy approach for producing conducting polymers such as

* Correspondence to: Swapan Kr Dolui, Department of Chemical Sciences, Tezpur University, Napaam, Tezpur, Assam 784028, India. E-mail: swapankdolui@gmail.com

Department of Chemical Sciences, Tezpur University, Napaam, Tezpur, Assam 784028, India

PPy, polyaniline, polythiophene and their nanocomposites.^{17–19} The electrochemical, electrical and various other properties of a composite are strongly influenced by the structure and the preparation method. To the best of our knowledge no previous work has been reported for preparing GR-based PPy composite by this route. Our challenge was to obtain a good dispersion of GR sheets within the polymer matrix and to introduce thermal stability along with high electrical conductivity and good electrochemical properties for PPy/GR composites.

EXPERIMENTAL

Materials

Pyrrole was purchased from Sigma Aldrich and was used as received. Graphite flakes were obtained from Carbon India Ltd, Guwahati, India, and were used as purchased. Sodium nitrate (Merck) India, sulfuric acid (Merck), potassium permanganate (Merck), hydrogen peroxide (Qualigens Fine Chemicals), ferric chloride (Aldrich), hydrazine monohydrate (Aldrich), chloroform (Merck), acetonitrile (Merck) and lithium perchlorate (Fluka) are commercial products and were used as received. For all purposes double-distilled water was used. Fourier transform infrared (FTIR) spectra were recorded at room temperature, over the frequency range 4000–500 cm⁻¹, using a Nicolet spectrometer. The samples were crushed well and then examined in KBr pellets. The ultraviolet–visible (UV–visible) absorption spectroscopy of the samples was recorded using a Shimadzu UV-2550 UV–visible spectrophotometer in the range 300–800 nm. Raman spectra were recorded using a Nanofinder 30 confocal Raman with He-Ne laser beam having a wavelength of 532 nm with a CCD detector. The XRD study was carried out at room temperature (*ca* 298 K) using a Rigaku X-ray diffractometer with Cu-K α radiation ($\lambda = 0.15418$ nm) at 30 kV and 15 mA using a scanning rate of 0.05 θ s⁻¹ in the range $2\theta = 10^\circ - 70^\circ$. SEM was carried out on a JSM-6390LV (JEOL, Japan). Transmission electron microscopy (TEM) measurements were conducted on a Philips CM 200 microscope at 200 kV. To study the thermal degradation of the samples, TGA was performed using a TG50 (Simadzu, Japan) thermogravimetric analyser in the temperature range 298–973 K with a heating rate of 283 K min⁻¹ under a nitrogen flow rate of 30 mL min⁻¹. Pellet shaped samples of 1.5 cm diameter and 3 mm width were prepared by pressing the composite materials using a compression-moulding machine at a high pressure (1.5–2 t) and were used to measure the electrical conductivity. The DC electrical conductivity of PPy and PPy/GR composites was measured using a four-probe technique in the temperature range 300 K $\leq T \leq$ 413 K. The electrical conductivity of the composite was calculated using the equations¹⁵

$$\text{resistivity } (\rho, \Omega \text{ cm}) = (V/I) 2\pi S \quad (1)$$

$$\text{conductivity } (\sigma, S \text{ cm}^{-1}) = 1/\rho \quad (2)$$

where ρ is the resistivity of the sample, V is the applied voltage, I is the measured current through the sample and S is the distance between probes. The electrochemical behaviour of the prepared samples was studied using a Sycopel AEW2-10 cyclic voltammeter. Measurements were performed with a standard one-compartment three-electrode configuration cell where platinum and an Ag/Ag⁺ electrode were used as counter and reference electrodes, respectively, in 0.1 mol L⁻¹ lithium

perchlorate (LiClO₄) in acetonitrile solution at a scan rate of 50 mV s⁻¹. The capacitor performance was characterized by means of galvanostatic charge–discharge tests using on an Autolab PGSTAT302N with a three-electrode system at room temperature. The specific capacitance (C_s) was measured by a charge–discharge method using the following equation:¹⁶

$$C_s = I\Delta t / (m\Delta V) \quad (3)$$

where I is the discharge current, ΔV is the potential drop during discharging, Δt is the discharge time and m is the mass of active material in a single electrode.

Preparation of GR by reduction of GO

A GO dispersion was prepared from natural graphite using a modified Hummers method²⁰ with KMnO₄ and H₂SO₄ as oxidizing agent. For purification, the mixture was washed with 5% HCl and then doubly ionized H₂O several times. The powdered GO was obtained by filtration, drying the reaction mixture under vacuum at 65 °C. To prepare GR, 0.1 g of GO was dispersed in 50 mL of doubly ionized water. Then 1 mL of hydrazine monohydrate was added to the mixture and heated at 95 °C for 12 h. After that the mixture was filtered and the reduced GO was obtained as a black powder. The product thus obtained was washed with doubly ionized water several times.

Preparation of PPy/GR composites

PPy/GR composites were prepared by liquid–liquid interfacial polymerization involving pyrrole and GR, as follows. First, the required amount of GR and 300 mg of FeCl₃·6H₂O were dispersed in 15 mL H₂O. The organic phase was obtained by dissolving 0.8 mL of pyrrole in 15 mL chloroform in a beaker. The water phase was added to the organic phase dropwise and the beaker was kept undisturbed for 24 h. During this time, a black film slowly grew on the interface between the two phases. Finally, the product was filtered and washed several times with water and alcohol and air dried. Composites of different weight percentages of GR to pyrrole (1%, 2% and 3%) were prepared and designated GRPPy1, GRPPy2 and GRPPy3. For comparison, pure PPy was prepared without GR by the same route.

RESULTS AND DISCUSSION

PPy/GR composite was prepared by liquid–liquid interfacial polymerization, illustrated in Fig. 1. The synthesis process involves polymerization of pyrrole at a water–chloroform interface with pyrrole monomer dissolved in the organic phase and GR along with the oxidant ferric chloride added to the aqueous phase. During the process the reactants diffuse to the water–chloroform interface and the pyrrole gets adsorbed on the GR sheets. The polymerization of pyrrole started at the interface of the two immiscible liquids and after a few hours a black film slowly appeared at the interface. It is noteworthy that the oxidative polymerization of pyrrole in solution is a rapid and uncontrollable reaction, while in interfacial polymerization the reaction is controllable, slow and completed in 24 h. Also the removal of the byproducts is easy due to their solubility in the aqueous or organic media. Moreover, the resulting PPy is insoluble in both aqueous and organic phase and therefore the product can be easily separated after completion of the reaction.

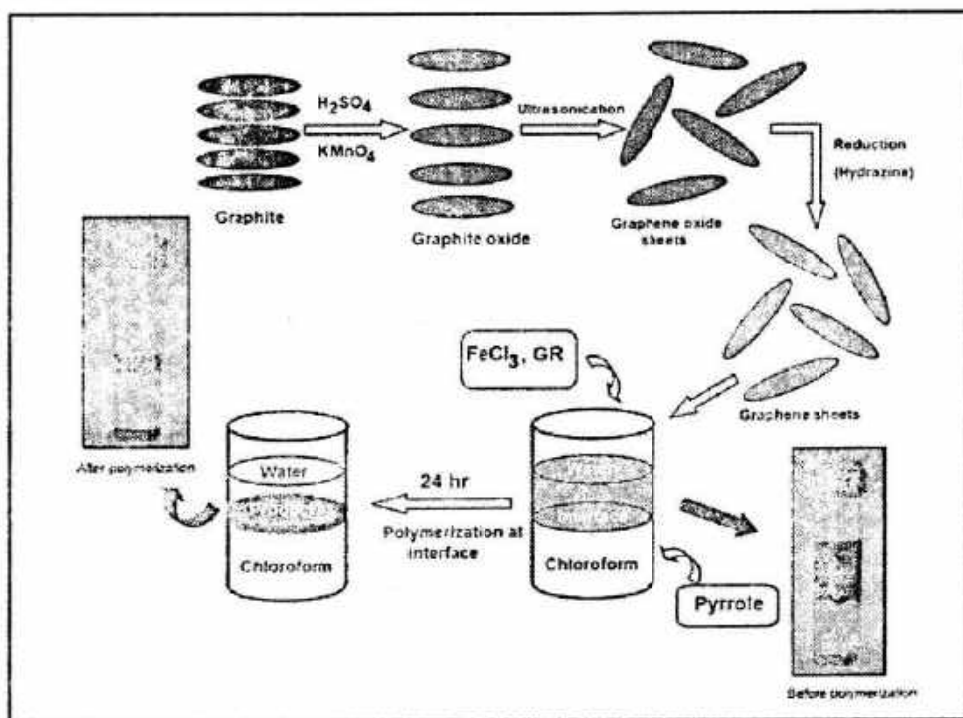


Figure 1. Illustration of the fabrication process for PPy/GR composites.

FTIR analysis

FTIR analyses of pure PPy, GO, GR and PPy/GR composites are presented in Fig. 2. In the FTIR spectra of PPy peaks at 1549, 1465 and 3460 cm^{-1} are associated with the C–C, C–N and N–H stretching vibration in the pyrrole ring (Fig. 2, curve (a)).^{21,22} The peaks located at 2920 and 2831 cm^{-1} are designated as the asymmetric stretching and symmetric vibrations of CH_2 .²³ In the FTIR spectrum of GO (Fig. 2, curve (b)), the broad peak at 3409 cm^{-1} and a peak at 1719 cm^{-1} can be assigned to the O–H stretching vibration and the carbonyl (C=O) stretching respectively. The peaks at 1370 and 1250 cm^{-1} represent the C–O–C and C–OH stretching vibrations.²⁴ The peak near 1065 cm^{-1} represents C–O stretching vibrations which confirm the presence of the epoxide group in the GO layers. Upon reduction of GO, the peaks at 1370 , 1250 and 1060 cm^{-1} disappear which indicates that the epoxide and the hydroxyl groups have been removed from the basal GR layer (Fig. 2, curve (c)). Also the characteristic peak at 1719 cm^{-1} for the carbonyl group becomes weaker in the FTIR spectrum of GR, indicating successful reduction of GO into GR. In the FTIR spectrum of PPy/GR composite we observed peaks for both PPy and GR (Fig. 2, curve (d)). The appearance of characteristic peaks of PPy at 1545 and 1450 cm^{-1} confirms the presence of PPy in the composite. However, the peaks have been downshifted compared with pure PPy. Also the peak intensity decreases in the composite. This indicates that GR has been successfully incorporated in the polymer matrix in the composite.

UV–visible analysis

Figure 3 demonstrates the UV spectra of GR, PPy and PPy/GR composites recorded in dimethylformamide. GR shows a characteristic absorption peak at 255 nm (Fig. 3, curve (a)) which is attributed to $\pi-\pi^*$ transitions of aromatic C–C bonds.²⁵ PPy shows two absorption peaks in the UV spectrum (Fig. 3, curve (b)). The first peak at around 260 nm is related to molecular conjugation and the second at around 455 nm is associated with

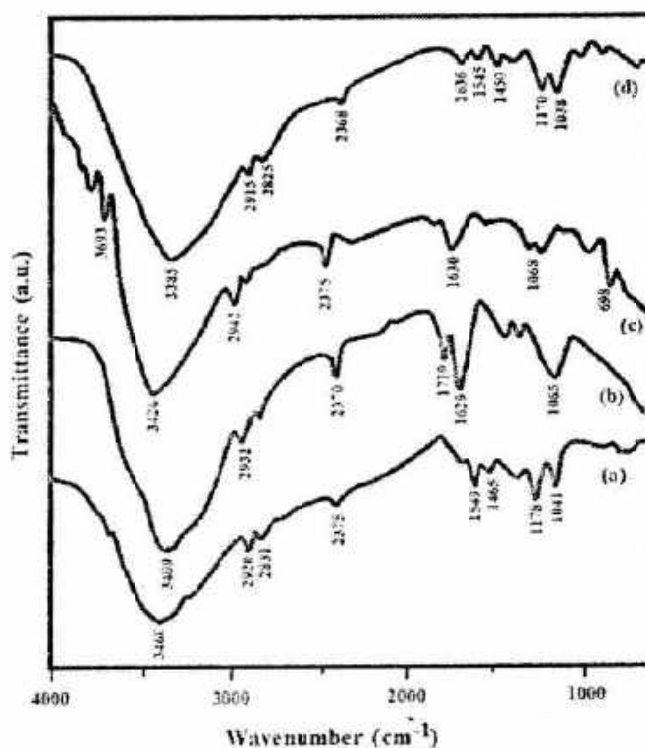


Figure 2. FTIR spectroscopic analysis of pure PPy (curve (a)), GO (curve (b)), GR (curve (c)) and PPy/GR composites (curve (d)).

the bipolaron state of PPy.^{26,27} PPy/GR shows similar absorption peaks (Fig. 3, curve (b)). The peaks related to molecular conjugation are observed at $270\text{--}300\text{ nm}$ and are attributed to $\pi-\pi^*$ interaction between PPy and GR of the composite. Also a strong band is observed at around $500\text{--}590\text{ nm}$ which confirms that PPy is also in the bipolaron state in the composite. Significantly, the absorption peaks have been red shifted in the composite

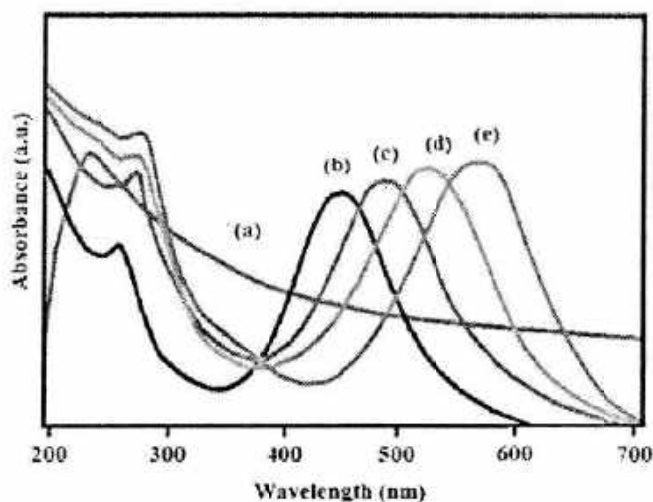


Figure 3. UV-visible spectra of GR (curve (a)), PPy (curve (b)), GRPPy1 (curve (c)), GRPPy2 (curve (d)) and GRPPy3 (curve (e)).

spectra with increasing GR percentage which is ascribed to the extended conjugation length of PPy chains resulting from the $\pi - \pi^*$ stacking between the polymer backbone and GR sheets. The optical absorption in conjugated polymers may be due to the transition of charge carriers through a forbidden energy gap. The optical band gaps of PPy and PPy/GR composites are calculated by using the following equation:²⁸

$$E_g^{\text{opt}} \text{ (eV)} = 1240/\lambda_{\text{edge}} \text{ (nm)} \quad (4)$$

where E_g^{opt} is the optical band gap and λ_{edge} is the absorption edge. The absorption edge and optical band gap of the polymer and composites are listed in Table 1. The band gap of PPy is found to be 2.23 eV whereas in PPy/GR composites the band gap is decreased from 2.10 eV to 1.82 eV.

Raman analysis

Raman spectroscopy is an effective non-destructive tool used for characterizing carbon products. The Raman spectra of PPy/GR, pure GR and GO are shown in Fig. 4. The Raman spectrum of GO (Fig. 4, curve (c)) exhibits two distinctive peaks for the D and G bands which appear at about 1350 cm^{-1} and 1590 cm^{-1} respectively.^{29,30} The D band is attributed to the K-point phonons of A_{1g} symmetry arising from the breathing vibration of aromatic rings, and the G band originates from the zone centre E_{2g} mode corresponding to ordered sp^2 -bonded carbon atoms. The G band is ascribed to the vibration of sp^2 -bonded carbon, whereas the D band is related to the edges, structural defects that correspond to the conversion of an sp^2 -hybridized carbon to an sp^3 -hybridized carbon. The intensity ratio between the D band and G band is a

Sample	$\varphi_{\text{onset}}^{\text{ox}}/ E_{\text{HOMO}}$	$\varphi_{\text{onset}}^{\text{red}}/ E_{\text{LUMO}}$	E^{ec} (eV)	λ_{edge} (nm)	E_g^{opt} (eV)
PPy	0.90/−6.01	−0.7/−4.01	1.60	550	2.23
GRPPy1	0.85/−5.56	−0.5/−4.21	1.35	590	2.10
GRPPy2	0.60/−5.31	−0.4/−4.31	1.00	650	1.90
GRPPy3	0.40/−5.11	−0.25/−4.46	0.65	680	1.82

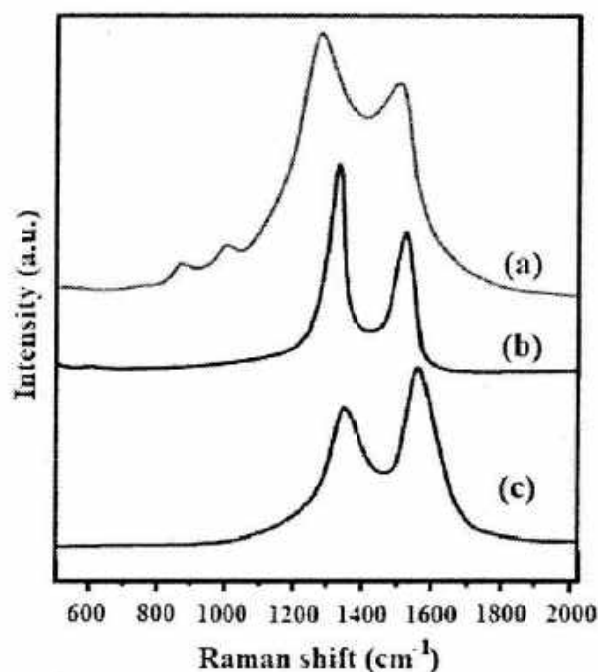


Figure 4. Raman spectra of PPy/GR composite (curve (a)), GR (curve (b)) and GO (curve (c)).

measure of the extent of disorderness. The intensity ratio (I_D/I_G) is found to be 0.80 for GO which indicates a high level of disorder of the GO layers due to the oxidation of graphite. In the Raman spectra of pure GR (Fig. 4, curve (b)), the D and G bands appear at 1340 and 1585 cm^{-1} respectively. However, the I_D/I_G value increased to 1.17 which may be attributed to the presence of unrepaired defects that remained after the removal of large amounts of oxygen-containing functional groups and a decrease in the average size of the sp^2 domains on reduction.^{16,31} In the Raman spectrum of PPy/GR composite (Fig. 4, curve (a)), a broad peak at 1050 cm^{-1} and two small peaks at 930 and 980 cm^{-1} reveal the presence of PPy in the composite. The bands at 930 cm^{-1} and 980 cm^{-1} are associated with the bipolaron and polaron structure of PPy. Moreover, the D and G bands shift to 1332 and 1560 cm^{-1} which indicates a $\pi - \pi$ interaction between the PPy and the GR sheets. The peak intensity ratio I_D/I_G of the composites was 1.14. This indicates the presence of localized sp^3 defects within the sp^2 carbon network which may favour the chemical grafting of polymers to the GR surface.³² Thus the Raman spectrum of the composite shows bands related to both the PPy and GR components which is consistent with the FTIR results.

XRD analysis

The structure of the composites was investigated by XRD measurements. The XRD patterns of GR, PPy/GR composite and pure PPy are shown in Fig. 5. Pure GR shows a broad reflection peak centred at $2\theta = 24.5^\circ$ and a peak at 43° (Fig. 5, curve (a)) corresponding to a d spacing of 0.35 nm which indicates loosely stacked GR sheets and is different from crystalline graphite. PPy exhibits a characteristic peak at $2\theta = 26^\circ$ (Fig. 5, curve (c)), which is attributed to the amorphous nature of PPy.¹⁶ The XRD pattern of the PPy/GR composite is similar to that of PPy however, the peak at 26° has been shifted to 25.2° with a slight increase in peak intensity. The disappearance of diffraction peaks at 43° reveals the full interaction between PPy and GR sheets (Fig. 5, curve (b)).

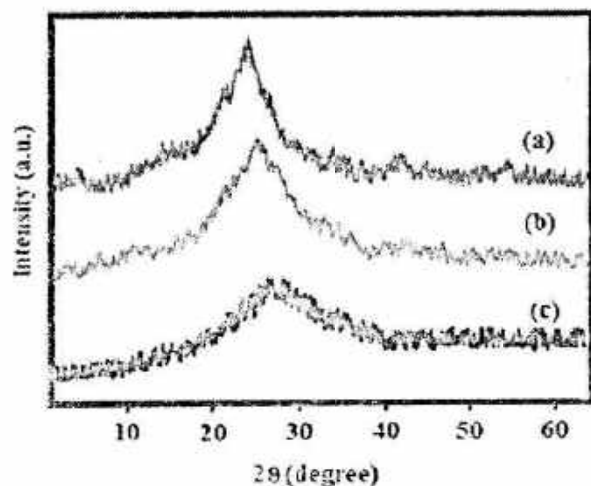


Figure 5. XRD patterns of GR (curve (a)), PPY/GR composite (curve (b)) and pure PPY (curve (c)).

Thus the XRD result indicates successful incorporation of GR in the polymer matrix.

Morphology and structure

The structure of the PPY, GR and PPY/GR composites was investigated using SEM and TEM. In the SEM image of GR a layered wrinkle-like structure is observed (Fig. 6(a)). Pure PPY exhibits a sphere-like structure (Fig. 6(b)) which is obtained as the polymerization is initiated at the interface between the two immiscible liquids. In case of the PPY/GR composite, the sphere-like structure of PPY disappears and a wrinkled multilayered structure is observed (Figs 6(c), 6(d)). This change in structure of the composite can be attributed to the polymerization of PPY on the surface of GR sheets.

TEM images for GR and PPY/GR composite are shown in Fig. 7. The TEM image of GR (Fig. 7(a)) shows a crumpled and agglomerated sheet-like structure over hundreds of nanometres. The wrinkled structure observed in the TEM image of GR sheets is due to the rapid removal of intercalated functional groups in GO during exfoliation.¹⁴ From the TEM image of the PPY/GR composite (Fig. 7(b)) it is observed that the exfoliated GR sheets are decorated by PPY nanoparticles, leading to the formation of well-dispersed composite sheets. Also it is clear from the TEM image that the composite sheets are folded with dark edges, thereby indicating the flexible character of the composite. GR acts as a template in the liquid–liquid interfacial polymerization, which results in the formation of such well dispersed flexible composite sheets.³³ These changes in structure of the composite from the individual components may introduce superior electrochemical properties. The structure of the PPY/GR composites obtained by liquid–liquid interfacial polymerization is quite different from structures described for earlier reported methods.^{15,16}

Thermogravimetric analysis

The thermal stability of PPY, PPY/GR composites and pure GR was studied by TGA. The TGA curves of pure PPY, GR and PPY/GR composites are shown in Fig. 8. GR exhibited around 20% weight loss in the temperature range 250–500 °C, which is attributed to removal of most of the oxygen-containing functional groups during the chemical reduction process. About 70% residual weight at 600 °C indicates the excellent thermal stability of GR (Fig. 8,

curve (a); Table 2). Pure PPY displays a major weight loss in the temperature range 250–500 °C and only 10% weight retention at 600 °C corresponds to complete degradation of the polymer (Fig. 8, curve (e)). PPY/GR composites exhibit a considerable enhancement in thermal stability on incorporation of GR (Fig. 8, curves (b)–(d)). In the case of the composites, major decomposition starts at higher temperatures compared with pure PPY. The major weight loss in the temperature range 250–500 °C can be attributed to decomposition of the PPY and functional groups of GR from the composite. Also, the weight retention value of the composites was found to be increased to 13%–35% at 600 °C compared with pure PPY. This residual weight is probably due to the existence of a carbon net structure in the composite.¹⁵

Measurements of electrical conductivity

The electrical conductivities of pure PPY and PPY/GR composites were determined using a four-point probe resistivity measurement system (Table 3). Pure PPY shows a conductivity of 0.210 S cm^{-1} . This value is lower than that of PPY synthesized by the electrochemical method ($10\text{--}50 \text{ S cm}^{-1}$)¹⁶ but higher than that of PPY synthesized by the chemical method using FeCl_3 as the oxidant (0.07 S cm^{-1}).³⁴ It is observed that incorporation of these highly conductive GR sheets (50.4 S cm^{-1}) into the PPY matrix greatly improved the conductivity of the composite. For GRPPY1, GRPPY2 and GRPPY3, the conductivities are 251, 4.52 and 8.45 S cm^{-1} respectively at room temperature (298 K). The increase in magnitude of the conductivity compared with pure PPY is perhaps due to the high aspect ratio and large specific surface area of the GR sheets which may act as effective percolative conducting bridges inside the composite system.

Electrochemical properties

Figure 9 illustrates the cyclic voltammogram (CV) of PPY and PPY/GR composites in $0.1 \text{ mol L}^{-1} \text{ LiClO}_4$ acetonitrile solution at 50 mV s^{-1} . The CV curve of pure PPY shows a couple of redox waves with a nearly rectangular shape (Fig. 9, curve (b)) which indicates the electrochemical double-layer capacitor character. The CVs of PPY/GR composites have large rectangular areas, indicating higher double-layer capacitances and better charge propagation within the electrode compared with PPY (Figs 9(c)–(e)). However, the CV of GR exhibits a much smaller rectangular area, perhaps due to its compact structure (Fig. 9, curve (a)). For PPY/GR composites the redox waves became wider, and shifted to more positive potentials compared with PPY. This is possibly due to the increased conductivity and surface area of the composite on introduction of GR.

The CV also gives us information about the electrochemical band gap of a system. The electrochemical band gap of the samples was calculated using the following formulae:³⁵

$$\text{HOMO} = -(\varphi_{\text{onset}}^{\text{ox}} + 4.71) \quad (5)$$

$$\text{LUMO} = -(\varphi_{\text{onset}}^{\text{red}} + 4.71) \quad (6)$$

$$E_{\text{ec}}^{\text{g}} = \varphi_{\text{onset}}^{\text{ox}} - \varphi_{\text{onset}}^{\text{red}} \quad (7)$$

where $\varphi_{\text{onset}}^{\text{ox}}$ and $\varphi_{\text{onset}}^{\text{red}}$ are the oxidation onset potential and reduction onset potential, respectively, and E_{ec}^{g} is the electrochemical band gap.

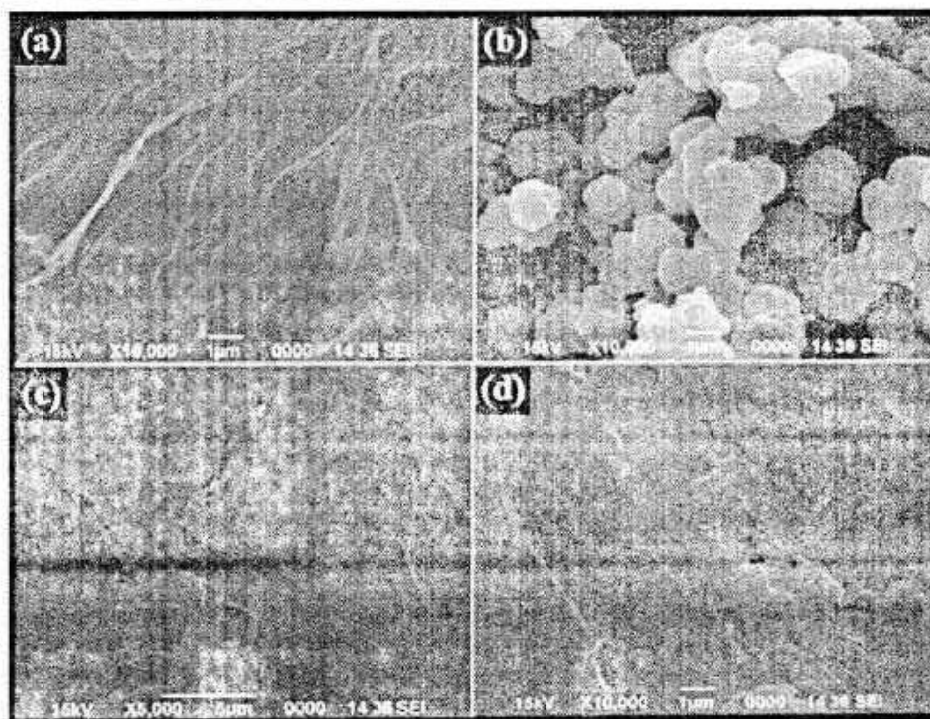


Figure 6. SEM images of (a) GR, (b) PPy, (c) PPy/GR composite at lower magnification and (d) PPy/GR composite at higher magnification.

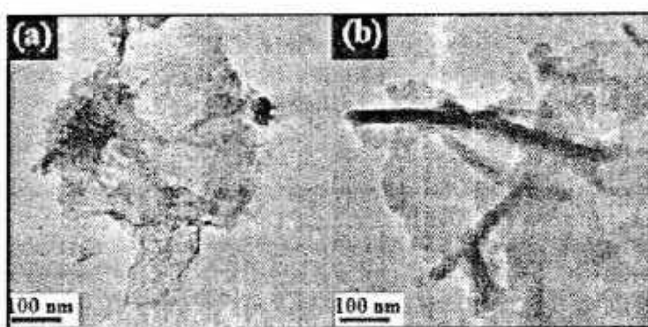


Figure 7. TEM images of (a) GR and (b) PPy/GR composite.

Sample	Weight loss (%) at				Major degradation temperature T_d ($^{\circ}\text{C}$)	Weight retention (%) at 600°C
	200°C	300°C	400°C	500°C		
PPy	10	20	44	75	240	10
GRPPy1	6	15	40	72	250	18
GRPPy2	4	10	36	65	265	24
GRPPy3	2	8	25	58	290	35
GR	1	10	15	25	310	70

The electrochemical band gap for PPy was calculated from the CV and was found to be 1.60 eV. The composites showed much lower band gaps (1.35 – 0.65 eV) compared with pure PPy. With an increase in the amount of GR in the PPy matrix the band gap decreases (Table 1). This may be due to changes in the electronic band structure of PPy/GR composites on incorporation of GR which manifests a new mid-gap state and thereby results in a decreasing band gap.

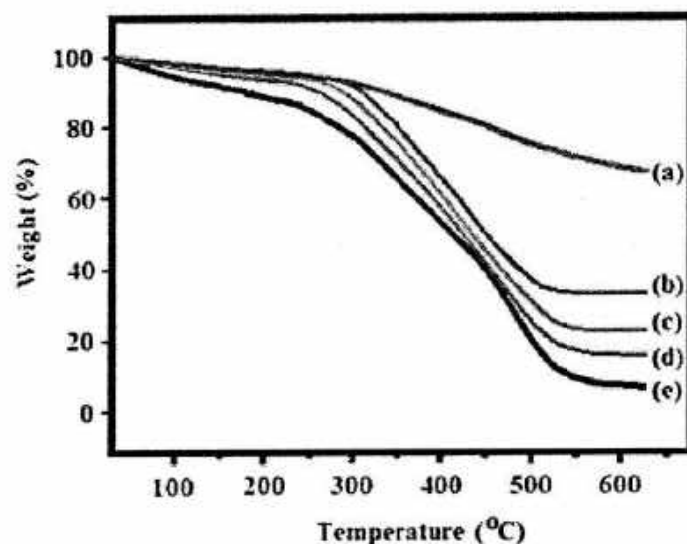


Figure 8. TGA curves of GR (curve (a)), PPyGR1 (curve (b)), PPyGR2 (curve (c)), PPyGR3 (curve (d)) and PPy (curve (e)).

The electronic properties, optical properties and electrical conductivity of conjugated polymers are affected by the band gap parameter. In our work we compared the optical band gap data with the electrochemical band gap of PPy and PPy/GR composites. The electrochemical determination of the band gap actually reveals the formation of charge carriers, while the optical transition does not lead to the formation of free charge carriers as the excited state in conjugated polymers may be viewed as a bound exciton. The band gaps of PPy/GR composites are found to be 2.10–1.82 eV (optically) and 1.35–0.65 eV (electrochemically). Thus it is observed that the composites showed lower electrochemical band gap values than optical band gaps; however, in both methods the same trend of band gap is observed.

Table 3. Conductivity measurements

Sample	Thickness d (cm)	Resistivity ρ (Ω cm)	Conductivity σ (S cm $^{-1}$)
PPy	0.3	5.07	0.210
GRPPy1	0.3	0.340	2.510
GRPPy2	0.3	0.210	4.520
GRPPy3	0.3	0.126	8.450
GR	0.3	0.021	50.400

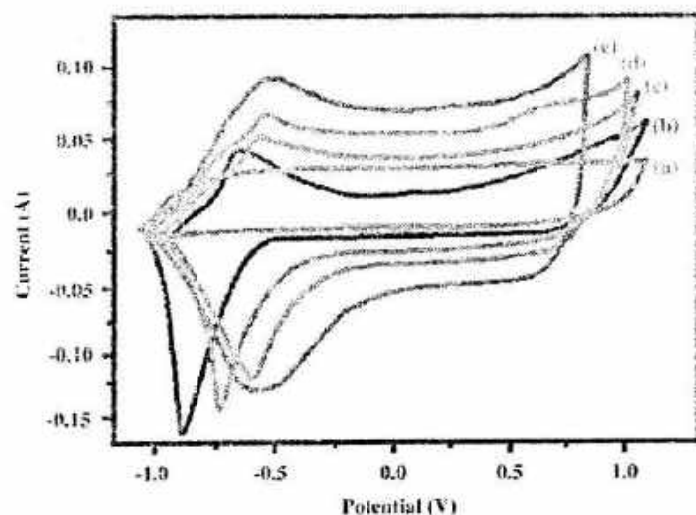


Figure 9. Cyclic voltammograms of GR (curve (a)), PPy (curve (b)), GRPPy1 (curve (c)), GRPPy2 (curve (d)) and GRPPy3 (curve (e)) at a scan rate of 50 mV s^{-1} .

The introduction of GR sheets can significantly improve the cycling stability of the composites due to the homogeneous dispersion of GR sheets in the PPy matrix. The composite was exposed to cyclic oxidation and reduction up to 100 cycles (Fig. 10). The curve exhibits clear redox peaks for the first cycle and as the cycling increases the peak shape becomes weaker and broader. However, there was no significant change in redox potential and the composite was quite stable even up to 100 repeated cycles indicating a good cycling performance. This improved stability of the composites is mainly due to the synergistic effect of GR and PPy in the composite. This result indicates that the composite bears a good application potential for rechargeable batteries.³⁶

Galvanostatic charge–discharge study

Galvanostatic charge–discharge behaviour was investigated to study the capacitance of the samples. Figure 11 demonstrates the galvanostatic charge–discharge curves of PPy and PPy/GR composite with a potential window from 0.0 to 1.0 V at a current density of 100 mA g^{-1} . The mass of active material used for the PPy and PPy/GR electrodes was 5 mg. The charge–discharge curves of PPy and PPy/GR composite electrodes are nearly triangular in shape, implying that the capacitance is mainly attributed to pure electrical double-layer capacitance.^{15,23} Compared with PPy, the PPy/GR composite exhibited longer discharge times at the same current density.

The PPy/GR composite shows a much higher specific capacitance value of 260 F g^{-1} compared with pure PPy (65 F g^{-1}). This increase in the specific capacitance of the composite is possibly

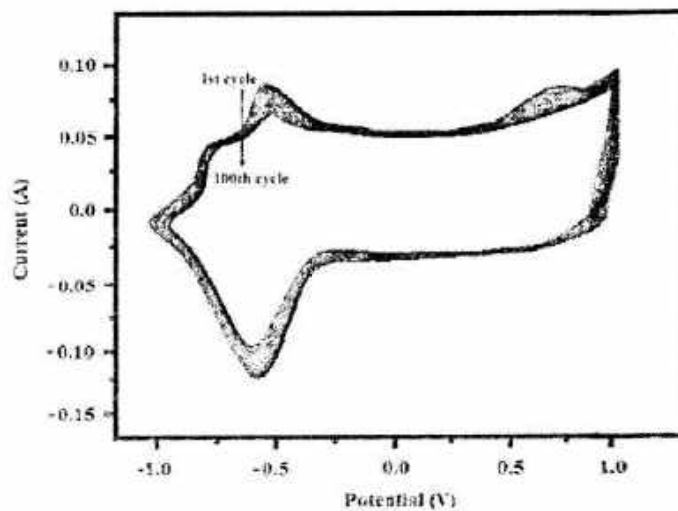


Figure 10. Successive electrochemical cycles of the PPy/GR (3 wt%) composite up to 100 cycles.

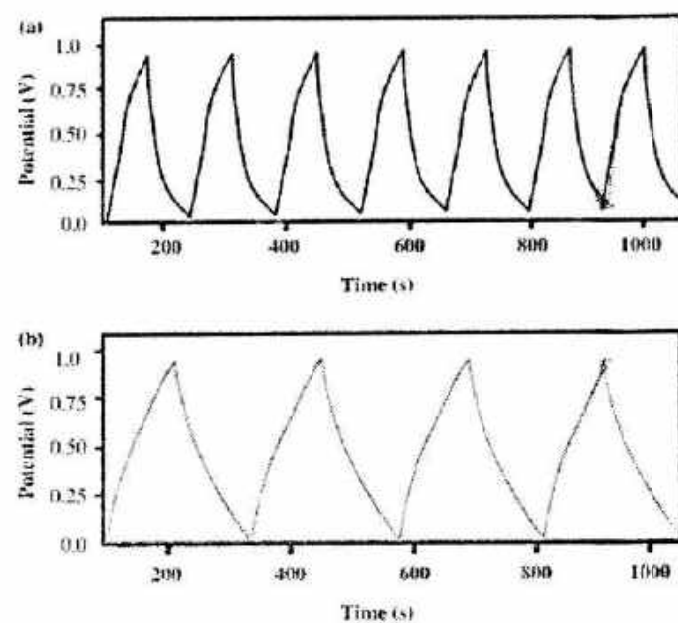


Figure 11. Galvanostatic charge–discharge curves of (a) PPy and (b) PPy/GR (3 wt%) composite at a current density of 100 mA g^{-1} .

due to the following factors. First, the incorporation of highly conductive GR favours the redox reaction of the PPy component, thereby increasing the pseudo-capacitance of PPy. Second, the presence of GR sheets within the PPy matrix greatly improves the double-layer capacitance of the composite by forming a porous structure which has a high specific surface area. We compared the specific capacitances of PPy/GR composites with some previous reports. Biswas *et al.*³⁷ synthesized nanocomposites based on GR nanosheets and PPy nanowire and obtained a specific capacitance value of 165 F g^{-1} . Bose *et al.*³⁸ developed a PPy/GR composite which exhibited a specific capacitance value of 267 F g^{-1} at a scan rate of 100 mV s^{-1} . Davies *et al.*³⁹ prepared a flexible, uniform PPy/GR composite by a pulsed electropolymerization technique which exhibited a specific capacitance value of 237 F g^{-1} . Thus it can be concluded that the specific capacitance value of the composite synthesized by interfacial polymerization is higher than that of various previously reported PPy/GR composites synthesized by other methods.

CONCLUSIONS

PPy/GR composite with improved properties and homogeneous dispersion was successfully prepared by liquid – liquid interfacial polymerization. This method provided a novel route to GR-based composites. Both XRD and FTIR spectroscopic analysis indicate successful formation of the composite. In Raman spectra, the ratio of D and G band intensity of the composites was 1.156 indicating the presence of localized sp^3 defects within the sp^2 carbon network of GR sheets. TEM and SEM showed a uniform distribution of GR throughout the PPy matrix. The PPy/GR composite exhibited a noticeable improvement in thermal stability compared with pure PPy. Both the optical and electrochemical band gaps of the composites showed a decreasing trend on incorporation of GR. The PPy/GR composites exhibit a high value of conductivity which may be attributed to the high aspect ratio and large specific surface area of GR nanosheets present within the polymer matrix. The composite shows a reversible electrochemical response and good cycling stability even up to 100 cycles. A charging – discharging study also reveals a consistent high capacitance value (260 F g^{-1}) for the PPy/GR composite at 100 mA g^{-1} . Thus, liquid – liquid interfacial polymerization has been found to be an effective method to fabricate PPy/GR composites which have vast application potential in supercapacitors, biosensors and many other fields.

ACKNOWLEDGEMENTS

The authors would like to thank the Council of Scientific and Industrial Research (CSIR) India for their financial support in the research under contract no. 02(0066)/12/EMR-II. The financial support received from UGC under the SAP program and DST under the FIST program is kindly acknowledged by the authors. The authors are also grateful to Professor S. K. Samdarshi (Department of Energy, Tezpur University) and Mr Ranjit G. Nair for the charge – discharge test.

REFERENCES

- Novoselov KS, Geim AK, Morozov SV, Jiang D, Zhang Y and Dubonos SV, *Science* **306**: 666–669 (2004).
- Kim H, Abdala AA and Macosko CW, *Macromolecules* **43**: 6515–6530 (2010).
- Allen MJ, Tung VC and Kaner RB, *Chem Rev* **110**: 132–145 (2010).
- Zhu Y, Murali S, Cai W, Li X, Suk JW and Potts JR, *Adv Mater* **22**: 3906–3924 (2010).
- Mishra AK and Ramaprabhu S, *J Phys Chem C* **115**: 14006–14013 (2011).
- Gomez H, Ram MK, Alvi F, Villalba P, Stefanakos EL and Kumar A, *J Power Sources* **196**: 4102–4108 (2011).
- Kuilla T, Bhadrab S, Yao D, Kim NH, Bose S and Lee JH, *Prog Polym Sci* **35**: 1350–1375 (2010).
- Potts JR, Dreyer DR, Bielawski CW and Ruoff RS, *Polymer* **52**: 5–25 (2011).
- Rao CNR, Sood AK, Subrahmanyam KS and Govindaraj A, *Angew Chem Int Ed* **48**: 7752–7757 (2009).
- Wang S, Tambraparni M, Qiu J, Tipton J and Dean D, *Macromolecules* **42**: 5251–5255 (2009).
- Fang M, Wang KG, Yang YL and Nutt S, *J Mater Chem* **19**: 7098–7105 (2009).
- Stankovich S, Dikin, Dommett GHB, Kohlhaas KM, Zimney EJ and Stach EA, *Nature* **442**: 282–286 (2006).
- Wu TM, and Lin SH, *J Polym Sci Polym Chem* **44**: 6449–6457 (2006).
- Zhang D, Zhang X, Chen Y, Yu P, Wang C and Ma Y, *J Power Sources* **196**: 5990–5996 (2011).
- Bose S, Kuilla T, Uddin ME, Kim NH, Lau T and Lee JH, *Polymer* **51**: 5921–5928 (2010).
- Liu A, Chun L, Bai H and Shi G, *J Phys Chem C* **114**: 22783–22789 (2010).
- Dallas P, Niarchos D, Vrbancic D, Boukos N, Pejovnik S, Trapalis C *et al.*, *Polymer* **48**: 2007–2013 (2007).
- Wu Q, Xu Yu, Yao Z, Liu A and Shi G, *ACS Nano* **4**: 1963–1970 (2010).
- Li XG, Li J, Meng QK and Huang MR, *J Phys Chem B* **113**: 9718–9727 (2009).
- Hummers WS and Offeman RE, *J Am Chem Soc* **80**: 1339 (1958).
- Sahoo S, Karthikeyan G, Nayak GC and Das CK, *Synth Met* **161**: 1713–1719 (2011).
- Chang HH, Chang CK, Tsai YC and Liao CS, *Carbon* **50**: 2331–2336 (2012).
- Zhang LL, Zhao S, Tian XN and Zhao XS, *Langmuir* **26**: 17624–17628 (2010).
- Patole AS, Patole SP, Kang H, Yoo JB, Kim TH and Ahn JHJ, *Colloid Interface Sci* **350**: 530–537 (2010).
- Zhao X, Zhang Q and Chen D, *Macromolecules* **43**: 257–2363 (2010).
- Konwer S, Maiti J and Dolui SK, *Mater Chem Phys* **128**: 283–290 (2011).
- Deng J, Peng Y, He C, Long X, Li P and Chan AS, *Polym Int* **52**: 1182–1187 (2003).
- Tsai FC, Chang CC, Liu CL, Chen WC and Jenekhe SA, *Macromolecules* **38**: 1958–1966 (2005).
- Kudin KN, Ozbas B, Schniepp HC, Prudhomme RK, Aksay IA and Car R, *Nano Lett* **8**: 36–41 (2008).
- Ren L, Liu T, Guo J, Guo S, Wang S and Wang W, *Nanotechnology* **21**: 335701–335708 (2010).
- Tsai F, Chang CC, Liu CL, Chen WC and Jenekhe SA, *Macromolecules* **38**: 1958–1966 (2005).
- Stankovich S, Dikin DA, Piner RD, Kohlhaas KA, Kleinhammes A and Jia Y, *Carbon* **45**: 1558–1565 (2007).
- Hao Q, Wang H, Yang X, Lu L and Wang X, *Nano Res* **4**: 323–333 (2011).
- Tsang SC, Chen YK and Green MLH, *Nature* **372**: 159–162 (1994).
- Konwer S, Boruah R and Dolui SK, *J Electron Mater* **40**: 2248–2255 (2011).
- Ghanbari K, Mousavi MF, Shamsipur M and Karami H, *J Power Sources* **170**: 513–517 (2007).
- Biswas S and Drazal LT, *Chem Mater* **22**: 5667–5671 (2010).
- Bose S, Kim NH, Kulia T, Lau L-t and Lee JH, *Nanotechnol* **22**: 295202 (2011).
- Davies A, Audette P, Farrow B, Hassan F, Chen Z and Choi J-Y, *J Phys Chem C* **15**: 17612–17620 (2011).

Synthesis of polythiophene/graphene oxide composites by interfacial polymerization and evaluation of their electrical and electrochemical properties

Chandramika Bora, Rupa Pegu, Bhaskar J Saikia and Swapan K Dolui*

Abstract

We report a new method for the synthesis of polythiophene (PTh)/graphene oxide (GO) nanocomposites by interfacial polymerization. Polymerization occurred at the interface of two immiscible solvents, i.e. *n*-hexane containing thiophene and nitromethane containing GO and an initiator. Characterizations were done using Fourier transform infrared spectroscopy, ultraviolet–visible spectroscopy, X-ray diffraction, scanning electron microscopy, thermogravimetric analysis, and electrochemical and electrical conductivity measurements. Spectroscopic analyses showed successful incorporation of GO in the PTh matrix. Morphological analysis revealed good dispersion of GO sheets in the polymer matrix. The PTh/GO composites showed marked improvements in thermal stability and electrical conductivity ($2.7 \times 10^{-4} \text{ S cm}^{-1}$) compared to pure PTh. The composites exhibited excellent electrochemical reversibility compared to pure PTh at a scan rate of 0.1 V s^{-1} . The composites were stable even up to 100 electrochemical cycles, indicating good cycle performance. The specific capacitance of the composites was calculated using cyclic voltammetry and was found to be 99 F g^{-1} .

© 2014 Society of Chemical Industry

Keywords: graphene oxide; polythiophene; electrical conductivity; electrochemical properties

INTRODUCTION

Conducting polymers such as polyaniline, polypyrrole and polythiophene (PTh) have received special attention from researchers due to their excellent electronic, magnetic and optical properties.¹ Among them, PTh is considered as one of the most promising materials due to its low cost, high environmental stability, good electrical conductivity and other specific properties. It has large areas of applications in electronics, photovoltaic cells, electrocatalysis, corrosion protection, sensors and actuators.^{2,3} A variety of nanofillers such as metals and metal oxides has been introduced into the PTh matrix for various improvements in properties including electrical conductivity and thermomechanical properties.^{4,5} In the last few years, carbon-based fillers such as carbon nanotubes, carbon black and carbon fibres in conducting polymer nanocomposites have been widely studied due to their outstanding electrochemical, thermal and mechanical properties.⁶ Karim *et al.*⁷ synthesized PTh/single-wall carbon nanotube composites using the *in situ* polymerization method. The composites showed good improvement in thermal as well as electrical conductivity (0.41 S cm^{-1}) compared to pure PTh. Wang *et al.*⁸ synthesized ordered PTh/fullerene composite core–shell nanorod arrays using melt-assisted wetting of porous alumina templates. The composites showed good application potential in solar cells. Zhao *et al.*⁹ synthesized an electromagnetic material of graphene nanosheet/PTh composites prepared using the *in situ* chemical polymerization method. The composites exhibited clear hysteretic behaviour as well as having the characteristics of a semiconductor.

Recently, graphene oxide (GO) has created a new era of carbon-filled nanocomposites owing to its superior mechanical, structural and thermal properties, and is preferred over other expensive fillers like carbon nanotubes.¹⁰ GO is an oxidized form of graphene, with various oxygen functional groups (i.e. hydroxyl, epoxide and carboxyl groups) on its basal planes. It is synthesized from low-cost graphite and imparts strong hydrophilicity to and has good compatibility with polymers which makes it attractive as a filler for the production of polymer nanocomposites. Nowadays nanocomposites based on conducting polymers with GO are widely studied to develop materials with excellent properties and good applicability.^{11,12} However, few studies have been reported of GO-based PTh nanocomposites so far, and mostly they are prepared using the solution polymerization method.¹³

In the work reported in the present paper, we developed a novel method to prepare PTh/GO composites by liquid/liquid interfacial polymerization. Interfacial polymerization is considered as a more simple, easy and controllable process than conventional polymerization techniques.¹⁴ Synthesis of polymers can be done at room temperature and higher molecular weight polymers

* Correspondence to: Swapan K Dolui, Department of Chemical Sciences, Tezpur University, Napaam, Tezpur, Assam 784028, India.
E-mail: swapankdolui@gmail.com

Department of Chemical Sciences, Tezpur University, Napaam, Tezpur, Assam 784028, India

can be obtained using this technique compared to bulk condensation polymerization. Also, in our previous work, we prepared polypyrrole/GO composites using the same route,¹⁵ which showed improved electrical, thermal and electrochemical properties. The work reported here was focused on getting a homogeneous dispersion of GO sheets in a PTh matrix and obtaining improved thermal, electrical and electrochemical properties compared to the pure polymer.

EXPERIMENTAL

Materials

Graphite flakes were purchased from Carbon India Ltd, Guwahati. Sodium nitrate (Merck), sulfuric acid (Merck), potassium permanganate (Merck), hydrogen peroxide (Qualigens Fine Chemicals) and ferric chloride (Aldrich) were used as received. Thiophene monomer was purchased from Sigma Aldrich. All solvents were of analytical grade and used without purification.

Preparation of GO

GO was prepared from natural graphite using the method of Hummers and Offeman.¹⁶ KMnO_4 and H_2SO_4 were used as oxidizing agents. The product was purified by washing many times with HCl (5%) and deionized water. After purification, the product was ultrasonicated for 1 h and thus a well-exfoliated GO dispersion was obtained.

Preparation of PTh/GO composites

PTh/GO composites of various weight percentages of GO to thiophene (1, 2 and 3%) were prepared by liquid/liquid interfacial polymerization and were labelled as PTGO1, PTGO2 and PTGO3. The interfacial polymerization was done as follows. The required amount of GO was dispersed in 20 mL of CH_3NO_2 (solvent) using an ultrasonicator. Then FeCl_3 (2.44 g) was added to the dispersion and mixed thoroughly. The solution as obtained was added dropwise into a thiophene (0.4 mL) solution in 10 mL of *n*-hexane and the mixture was continuously stirred for 24 h. The product was obtained from the reaction mixture by centrifugation and then washed with ethanol for purification. Finally, the powdery composite was dried at 60 °C for 24 h.

Characterization

Fourier transform infrared (FTIR) spectra were obtained using a Nicolet Impact 410 spectrophotometer in the frequency range 500–4000 cm^{-1} at room temperature. UV-visible spectra of GO, PTh and PTh/GO composites in *N*-methyl-2-pyrrolidone were recorded with a Shimadzu UV-2550 UV-visible spectrophotometer. XRD was done using a Rigaku X-ray diffractometer with $\text{Cu K}\alpha$ radiation at a scan rate of 0.05° s^{-1} . SEM analysis was done with a JSM-6390LV instrument (JEOL, Japan). The surface of samples was coated with platinum before SEM analysis. Transmission electron microscopy (TEM) analysis was performed with a Philips CM 200 TEM microscope. A small amount of powdery sample was dispersed in ethanol for TEM analysis. Then, the suspension was dropped on 300 mesh copper TEM grids covered with thin carbon films. TGA was carried out with a Shimadzu TGA 50 (Japan) thermal analyser in the temperature range 25–700 °C at a heating rate of 10 °C min^{-1} under nitrogen flow. To measure the electrical conductivity, pellet-shaped (1.5 cm diameter, 2 mm thick) composite samples were made using a compression-moulding

machine at a high pressure (1–2 tonnes). To measure the electrical conductivity of PTh and PTh/GO composites, the four-probe technique was used in the temperature range 300–400 K. The electrical conductivity (σ , S cm^{-1}) of the composite was calculated using the following equations:¹⁷

$$\rho = \frac{V}{I} \times 2\pi S \quad (1)$$

$$\sigma = \frac{1}{\rho} \quad (2)$$

where ρ ($\Omega \text{ cm}$) is the resistivity of the sample, I is the measured current, V is the applied voltage and S is the distance between the probes. The electrochemical properties of the prepared samples were analysed using a Sycopel AEW2-10 cyclic voltammeter. The capacitances were calculated with the following equation:¹⁸

$$C_{\text{sp}} = \frac{I_+ - I_-}{v \times m} \quad (3)$$

where I_+ and I_- are maximum currents in positive and negative voltage scans, respectively, v is the scan rate (50 mV s^{-1}) and m is the mass of the composite material (10 mg).

RESULTS AND DISCUSSION

The method of preparation of the PTh/GO composites by interfacial polymerization is shown in Fig. 1. In this method, monomer thiophene is dissolved in *n*-hexane forming the organic phase and GO along with the oxidant ferric chloride is dissolved in CH_3NO_2 which forms the aqueous phase. The polymerization occurs at the interface between these two immiscible phases. After 24 h of constant stirring, black-coloured PTh microparticles are obtained as a suspension in CH_3NO_2 which are further washed and dried. The process is controllable, slow and the separation of the product is easy due to its insolubility in both aqueous and organic phases.

FTIR analysis

FTIR spectra of PTh, GO and PTh/GO composite are shown in Fig. 2. In the PTh spectrum, a broad band appears at around 3423 cm^{-1} which is due to the O–H stretching vibration (Fig. 2(a)). The bands at 2923, 1640 and 1426 cm^{-1} are ascribed to C–H stretching vibration and C=C asymmetric and symmetric stretching vibrations of thiophene units, respectively.¹⁹ The band at 1167 cm^{-1} is assigned to C–H (in-plane) bending vibration of thiophene. A band at 790 cm^{-1} appears due to C–H (out-of-plane) bending vibration of thiophene units indicating the α -position linkage between the thiophene rings. Moreover, the bands at 830 and 692 cm^{-1} may be assigned to C–S stretching and C–S–C bending vibrations indicating the presence of thiophene rings.²⁰ The FTIR spectrum of GO (Fig. 2(c)) shows a broad peak at 3409 cm^{-1} for O–H stretching and a peak at 1719 cm^{-1} which can be assigned to the carbonyl (C=O) stretching vibration. The peak at 1066 cm^{-1} for C–O stretching vibration appears due to the presence of the epoxide group in the GO layers. The peaks at 1236 and 1411 cm^{-1} can be ascribed to the C–OH stretching vibration and O–H deformation, respectively.²¹ The FTIR spectrum of PTh/GO composite (Fig. 2(b)) shows almost the same bands as that of PTh; however, the bands are shifted to longer wavelength. Also a peak near 1720 cm^{-1} for the carbonyl (C=O) stretching vibration appears in the spectrum of the composite which is absent in that of pure polymer.

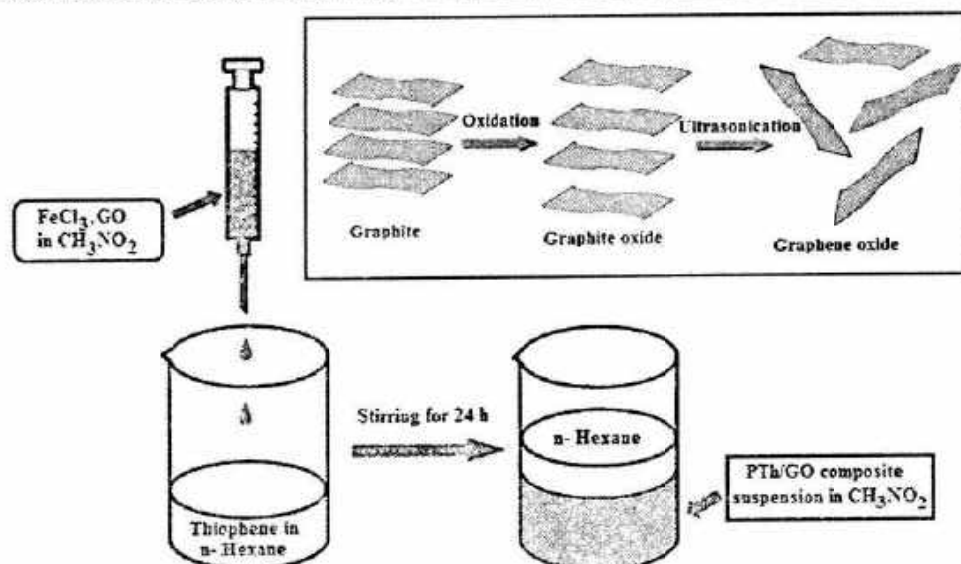


Figure 1. Fabrication process for PTh/GO composites.

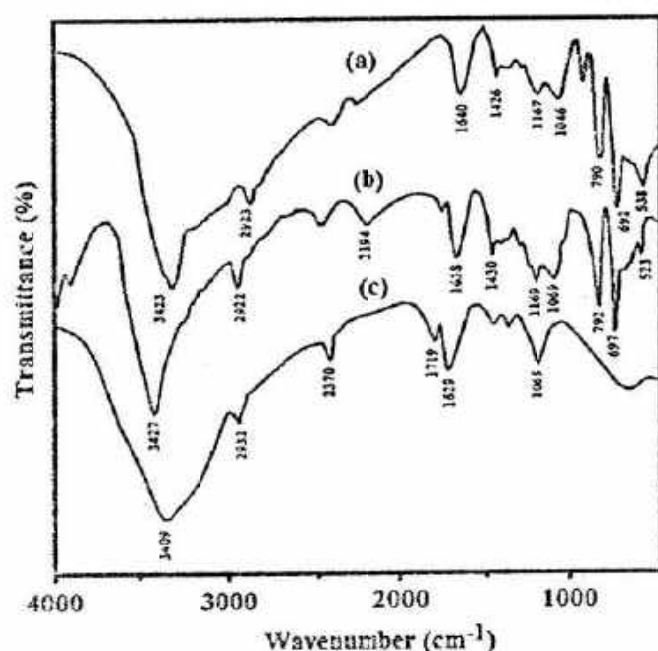


Figure 2. FTIR spectra of (a) PTh, (b) PTh/GO composite and (c) GO.

Thus the FTIR results show characteristic peaks of both the components and thereby reveal the successful incorporation of GO in the PTh matrix.

UV-visible analysis

UV-visible spectra of the samples are shown in Fig. 3. A characteristic absorption peak of GO is observed at 236 nm.²² The spectrum of PTh shows a strong band at 260 nm which is attributed to the $\pi-\pi^*$ transition of the 2,5-thiophenylene unit.²³ An additional broad band appears at around 435 nm which is related to the bipolaron state of PTh. Similar peaks are observed for the PTh/GO composites (Figs 3(c)–(e)). The peaks at 264–270 nm indicate the $\pi-\pi$ interaction between PTh and GO of the composite. A band at around 441–460 nm (2.15–2.01 eV) is also observed which confirms the bipolaron state of PTh in the composite. The absorption bands of PTh/GO nanocomposites show a red shift in the ranges for

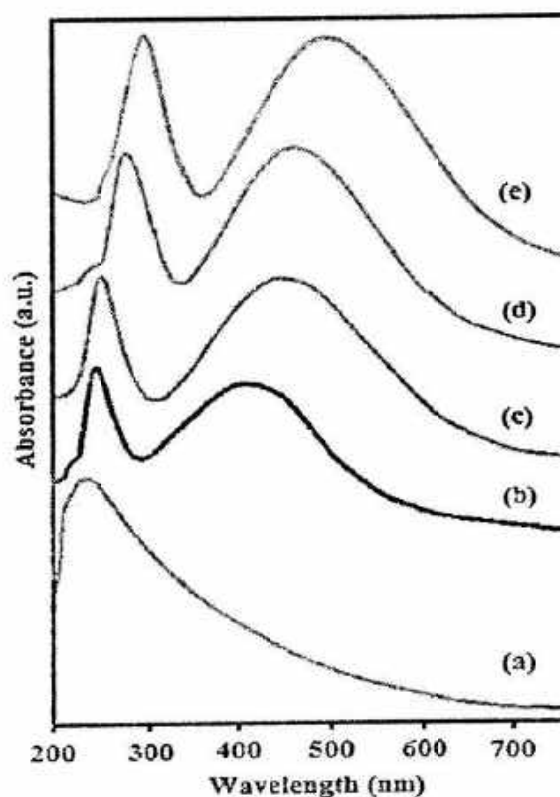


Figure 3. UV-visible spectra of (a) GO, (b) PTh, and composites (c) PTGO1, (d) PTGO2 and (e) PTGO3.

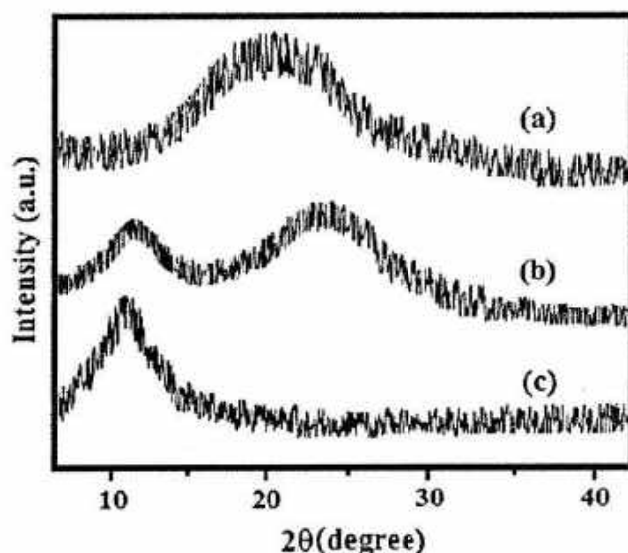
the $\pi-\pi^*$ transition and for the polaron–bipolaron band transition with increasing GO percentage. This shifting results from the $\pi-\pi$ stacking between polymer chains and GO sheets. Incorporation of GO extends the conjugation length of PTh chains.

In conjugated polymers, the optical absorption may be attributed to the transition of charge carriers, through a forbidden energy gap. The optical band gaps are calculated from the following equation²⁴ and are listed in Table 1:

$$E_g^{\text{opt}} = \frac{1240}{\lambda_{\text{edge}}} \quad (4)$$

Table 1. Electrochemical and optical data for PTh and PTh/GO composites

Sample	$\varphi_{\text{onset}}^{\text{ox}}/ E_{\text{HOMO}}$	$\varphi_{\text{onset}}^{\text{red}}/ E_{\text{LUMO}}$	E^{gc} (eV)	λ_{edge} (nm)	E^{opt} (eV)
PTh	1.30/−6.01	−1.10/−3.61	2.40	556	2.23
PTGO1	1.13/−5.84	−1.10/−3.61	2.23	575	2.15
PTGO2	1.10/−5.81	−1.06/−3.65	2.16	593	2.09
PTGO3	1.08/−5.79	−0.99/−3.72	2.07	615	2.01

**Figure 4.** XRD patterns of (a) pure PTh, (b) PTh/GO composite and (c) GO.

where E_g^{opt} (eV) is the optical band gap and λ_{edge} (nm) is the absorption edge. Pure PTh shows a band gap of 2.23 eV. In the PTh/GO composites, the band gap decreases from 2.15 to 2.01 eV on increasing the GO content.

XRD analysis

The XRD patterns of GO, PTh/GO composite and pure PTh are presented in Fig. 4. The XRD pattern of GO (Fig. 4(c)) shows a strong peak at $2\theta = 11.46^\circ$ corresponding to (001) reflection peak.²⁵ Pure PTh exhibits a broad diffraction peak at $2\theta = 22^\circ$ (Fig. 4(a)) indicating the amorphous nature of the polymer. For the PTh/GO composite, the characteristic broad peak of PTh appears at $2\theta = 23.5^\circ$ (Fig. 4(b)) indicating the presence of PTh in the composite. Also a peak appears at $2\theta = 11.6^\circ$ which indicates the presence of GO in the composite. Thus the XRD analysis indicates the interactions between GO and PTh.

Morphological analysis

The surface morphologies of GO, PTh and PTh/GO composites were investigated using SEM. In the SEM image of GO (Fig. 5(a)), a multilayered sheet structure is observed which is in accordance with an earlier report.²⁶ The SEM image of pure PTh shows a granular structure of a few micrometres (Fig. 5(b)). This granular morphology vanishes and an uneven, flaky morphology is observed in the composites (Fig. 5(c)) indicating successful polymerization of PTh on the GO sheets.

Figure 6 shows TEM images of GO and PTGO3 composite. In the TEM image of GO, a layered structure of GO sheets of a

few micrometres in dimension is observed (Fig. 6(a)). In the TEM image of the composite (Fig. 6(b)), some spherical structures of PTh decorating the surface of the GO sheets are observed which indicate the formation of PTh chains on the surface of the GO sheets. These changes in morphology as obtained from TEM and SEM results indicate the possibility of improved electrochemical properties of the composites on the introduction of GO.

Thermogravimetric analysis

The thermal stability of the samples was investigated using TGA. The TGA curves of GO, PTh and PTh/GO composites are shown in Fig. 7 and the corresponding data are summarized in Table 2. The TGA curve of pure PTh (Fig. 7(a)) shows that PTh is stable up to 200 °C. Major degradation then starts at 240 °C which is due to the thermal decomposition of PTh. In the TGA curve of GO, major weight loss occurs in the temperature range 200–300 °C, which is due to the removal of most of the oxygen functionalities (Fig. 7(e)). For the composites, major degradation starts at higher temperatures (248–260 °C) compared to pure PTh. Further, it is observed that the weight retention of the PTGO3 composite increases up to 19% on incorporation of GO compared to pure PTh which shows only 4% weight retention at 600 °C. Thus from the TGA data, it is evident that both the decomposition temperature and the residual weight increase on incorporating GO. Hence we can say that by incorporating GO in the PTh matrix the thermal stability of the polymer can be increased. The results are consistent with the earlier report of Karim *et al.*⁷

Electrical conductivity measurements

The DC electrical conductivities of the samples were measured using a four-point probe resistivity measurement system. The conductivity measurements were carried out on pellet-shaped samples pressed from powders. The average conductivity values are given in Table 3. Pure PTh shows a conductivity of $5.8 \times 10^{-5} \text{ S cm}^{-1}$. The conductivity of the resulting PTGO3 composite is $2.7 \times 10^{-4} \text{ S cm}^{-1}$ at room temperature, which is higher than that of pure PTh. The DC conductivity values of the composites are seen to increase with increasing GO content. This increase in conductivity may be attributed to the increased electron mobility arising from the π - π stacking between the GO layers and PTh within the composite system.

Electrochemical behaviour

Cyclic voltammetry (CV) was performed to study the electrochemical properties of the composites. Figure 8 shows the CV curves of PTh and PTh/GO composites in $0.1 \text{ mol L}^{-1} \text{ LiClO}_4$ -acetonitrile solution obtained at a scan rate of 50 mV s^{-1} . Platinum wire and Ag/AgCl were used as counter and reference electrodes, respectively. It is seen that the CV curves are almost rectangular in shape within the measured potential indicating good redox behaviour of the samples. The CV curves of the PTh/GO composites have large rectangular areas, indicating good electrochemical double-layer capacitances. Also the redox waves shift to more positive potentials compared to PTh. This is possibly due to the increased conductivity and surface area of the composites as a result of the introduction of GO.

We also determined the electrochemical band gap energies of the samples from CV data. The band gap of the samples was calculated using the following formulae:²⁷

$$\text{HOMO} = - \left[\varphi_{\text{onset}}^{\text{ox}} + 4.71 \right] \quad (5)$$

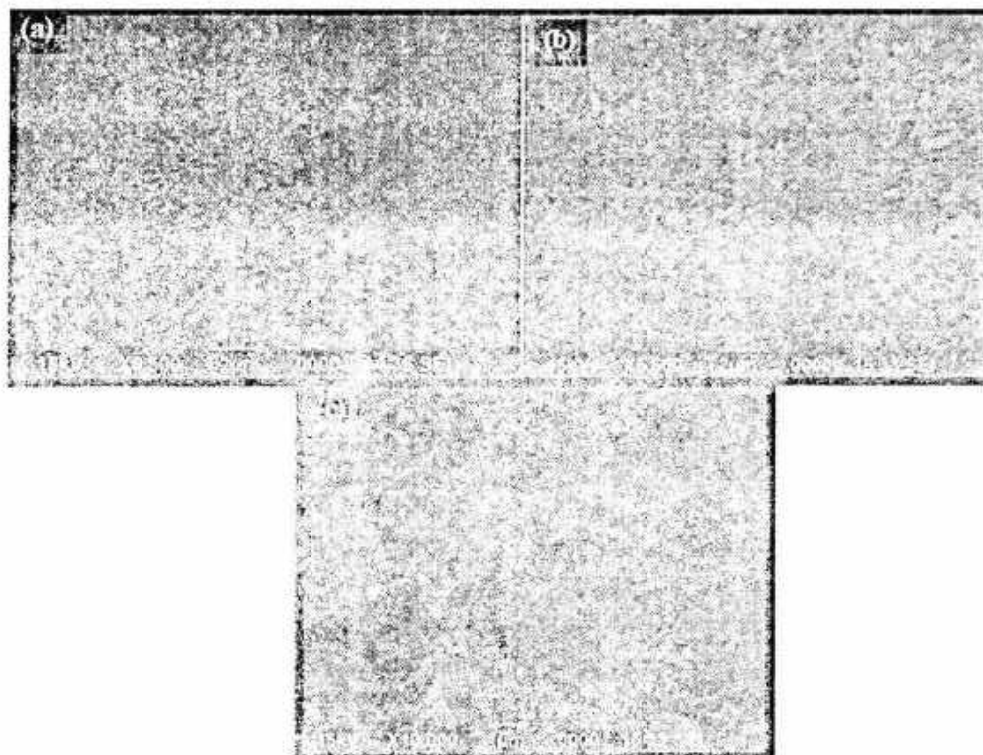


Figure 5. SEM images of (a) GO, (b) PTh and (c) PTh/GO composite.

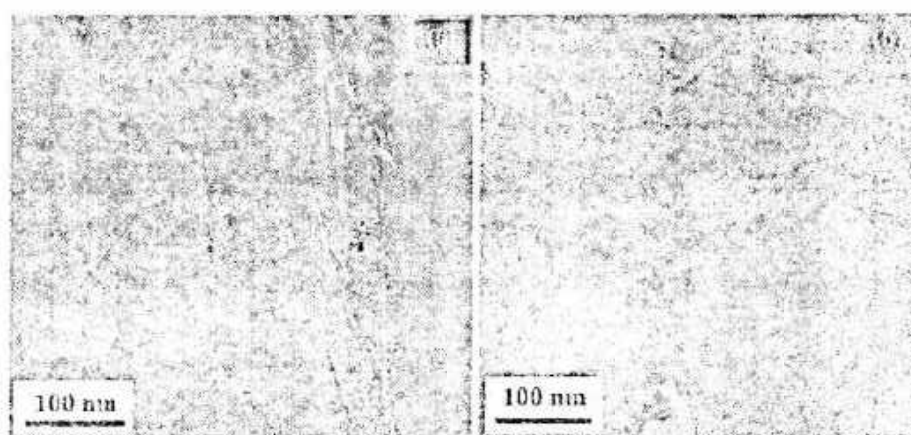


Figure 6. TEM images of (a) GO and (b) PTh/GO composite.

$$\text{LUMO} = -[\varphi_{\text{onset}}^{\text{red}} + 4.71] \quad (6)$$

$$E_{\text{ec}}^{\text{g}} = (\varphi_{\text{onset}}^{\text{ox}} - \varphi_{\text{onset}}^{\text{red}}) \quad (7)$$

where $\varphi_{\text{onset}}^{\text{ox}}$ and $\varphi_{\text{onset}}^{\text{red}}$ are the oxidation onset potential and reduction onset potential, respectively, and E_{ec}^{g} is the electrochemical band gap.

The electrochemical data obtained are summarized in Table 1. The electrochemical band gap for PTh is found to be 2.40 eV. The composites show much lower band gap value (2.07–2.33 eV) compared to pure PTh. The band gap decreases with increasing GO content in the composites. This decrease in band gap may be due to the changes in the electronic band structure of PTh/GO composites which demonstrates a new mid-gap state. We compare the optical band gaps with the electrochemical band gaps of PTh and PTh/GO composites. The electrochemical band gaps are found to be higher than the optical band gaps. The electrochemical band

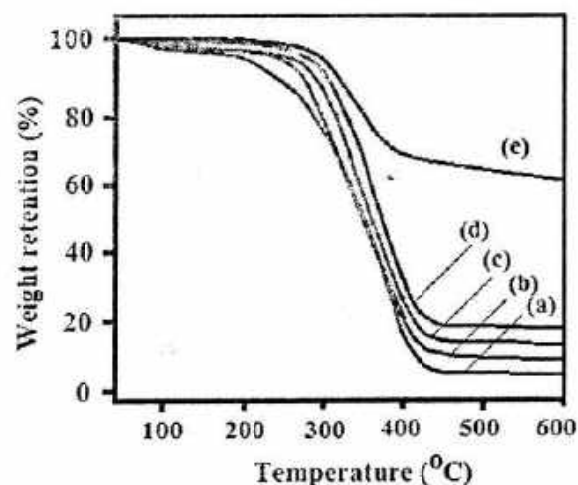


Figure 7. TGA curves: (a) PTh; (b) PTGO1, (c) PTGO2 and (d) PTGO3 composites; (e) GO.

Table 2. TGA data for PTh, GO and PTh/GO composites

Sample	Major degradation temperature, T_d (°C)	Weight loss (%)				Weight retention at 600 °C (%)
		200 °C	300 °C	400 °C	500 °C	
PTh	240	10	15	40	80	4
PTGO1	248	8	13	36	77	11
PTGO2	256	7	12	34	73	17
PTGO3	260	6	10	30	70	19
GO	266	1	25	30	35	60

Table 3. Electrical conductivity and specific capacitance of PTh and PTh/GO composites

Sample	Thickness, d (cm)	Resistivity, ρ (Ω cm)	Conductivity, σ (S cm $^{-1}$)	Specific capacitance (F g $^{-1}$)
PTh	0.3	4.90	5.8×10^{-5}	71
PTGO1	0.3	2.80	0.8×10^{-4}	84
PTGO2	0.3	2.36	1.2×10^{-4}	92
PTGO3	0.3	1.97	2.7×10^{-4}	99

gap actually reveals the formation of charge carriers, while in optical transitions no such charge carriers form as the excited state in conjugated polymers may be viewed as a bound exciton. Although, the optical band gap cannot be directly compared to the

electrical band gap, same trend of band gap is observed in both the cases.

The cycling performance of the composites was estimated by repeating the CV tests for 100 oxidation and reduction cycles at a scan rate of 10 mV s^{-1} (Fig. 9). The curves show clear redox peaks for the first cycle and, as the cycling increases, the peak shape becomes weaker and broader. However, the redox potentials remain same even up to 100 repeated cycles. This improved cycling stability of the composites is mainly due to the interaction of GO and PTh which restricts the change of network structure during cycling. Thus the composites exhibit good potential for application in capacitors and rechargeable batteries.²⁸

Charge capacity

The specific capacitances of PTh and the composites were measured from the CV curves (Fig. 8) and are given in Table 3. Pure

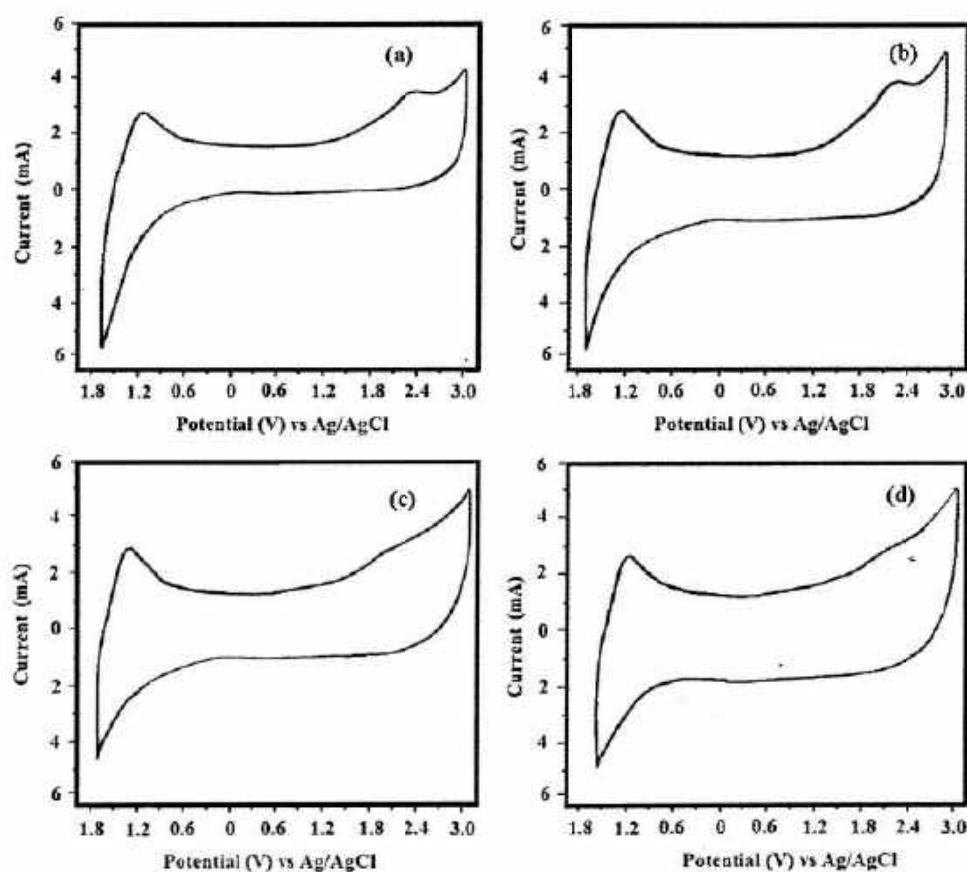


Figure 8. Cyclic voltammograms of (a) PTh, and (b) PTGO1, (c) PTGO2 and (d) PTGO3 composites obtained at a scan rate of 50 mV s^{-1} .

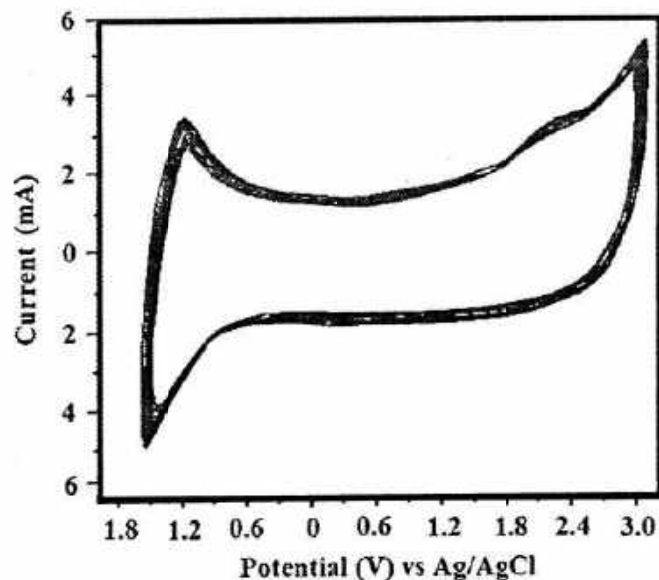


Figure 9. Successive electrochemical cycles of the PTGO3 composite up to 100 cycles.

PTh shows a specific capacitance value of 71 F g^{-1} . The PTGO3 composite exhibits a capacitance value of 99 F g^{-1} , which is much higher than that of pure PTh. The specific capacitance of the composites increases with increasing GO content. This is because the sheet-like structure of GO provides more active surfaces for facile oxidation–reduction reaction. Also, due to the increase in conjugation length (as evident from FTIR and UV-visible spectroscopic results) and conductivity of PTh on incorporation of GO, the specific capacitance of the composites increases.

CONCLUSIONS

PTh/GO nanocomposites have been successfully prepared by liquid/liquid interfacial polymerization. Both FTIR and XRD results indicate the incorporation of GO in the polymer matrix. SEM and TEM analyses indicate the uniform distribution of GO in the PTh matrix. The PTh/GO composites exhibited an improved thermal stability compared to pure PTh. Both optical and electrochemical band gaps of the composites were calculated and found to decrease dramatically on incorporation of GO into the polymer matrix. Electrical conductivity of the composites was found to be higher ($2.7 \times 10^{-4} \text{ S cm}^{-1}$ for PTGO3) than that of pure PTh. The composites showed reversible electrochemical response and a good cycling stability even up to 100 cycles. A specific capacitance value of 99 F g^{-1} (scan rate of 50 mV s^{-1}) was obtained for the PTGO3 composite. The present work shows that the PTh/GO composites prepared using the interfacial polymerization method possess great promise for a range of potential applications in batteries and optoelectronic devices.

ACKNOWLEDGEMENTS

The authors thank the Council of Scientific and Industrial Research (CSIR), India, for its financial support of the research under contract no. 02(0066)/12/EMR-II. The financial support received from UGC under SAP programme and DST under FIST programme is gratefully acknowledged by the authors.

REFERENCES

- Carswell ADW, O'Rear EA and Grady BP, *J Am Chem Soc* **125**:14793–14799 (2003).
- Sakurai Y, Jung HS, Shimanouchi T, Inoguchi T, Morita S and Kuboi R, *Sens Actuators B* **83**:270–274 (2002).
- Otsuka Y, Okamoto Y, Akiyama HY, Umekita K, Tachibana Y and Kuwabata S, *J Phys Chem C* **112**:4767–4772 (2008).
- Lu Q and Zhou Y, *J Power Sources* **196**:4088–4094 (2011).
- Uygun A, Yavuz AG, Sen S and Omastova M, *Synth Met* **159**:2022–2028 (2009).
- Wang SH, Chen SY, Su MH, Wang YL and Wei KH, *Nanotechnology* **21**:145203 (2010).
- Karim MR, Lee CJ and Lee MS, *J Polym Sci A: Polym Chem* **44**:5283–5290 (2006).
- Wang HS, Lin LH, Chen SY, Wang YL and Wei KW, *Nanotechnology* **20**:75201–75206 (2009).
- Zhao J, Xie Y, Le Z, Yu J, Gao Y, Zhong R et al., *Synth Met* **181**:110–116 (2013).
- Cassagneau T, Guerin F and Fendler JH, *Langmuir* **16**:7318–7324 (2000).
- Wang DW, Li F, Zhao JP, Ren WC, Chen ZJ and Tan J, *ACS Nano* **3**:1745–1752 (2009).
- Wei T, Luo GL, Fan ZJ, Zheng C, Yan J and Yao CZ, *Carbon* **47**:2290–2299 (2009).
- Wang S, Nai CT, Jiang XF, Pan Y, Tan CH, Nesladek M et al., *J Phys Chem Lett* **3**:2332–2336 (2012).
- Dallas P, Niarchos D, Vrbanic D, Boukos N, Trapalis SP and Petridis D, *Polymer* **48**:2007–2013 (2007).
- Bora C and Dolui SK, *Polymer* **53**:923–932 (2012).
- Hummers WS and Offeman RE, *J Am Chem Soc* **80**:1339 (1958).
- Konwer S, Maiti J and Dolui SK, *Mater Chem Phys* **128**:283–290 (2011).
- Sahoo S, Karthikeyan G, Nayak GC and Das CK, *Synth Met* **161**:1713–1719 (2011).
- Gok A, Omastova M and Yavuz AG, *Synth Met* **157**:23–25 (2007).
- Gao HX, Jiang T, Han BX, Wang Y, Du JM and Liu ZM, *Polymer* **45**:3017–3024 (2004).
- Jeong HK, Noh HJ, Kim JY, Jin MH, Park CY and Lee YH, *J Explor Front Phys* **82**:6700–6704 (2008).
- Wang H, Hao Q, Yang X, Lu L and Wang X, *ACS Appl Mater Interfaces* **2**:821–828 (2010).
- Li XG, Li J, Meng OK and Huang MR, *J Phys Chem B* **113**:9718–9727 (2009).
- Tsai FC, Chang CC, Liu CL, Chen WC and Jenekhe SA, *Macromolecules* **38**:1958–1966 (2005).
- Bose S, Kuila T, Uddin ME, Kim NH, Lau AT and Lee JH, *Polymer* **51**:5921–5928 (2010).
- Zhang LL, Zhao S, Tian XN and Zhao XS, *Langmuir* **26**:17624–17628 (2010).
- Pokhrel B and Dolui SK, *J Polym Mater* **26**:417–501 (2009).
- Zengin H and Ballato J, *Adv Mater* **14**:1480–1484 (2002).

Cite this: *RSC Adv.*, 2015, 5, 60763

Synthesis of copper oxide/reduced graphene oxide nanocomposite and its enhanced catalytic activity towards reduction of 4-nitrophenol†

Chandrama Sarkar and Swapan K. Dolui*

Graphene oxide (GO) and its derivatives have attracted extensive interest in many fields, including catalytic chemistry, organic synthesis, and electrochemistry. Integrating nanoparticles into GO enhances the properties and functionality of the nanocomposites due to the synergetic effects between GO nanosheets and the nanoparticles. A facile and novel hydrothermal method of preparing copper oxide-reduced graphene oxide (CuO-rGO) nanocomposites has been developed. The nanocomposites were prepared from a mixture of GO and cuprous chloride (CuCl). In this method simultaneous formation of CuO and reduction of GO takes place without using any foreign materials. The synthesized composites were characterized by Fourier transform infrared spectroscopy (FTIR), X-ray diffraction (XRD), scanning electron microscopy (SEM), and energy dispersive X-ray (EDX) spectroscopy. 4-Nitrophenol (4-NP) was used as a probe to assess the catalytic activities of the prepared CuO-rGO nanocomposites. The nanocomposites exhibited excellent and stable catalytic activity towards reduction of 4-NP to 4-aminophenol (4-AP) in the presence of NaBH₄. The catalytic activities of the nanocomposites were also studied by changing the ratio of GO and Cu. The reaction kinetics followed a pseudo-first-order rate law and the maximum value of the rate constant is 13.951 min⁻¹, which is superior to all other reported works. The catalyst can be easily regenerated and reused with good recyclability even for up to five catalytic cycles.

Received 3rd June 2015

Accepted 9th July 2015

DOI: 10.1039/c5ra10551j

www.rsc.org/advances

1. Introduction

Graphene (GR), a monolayer or few layers (<10) of hexagonally arrayed sp²-bonded carbon atoms, has attracted tremendous interest in recent years in many fields of science and engineering since it was first reported in 2004.^{1,2} This interest can be attributed to the extraordinary electrical, optical, thermal, mechanical and chemical properties of GR and its related carbon nanostructures.³⁻⁶ In addition, it possesses high thermal conductivity, excellent mobility of charge carriers, large specific surface area, good mechanical stability, good biocompatibility and high adsorption capacity.⁷⁻¹¹ To date, various synthetic strategies have been developed for producing GR such as micromechanical exfoliation, oxidation/reduction protocols, epitaxial growth, and chemical vapour deposition.^{12,13} GR and its derivatives have been used for a wide range of applications, including electrocatalysis,¹⁴ catalytic oxidation reaction,¹⁵ photocatalysis,¹⁶ memory devices,¹⁷ energy storage,¹⁸ solar cells,¹⁹ sensing platforms,²⁰ Raman enhancement²¹ and even drug

delivery.²² GO is the common choice over pristine GR owing to its facile synthetic nature in a controlled, scalable, and reproducible manner. Also, its abundant oxygen-containing functional groups such as epoxide, alcohol, and carboxylic acids provide GO with excellent aqueous dispersity and offer anchors for further chemical modifications.²³ In catalysis, GR-based materials are used as catalytic supports, due to their high electrical, thermal conductivity, great mechanical strength, huge specific surface area and good adsorption capacities. GO nanosheets are also emerging as promising supports for the creation of hybrid nanomaterials and, in particular, in catalytic applications.

Recently, a variety of metal, metal oxide, semiconducting, and magnetic nanoparticles including Pd,²⁴ Pt,²⁵ Au,²⁶ TiO₂,²⁷ and Fe₃O₄ (ref. 28) have been hosted on the surface of GO. Nanoparticles can act as spacers between GO nanosheets to minimize the agglomeration of them and can also prevent the aggregation of these active nanoblocks with high surface energy. The nanocomposites often exhibit enhanced properties and improved functionalities due to the synergetic effects between GO nanosheets and the nanoparticles.^{29,30} Most of these hybrid nanocomposites find applications as electrocatalysts. However, a few papers have reported on their catalytic activity for organic transformation.²⁴ For example, Choi and co-workers have reported the catalytic activity of Au nanoparticles

Department of Chemical Science, Tezpur University, Napaam, Assam, 784028, India
E-mail: chandrama006@gmail.com; Fax: +91 03712267006; Tel: +91 03712267006

† Electronic supplementary information (ESI) available: The standard deviation values for the entire kinetic study are given in electronic supplementary information. See DOI: 10.1039/c5ra10551j

supported on GO for catalytic reduction of nitroarenes.³¹ Compared with the expensive noble metal or metal oxide nanoparticles CuO is a cheap alternative with a broad potential applications. It has been widely used in active anode materials, superconductors, sensors and heterogeneous catalysts due to its abundant resources, environmental compatibility, cost effectiveness and favorable pseudocapacitive characteristics.^{32,33} Integrating nanoparticle into GR currently has been an active research field. Recently, Zhao *et al.* has synthesized CuO-GR nanostructure by a hydrothermal method in presence of ammonia solution for use in supercapacitors.³⁴ CuO-GR nanocomposites are also exhibited high capacity and capacity retention as anode materials in lithium ion batteries.^{34,35} To the best of our knowledge, there is no research studying their catalytic application.

In this article, we present a simple and facile approach for integrating CuO onto the surface of GO by hydrothermal method. During the hydrothermal treatment, GO was successfully reduced to GR and CuCl was oxidized to CuO due to the redox reaction. This method eliminates the use of reducing agents and offers the necessary stability of the resulting nanocomposite for catalytic transformation. Furthermore, the resulting CuO-rGO nanocomposites exhibit excellent catalytic activity toward the reduction of 4-NP in presence of NaBH₄. The catalytic activities of the nanocomposites were also studied by changing the ratio of GO and Cu. The reaction was completed in only 20 s at room temperature and the catalyst can be easily regenerated and reused with good recyclability up to five catalytic cycles. Considering the wide-ranging potential applications of GO as a host material for a variety of nanoparticles, the approach developed here may lead to new possibilities for the fabrication of GO by nanomaterials endowed with multiple functionalities.

2. Experimental section

2.1. Chemicals

Graphite power (<20 micron, Aldrich) was used as received. Sodium nitrate (NaNO₃), potassium permanganate (KMnO₄), hydrogen peroxide (50% v/v), cuprous chloride (CuCl), 4-nitrophenol, sodium borohydride (NaBH₄), concentrated sulfuric acid (98%), hydrochloric acid were procured from Merck.

2.2. Preparation of GO, CuO-rGO nanocomposites

GO was synthesized from natural graphite powder using modified Hummers method.³⁶ CuO-rGO nanocomposites was synthesized by hydrothermal method from mixture of GO and CuCl. In this process, 10.0 mg of GO was dispersed in 10.0 mL of distilled water and 9.89 mg of CuCl (0.01 mol CuCl in 1000 mg GO, labelled as CuO_{0.01}-rGO) was dispersed with 20 mL distilled water by ultrasonication to form a homogeneous dispersion. Then, the GO dispersion was gradually added to the CuCl solution. The solution mixture was stirred magnetically at 25 °C for 120 min and transferred into an autoclave with a volume of 50 mL. Hydrothermal treatment of the mixed solution was done at 150 °C for 4 h, and the solid product was washed with

distilled water by centrifugation several times. Then, the composites were dried at 100 °C to obtain the desired CuO-rGO nanocomposites. In addition, for optimization, 0.05 mol CuCl in 1000 mg (CuO_{0.05}-rGO) and 0.1 mol CuCl in 1000 mg (CuO_{0.1}-rGO) was also synthesized following the same procedure.

2.3. Characterization

The infrared spectra were recorded with samples on KBr pellets over a frequency range of 4000–500 cm⁻¹ in a Nicolet model impact 410 FT-IR Spectrophotometer. The X-ray diffraction (XRD) study was carried out at room temperature (*ca.* 298 K) using a Rigaku X-ray diffractometer with Cu-K α radiation (λ = 0.15418 nm) at 30 kV and 15 mA using a scanning rate of 0.05 θ sec⁻¹ in the range of 2θ = (10–70 $^\circ$). The morphology of CuO-rGO nanocomposites was characterized with scanning electron microscope (SEM). The SEM analysis was conducted on JSM-6390LV (Jeol, Japan) scanning electron micrograph attached with energy dispersive X-ray detector. Scanning was done at micrometer range; images were taken at an accelerating voltage of 15–20 kV with magnification of $\times 15\ 000$ and $\times 20\ 000$ and data were obtained by using INCA software.

2.4. Catalytic reduction of *p*-nitrophenol (4-NP) by CuO-rGO nanocomposite

In a typical reaction, freshly prepared aqueous solution of NaBH₄ (0.1 mL, 0.3 M) was added in 10.0 mL of 4-NP aqueous solution (1×10^{-4} M). This was leading to a color change from light yellow to yellow green. To that solution, 1.0 mg catalyst was added and the reaction solution was allowed to stir until the solution became colorless. The green yellow color of the solution gradually vanished, indicating the reduction of 4-NP. The reaction progress was checked by assessing a small portion of the reaction mixture at a given time interval. The concentration of 4-NP was recorded in the UV-vis spectrophotometer at a wavelength of 400 nm.

To study the recycling ability of the catalyst, the catalyst was separated from the solution by centrifugation and washed with distilled water several times. Then the catalyst was added into another freshly prepared mixed solution of 4-NP and NaBH₄ to start the next round of reaction. The recyclability test was carried out for five catalytic cycles.

3. Result and discussion

3.1. Characterization of CuO-rGO nanocomposite

3.1.1. FTIR study. Fig. 1 shows the FTIR spectra of GO, CuCl and CuO-rGO nanocomposite. In the FTIR spectrum of GO (Fig. 1a), the peaks obtained at 1264 cm⁻¹, 1067 cm⁻¹ and 1721 cm⁻¹ are attributed to the C–O epoxy stretching, C–O alkoxy stretching and C=O carbonyl stretching vibrations, respectively. The absorption band at 1623 cm⁻¹ and 3421 cm⁻¹ correspond to the aromatic C=C stretching vibration and O–H stretching vibration respectively. Normally, CuCl vibrations are observed at wavenumbers less than 500 cm⁻¹.³⁷ In the FTIR spectrum of CuCl (Fig. 1b), peak at 442 cm⁻¹ corresponds to

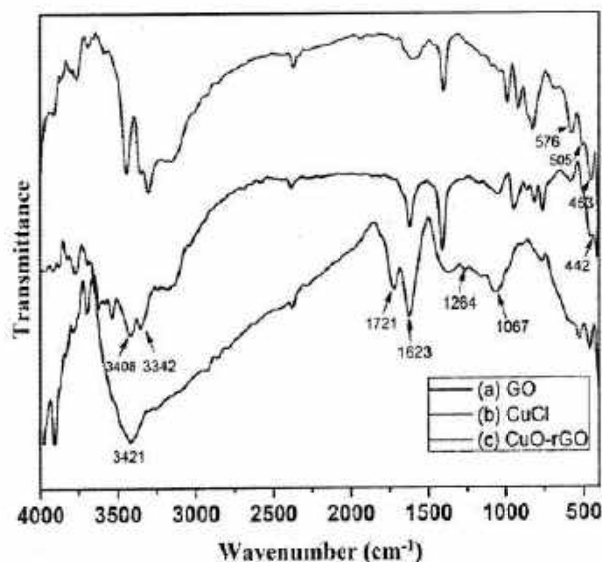


Fig. 1 FTIR spectrum of (a) GO, (b) CuCl and (c) CuO-rGO nanocomposite.

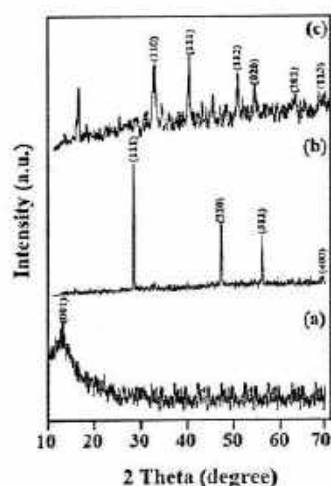


Fig. 2 XRD patterns of (a) GO, (b) CuCl and (c) CuO-rGO nanocomposite.

Cu-Cl stretching vibration. Bands at 3408 cm^{-1} and 3342 cm^{-1} may be attributed to the Cu-OH groups. Peaks between 500 cm^{-1} to 1500 cm^{-1} is made for the observation of hydroxyl

deformation modes. In the FTIR spectrum of CuO-rGO nanocomposite (Fig. 1c), the peak intensity of C=O, C-OH, and C-O groups decreases significantly, indicating reduction of GO. Again, some new peaks appeared at 576 cm^{-1} , 505 cm^{-1} and 453 cm^{-1} corresponding to Cu-O stretching vibrations. These results implied simultaneous reduction of GO along with formation of CuO by hydrothermal treatment.

3.1.2. XRD analysis. Fig. 2 shows XRD patterns of GO, CuCl and CuO-rGO nanocomposite. GO exhibited the strong diffraction peak at $2\theta = 11.45^\circ$ (Fig. 2a), attributed to the (001) plane due to oxygen containing functional groups on carbon sheets. In the XRD pattern of CuCl and CuO-rGO, the positions of diffraction peaks matched well with standard CuCl, CuO and rGO. The peaks at 2θ values of 28.45° (111), 47.35° (220), 56.2° (311) and 68.5° (400) were consistent with the standard XRD data for the CuCl cubic phase of face centered crystal lattice (JCPDS Card no. 82-2114, Fig. 2b). The XRD spectra of CuO-rGO exhibits peaks at 2θ values of 32.55° (110), 39.95° (111), 50.25° (112), 53.85° (020), 58.5° (202) and 63.6° (113) which were consistent with the standard XRD data for the CuO monoclinic phase of end-centered crystal lattice (JCPDS Card no. 89-2530, Fig. 2c). Again, the spectrum shows small additional peaks at 25.2° and 44.9° which could be attributed to rGO. These results demonstrated that GO was successfully reduced to rGO and CuCl was oxidized to CuO during the redox reaction.

3.1.3. SEM and EDX analysis. A difference in surface morphology between CuCl and CuO-rGO nanocomposite is observed (Fig. 3). The SEM image of CuO-rGO revealed that the copper nanoparticles are homogeneously distributed over crumpled, paper-like surface of GO confirming that the incorporation of Cu nanoparticle into GO (Fig. 3b). Again, the EDX spectrum of CuO-rGO (Fig. 4) exhibited the presence of C, O, and Cu elements, further confirming the formation of CuO-rGO composite.

3.2. Catalytic properties of CuO-rGO nanocomposite

The catalytic properties of the CuO-rGO nanocomposite were quantitatively evaluated with the reduction 4-NP into of 4-aminophenol (4-AP) by NaBH_4 as a model system. As shown in Fig. 5, this reaction could be easily monitored by the time-dependent UV-vis absorption spectra. In the absence of the catalysts, the mixture of 4-NP and NaBH_4 show a strong peak at

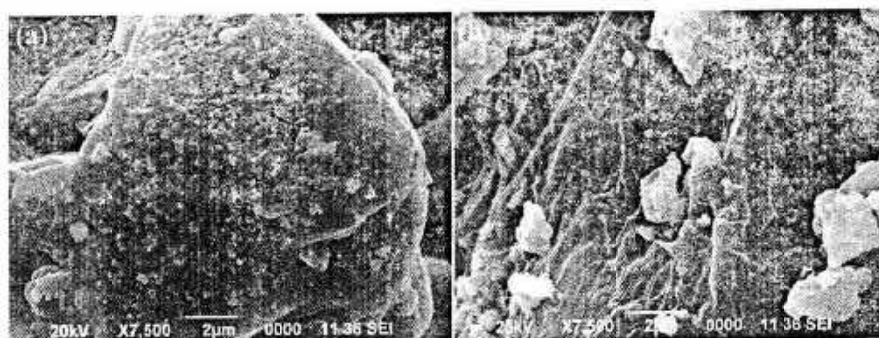


Fig. 3 SEM images of (a) CuCl and (b) CuO-rGO nanocomposite.

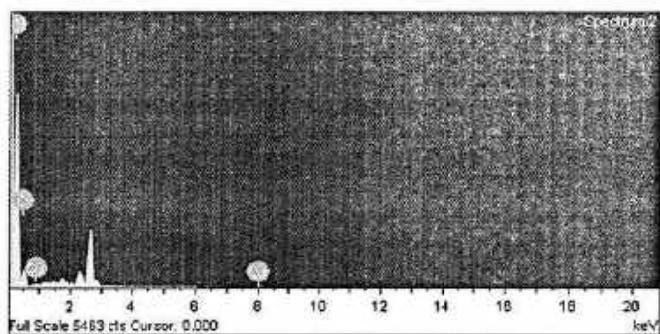


Fig. 4 EDX spectrum of CuO-rGO nanocomposite.

400 nm due to the formation of 4-NP ions under alkaline condition. After the catalysts were added into the system, the absorption peak of 4-NP at 400 nm decreases rapidly with a concomitant increase in the peak at 300 nm, which is attributed to the reduced product, 4-AP. As the initial concentration of NaBH_4 is large excess in comparison to 4-NP, the pseudo-first-order reaction kinetics was applied for the evaluation of the catalytic rate. Therefore, the kinetic equation can be written as:

$$\ln(C/C_0) = -kt$$

where C_0 is the initial concentration of 4-NP in absence of catalyst; C is the concentration of 4-NP at any time, t after catalyst was added; and ' k ' is the rate constant, which can be obtained from the decrease in the peak intensity at 400 nm with time.

Fig. 5 shows the UV-vis absorption spectra of the reduction of 4-NP by NaBH_4 and Fig. 6 shows the corresponding plots of

$\ln(C/C_0)$ of 4-NP versus reaction time in the presence of (a) $\text{CuO}_{0.01}$ -rGO (b) $\text{CuO}_{0.05}$ -rGO (c) $\text{CuO}_{0.1}$ -rGO. From the linear relations of $\ln(C/C_0)$, shown in Fig. 6, the maximum value of rate constant, k , for this reaction is 13.951 min^{-1} , which is very high compared to those reported previously (Table 2). The results are summarised in Table 1. Good linear correlations ($R^2 > 0.996$) of $\ln(C/C_0)$ vs. t are observed for all nanocomposites, confirming the pseudo-first-order kinetics (Table 1).

It should be noted that the $\text{CuO}_{0.05}$ -rGO shows the highest catalytic activity with only 20 s to finish the reaction (Fig. 5b), whereas $\text{CuO}_{0.01}$ -rGO shows the lowest catalytic activity and can't achieve the full reduction of 4-NP even with a reaction time of 18 min (Fig. 5a). On the other hand, $\text{CuO}_{0.1}$ -rGO required 3 min to finish the reaction. The higher catalytic activity for the CuO-rGO catalysts may be ascribed to the two dimensional structure of rGO, which has a high affinity for the adsorption of 4-NP due to π - π stacking interactions. This increases the concentration of 4-NP near CuO. The high catalytic activity occurs from the synergistic effect of: (1) the high adsorption ability of rGO towards 4-NP, providing a high concentration of 4-NP near to the CuO which accelerates the reaction; and (2) electron transfer from rGO to CuO, facilitating the uptake of electrons by 4-NP molecules. Thus, the catalytic activity of the CuO-rGO catalyst depends on both CuO and rGO. With increase in the amount of CuO the catalytic activity increase and after a certain amount the activity decreases. This may be due to the decrease in the available active surface of rGO for adsorption of 4-NP.

The representative sample of $\text{CuO}_{0.05}$ -rGO was also tested for reusability in the reduction of 4-NP by NaBH_4 . The catalyst was separated by centrifugation and reused to carry out the

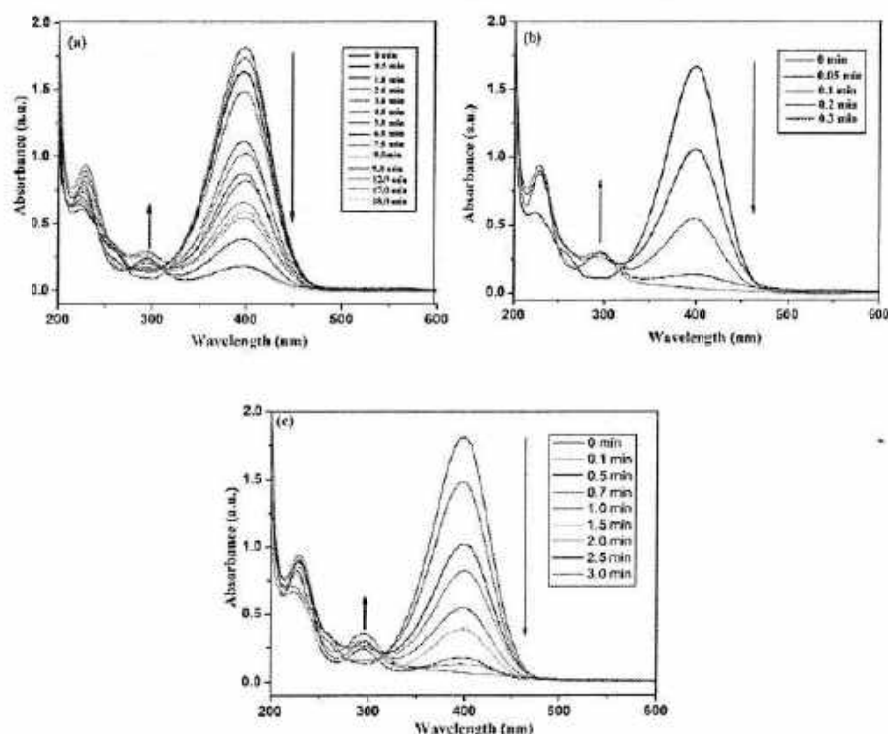


Fig. 5 UV-vis absorption spectra of the reduction of 4-NP by NaBH_4 in the presence of (a) $\text{CuO}_{0.01}$ -rGO (b) $\text{CuO}_{0.05}$ -rGO (c) $\text{CuO}_{0.1}$ -rGO.

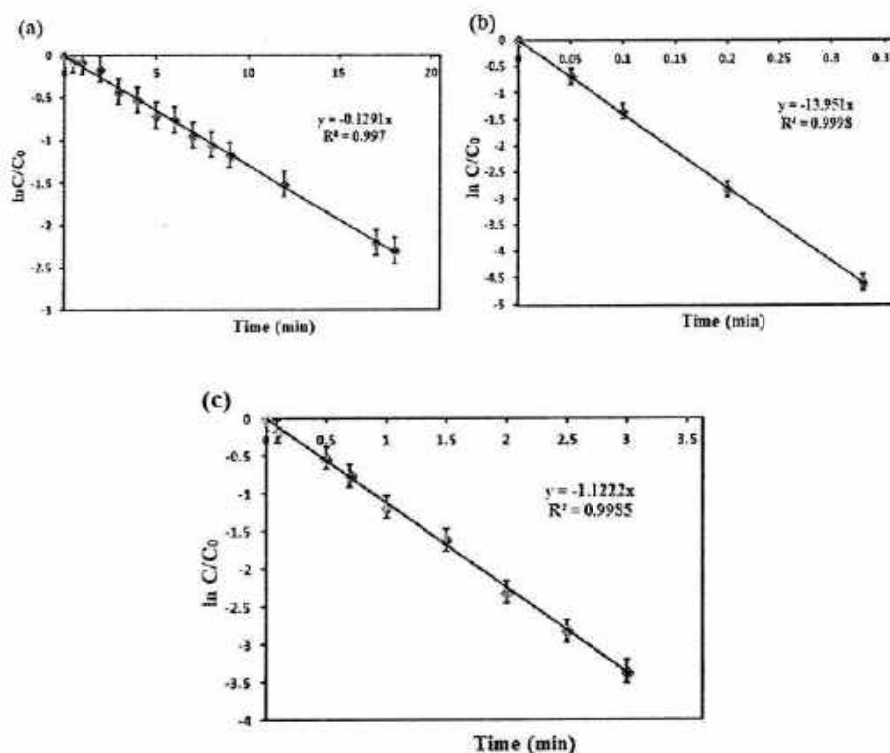


Fig. 6 Plots of $\ln(C/C_0)$ of 4-NP versus reaction time in the presence of (a) $\text{CuO}_{0.01}$ -rGO (b) $\text{CuO}_{0.05}$ -rGO (c) $\text{CuO}_{0.1}$ -rGO.

Table 1 Catalytic rate constants of reduction of 4-NP in the presence of CuO_x -rGO nanocomposites and the R^2 values for the $\ln(C/C_0)$ vs. t plots

Entry	Catalyst	4-NP (M)	NaBH_4 (M)	Rate constant (min^{-1})	R^2
1	$\text{CuO}_{0.01}$ -rGO	1×10^{-4}	0.3	0.1291	0.997
2	$\text{CuO}_{0.05}$ -rGO	1×10^{-4}	0.3	13.951	0.9998
3	$\text{CuO}_{0.1}$ -rGO	1×10^{-4}	0.3	1.1222	0.9985

reduction process for an additional four times. After the completion of five cycles, the values of k for each round of catalytic reaction were obtained from the plots of $\ln(C/C_0)$ vs. t (Fig. 7a). The k values for the successive five cycles was shown in

Fig. 7b, there is only a slight decrease in the k value with the increasing cycle. The main reason for the decrease in the catalytic activity is loss of catalyst during the separation process.

4. Comparison with other catalysts

For comparison of the present work with some of the earlier reports, different catalysts employed for the catalytic reduction of 4-NP are highlighted in Table 2. It is evident from Table 2 that the value of k of present work is much larger than Cu nanocatalyst²⁸ and pristine GO.³⁷ The catalytic activity of the synthesized catalyst is superior compared to all other metal nanocatalysts as well as noble metal/GR based catalysts reported earlier.^{31,38}

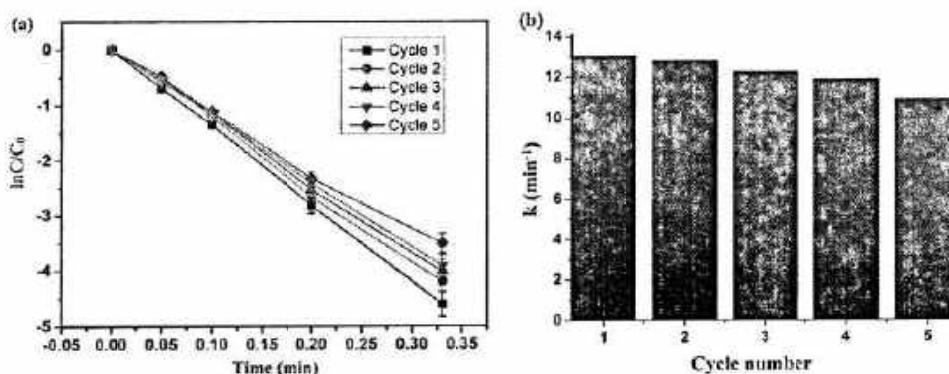


Fig. 7 (a) Plots of $\ln(C/C_0)$ of 4-NP versus reaction time for successive 5 cycles (b) value of k for each cycle with $\text{CuO}_{0.05}$ -rGO nanocomposite as catalyst.

Table 2 Comparison of values of rate constant for 4-NP reduction to 4-AP catalyzed by various catalysts

Entry	Catalyst	4-NP (M)	NaBH ₄ (M)	k (min ⁻¹)	Ref.
1	CuO _{0.05} -rGO	1 × 10 ⁻⁴	0.3	13.951	Present work
2	Cu nanoparticle	1.2 × 10 ⁻⁴	0.02	0.095	38
3	Au nanocages	1.4 × 10 ⁻⁴	0.042	5.58	39
	Au nanoboxes	1.4 × 10 ⁻⁴	0.042	3.25	(at 43 °C)
	Au nanoparticles	1.4 × 10 ⁻⁴	0.042	0.95	(at 43 °C)
4	Au-GR hydrogel	1 × 10 ⁻³	0.1	0.19	40
5	Au-rGO	7.5 × 10 ⁻⁴	2.22	6.478	31
	Au			0.069	
	GO			0.038	
6	Au-Ag/GO	1.54 × 10 ⁻³	0.88	8.56	41
	Au/GO			0.368	
	Ag/GO			0.208	

5. Conclusions

In summary, a facile and novel method to prepare GO-supported CuO nanoparticles was successfully developed. The prepared nanocomposite is successfully employed in the catalytic reduction of 4-NP with excellent catalytic activities and stabilities by the synergistic catalytic effect of CuO nanoparticle and rGO, further highlighting the importance of hybrid CuO-rGO nanocomposites. Considering the wide applications of rGO as a host material for a variety of nanoparticles, the present approach may lead to new possibilities for integrating active nanoparticles with rGO for advanced electronic, energy, and catalytic applications.

Acknowledgements

The authors would like to thank the Council of Scientific and Industrial Research (CSIR) India for their financial support in the research under contract no. 02(0066)/12/EMR-II.

References

- 1 K. S. Novoselov, A. K. Geim, S. V. Morozov, D. Jiang, Y. Zhang, S. V. Dubonos, I. V. Grigorieva and A. A. Firsov, *Science*, 2004, **306**, 666–669.
- 2 C. N. R. Rao, A. K. Sood, K. S. Subrahmanyam and A. Govindaraj, *Angew. Chem., Int. Ed.*, 2009, **48**, 7752–7777.
- 3 S. Stankovich, D. A. Dikin, G. H. B. Dommett, K. M. Kohlhaas, E. J. Zimney, E. A. Stach, R. D. Piner, S.-B. T. Nguyen and R. S. Ruoff, *Nature*, 2006, **442**, 282–286.
- 4 A. A. Balandin, S. Ghosh, W. Bao, I. Calizo, D. Teweldebrhan, F. Miao and C. N. Lau, *Nano Lett.*, 2008, **8**, 902–907.
- 5 Z. Lee, K.-J. Jeon, A. Dato, R. Erni, T. J. Richardson, M. Frenklach and V. Radmilovic, *Nano Lett.*, 2009, **9**, 3365–3369.
- 6 K. P. Loh, Q. Bao, G. Eda and M. Chhowalla, *Nat. Chem.*, 2010, **2**, 1015–1024.
- 7 A. A. Balandin, *Nat. Mater.*, 2011, **10**, 569–581.
- 8 A. K. Geim and K. S. Novoselov, *Nat. Mater.*, 2007, **6**, 183–191.
- 9 M. J. Allen, V. C. Tung and R. B. Kaner, *Chem. Rev.*, 2010, **110**, 132–145.
- 10 M. C. Duch, G. R. S. Budinger, Y. T. Liang, S. Soberanes, D. Urich, S. E. Chiarella, L. A. Campochiaro, A. Gonzalez, N. S. Chandel, M. C. Hersam and G. M. Mutlu, *Nano Lett.*, 2011, **11**, 5201–5207.
- 11 J. Xu, L. Wang and Y. Zhu, *Langmuir*, 2012, **28**, 8418–8425.
- 12 G. Eda, G. Fanchini and M. Chhowalla, *Nat. Nanotechnol.*, 2008, **3**, 270–274.
- 13 K. S. Kim, Y. Zhao, H. Jang, S. Y. Lee, J. M. Kim, K. S. Kim, J.-H. Ahn, P. Kim, J.-Y. Choi and B. H. Hong, *Nature*, 2009, **457**, 706–710.
- 14 F. Yu, J. Ma and D. Bi, *Mater. Horiz.*, 2014, **1**, 379–399.
- 15 X.-K. Kong, C.-L. Chen and Q.-W. Chen, *Chem. Soc. Rev.*, 2014, **43**, 2841–2857.
- 16 N. Zhang, Y. Zhang and Y.-J. Xu, *Nanoscale*, 2012, **4**, 5792–5813.
- 17 D. Gunlycke, D. A. Areshkin, J. Li, J. W. Mintmire and C. T. White, *Nano Lett.*, 2007, **7**, 3608–3611.
- 18 A. K. Mishra and S. Ramaprabhu, *J. Phys. Chem. C*, 2011, **115**, 14006–14013.
- 19 J. D. Roy-Mayhew and I. A. Aksay, *Chem. Rev.*, 2014, **114**, 6323–6348.
- 20 F. Schedin, A. K. Geim, S. V. Morozov, E. W. Hill, P. Blake, M. I. Katsnelson and K. S. Novoselov, *Nat. Mater.*, 2007, **6**, 652–655.
- 21 X. Ling, L. Xie, Y. Fang, H. Xu, H. Zhang, J. Kong, M. S. Dresselhaus, J. Zhang and Z. Liu, *Nano Lett.*, 2010, **10**, 553–561.
- 22 O. Akhavan, E. Ghaderi and A. Esfandiari, *J. Phys. Chem. B*, 2011, **115**, 6279–6288.
- 23 D. C. Wei and Y. Q. Liu, *Adv. Mater.*, 2010, **22**, 3225–3241.
- 24 G. M. Scheuermann, L. Rumi, P. Steurer, W. Bannwarth and R. Mülhaupt, *J. Am. Chem. Soc.*, 2009, **131**, 8262–8270.
- 25 S. Guo, D. Wen, Y. Zhai, S. Dong and E. Wang, *ACS Nano*, 2010, **4**, 3959–3968.
- 26 R. Muszynski, B. Seger and P. V. Kamat, *J. Phys. Chem. C*, 2008, **112**, 5263–5266.
- 27 K. K. Manga, S. Wang, M. Jaiswal, Q. Bao and K. P. Loh, *Adv. Mater.*, 2010, **22**, 5265–5270.
- 28 B. Li, H. Cao, J. Shao, M. Qu and J. H. Warner, *J. Mater. Chem.*, 2011, **21**, 5069–5075.
- 29 B. Li, H. Cao and G. Yin, *J. Mater. Chem.*, 2011, **21**, 13765–13768.
- 30 B. Li and H. Cao, *J. Mater. Chem.*, 2011, **21**, 3346–3349.
- 31 Y. Choi, H. S. Bae, E. Seo, S. Jang, K. H. Park and B.-S. Kim, *J. Mater. Chem.*, 2011, **21**, 15431–15436.
- 32 J. S. Shaikh, R. C. Pawar, A. V. Mpholkar, J. H. Kim and P. S. Patil, *Appl. Surf. Sci.*, 2011, **257**, 4389–4397.
- 33 H. X. Zhang and M. L. Zhang, *Mater. Chem. Phys.*, 2008, **108**, 184–187.
- 34 B. Zhao, P. Liu, H. Zhuang, Z. Jiao, T. Fang, W. Xu, B. Lub and Y. Jiang, *J. Mater. Chem. A*, 2013, **1**, 367–373.
- 35 B. Wang, X. L. Wu, C. Y. Shu, Y. G. Guo and C. R. Wang, *J. Mater. Chem.*, 2010, **20**, 10661–10664.

- 36 W. S. Hummers and R. E. Offeman, *J. Am. Chem. Soc.*, 1958, **80**, 1339.
- 37 R. L. Frost, W. Martens, J. T. Kloprogge and P. A. Williams, *J. Raman Spectrosc.*, 2002, **33**, 801–806.
- 38 P. Deka, R. C. Deka and P. Bharali, *New J. Chem.*, 2014, **38**, 1789–1793.
- 39 J. Zeng, Q. Zhang, J. Chen and Y. Xia, *Nano Lett.*, 2010, **10**, 30–35.
- 40 J. Li, C.-Y. Liu and Y. Liu, *J. Mater. Chem.*, 2012, **22**, 8426–8430.
- 41 T. Wu, L. Zhang, J. Gao, Y. Liu, C. Gaob and J. Yan, *J. Mater. Chem. A*, 2013, **1**, 7384–7390.

Utilization Certificate

Project Title: Graphene/graphene oxide based polymer nanocomposites and their applications as biosensor and supercapacitor


CSIR Sanction No: 02(0066)/12/EMR-II


Dated: 29-01-2016


Funded by Council of Scientific and Industrial Research (CSIR)

Sl No.	Amount	
	Rs. 11,39,250/-	Certified that out of Rs. 11,39,250/- of grant -in-aid received during the year 2012-2015 in the favor of Registrar, Tezpur University under this Ministry/Department grant no. given in the margin and a sum of Rs 12,43,692/- has been spent. The excess expenditure of Rs. 1,04,442/- incurred by the University and the same to be released to Registrar, Tezpur University.
		CSIR Sanction No: 02(0066)/12/EMR-II

Certified that I have satisfied myself that the condition on which the grants-in-aid was sanctioned have been fulfilled and that I have exercised the following checks to see that the money was utilized for the purpose for which it was sanctioned.


Principal Investigator
S.K. Dolui


Registrar
Tezpur University


Finance Officer
Tezpur University

ANEXURE-II

Consolidated Statement of Expenditure

(From the date of commencement 14-08-2012)

Title of the research scheme: Graphene/graphene oxide based polymer nanocomposites and their applications as biosensor and supercapacitor.

Date of commencement: 14-08-2012

Date of Termination: 31-08-2015

Period	Cheque No. Date & Amount	Stipend	Contingency	Scientist Allowance (For emeritus scientist scheme only)	Equipment	HRA + MA	Total	Payments (particulars of grants spent) (Rs.)					Balance	
								Stipend	Contingency	Scientist Allowance (For emeritus scientist scheme only)	Equipment	HRA + MA		Total
14.8.12-31.3.13	8,74,000	2,64,000	1,60,000	Nil	4,50,000	Nil	8,74,000	1,06,129	1,66,780	Nil	72,697	Nil	3,45,606	5,28,394
14.13-31.3.14	1,10,344							1,02,258	83,612		3,03,774		4,89,644	(-) 3,79,300
14.14-31.3.15	1,54,906							1,32,000	1,73,863		30,579		3,36,442	(-) 1,81,536
31.3.15-31.8.15	Nil							72,000	Nil		Nil		72,000	(-) 72,000
Total	11,39,250							4,12,387	4,24,255		4,07,050		12,43,692	(-) 1,04,442

Prof. S. K. Dohi
(Project Investigator)

Registrar
Tezpur University

Finance Officer
Tezpur University

Finance Officer
Tezpur University